Doctoral Thesis

Computational Modelling of Transcranial Magnetic Stimulation

by

Nicholas Hananeia

Institut für Theoretische Physik

Justus-Liebig-Universität Gießen

Gießen, 2024

Supervised by

Prof. Dr. Christian Heiliger

Prof. Dr. Peter Jedlička

Contents

List of Figures

Abstract

Transcranial magnetic stimulation (referred to as TMS) is a form of non-invasive brain stimulation that has been in widespread clinical use in recent decades. In spite of its widespread applicability to a variety of mental and neurological ailments, there are a great many unknowns in the understanding of how and why TMS has beneficial effects. In this work we model transcranial magnetic stimulation in-silico, with a focus on the propagation of action potentials and implications for synaptic plasticity.

The first piece of modelling work that will be focused on in this thesis is the toolbox "Neuron Modelling for Transcranial Magnetic Stimulation" (NeMo-TMS). NeMo-TMS is a tool developed to synergize modelling of transcranial magnetic stimulation across multiple scales of brain organization. NeMo-TMS links modelling of magnetically-induced electric fields in large volumes of neural tissue (such as whole brains, segments of brain tissue, or even volumes placed in-vitro) to smaller scales. These fields are coupled to single-cell models. NeMo-TMS is capable of importing arbitrary morphologies which are reconstructed from observations of real cells. With the realistic electric field and the realistic morphology, the tool enables modelling of the propagation of action potentials through the axons and dendrites of these cells, and subsequent modelling of calcium accumulation and dispersion within the cells. This thesis details the function of this tool, and provides a worked example of the tool's use and observations of the induction and propagation of cellular action potentials in NeMo-TMS.

The second major piece of modelling in this thesis is the induction of synaptic plasticity by TMS stimulation. We implement in NeMo-TMS a well-validated model of the CA1 pyramidal cell with a reduced morphology and detailed biophysical properties. This model is then combined with a model of a combined AMPA/NMDA glutamatergic synapse, with multiple detailed phenomenological synaptic plasticity pathways representing biophysical pathways.

With this model, we simulate induction of long-term potentiation by application of both low-frequency TMS stimulation as well as that induced by high-frequency theta burst TMS stimulus, and simulate the dependence of plasticity outcomes on stimulation frequency, synaptic location, and pharmacological perturbation.

Finally, with the tools we developed, we investigate the degree to which axonal/dendritic morphology explains discrepancies in plasticity induction thresholds between cells sourced from different species of rodent, using detailed reconstructions of the dendrites and large, branching axons sourced from mice and rats.

In summary, this thesis demonstrates the development and implementation of novel tools for modelling transcranial magnetic stimulation, and demonstrates their use with scientifically relevant applications to plasticity and modelling of action potential initiation.

Zusammenfassung

Die transkranielle Magnetstimulation (TMS) ist eine Form der nicht-invasiven Hirnstimulation, die in den letzten Jahrzehnten in großem Umfang klinisch eingesetzt wurde. Trotz ihrer weit verbreiteten Anwendbarkeit bei einer Vielzahl von psychischen und neurologischen Erkrankungen gibt es noch viele Unbekannte im Verständnis, wie und warum TMS positive Effekte hat. In dieser Arbeit modellieren wir die transkranielle Magnetstimulation in-silico, wobei wir uns auf die Ausbreitung von Aktionspotentialen und die Auswirkungen auf die synaptische Plastizität konzentrieren.

Der erste Teil der Modellierungsarbeit, auf den wir uns in dieser Arbeit konzentrieren, ist der Werkzeug "Neuron Modelling for Transcranial Magnetic Stimulation" (NeMo-TMS). NeMo-TMS ist ein Werkzeug, das entwickelt wurde, um die Modellierung der transkraniellen magnetischen Stimulation über mehrere Skalen der Gehirnorganisation hinweg zu synergetisieren. NeMo-TMS verbindet die Modellierung magnetisch induzierter elektrischer Felder in großen Volumina neuronalen Gewebes (wie ganze Gehirne, Segmente von Hirngewebe oder sogar in vitro platzierte Volumina) mit kleineren Maßstäben. Diese Felder werden mit Einzelzellmodellen gekoppelt. NeMo-TMS ist in der Lage, beliebige Morphologien zu importieren, die aus Beobachtungen realer Zellen rekonstruiert werden. Mit dem realistischen elektrischen Feld und der realistischen Morphologie ermöglicht das Tool die Modellierung der Ausbreitung von Aktionspotenzialen durch die Axone und Dendriten dieser Zellen sowie die anschließende Modellierung der Kalziumakkumulation und -dispersion innerhalb der Zellen. In dieser Arbeit wird die Funktion dieses Werkzeugs detailliert beschrieben und ein praktisches Beispiel für die Verwendung des Werkzeugs sowie Beobachtungen der Induktion und Ausbreitung von zellulären Aktionspotenzialen bei NeMo-TMS gegeben.

Der zweite wichtige Teil der Modellierung in dieser Arbeit ist die Induktion von synaptischer Plastizität durch TMS-Stimulation. Wir implementieren in NeMo-TMS ein gut validiertes Modell der CA1-Pyramidenzelle mit einer reduzierten Morphologie und detaillierten biophysikalischen Eigenschaften. Dieses Modell wird dann mit einem Modell einer kombinierten glutamatergen AMPA/NMDA-Synapse kombiniert, wobei mehrere detaillierte phänomenologische synaptische Plastizitätspfade biophysikalische Pfade darstellen.

Mit diesem Modell simulieren wir die Induktion der Langzeitpotenzierung sowohl durch niederfrequente TMS-Stimulation als auch durch einen hochfrequenten Theta-Burst-TMS-Stimulus und simulieren die Abhängigkeit der Plastizitätsergebnisse von der Stimulationsfrequenz, dem synaptischen Ort und der pharmakologischen Störung.

Schließlich untersuchen wir mit den von uns entwickelten Werkzeugen, inwieweit die axonale/dendritische Morphologie Unterschiede in den Schwellenwerten für die Plastizitätsinduktion zwischen Zellen verschiedener Nagetierarten erklärt, indem wir detaillierte Rekonstruktionen der Dendriten und großen, verzweigten Axone von Mäusen und Ratten verwenden.

Zusammenfassend zeigt diese Arbeit die Entwicklung und Implementierung neuartiger Werkzeuge für die Modellierung der transkraniellen Magnetstimulation und demonstriert deren Einsatz in wissenschaftlich relevanten Anwendungen zur Plastizität und zur Modellierung der Initiierung von Aktionspotentialen.

Chapter 1

Introduction

The history of electrical stimulation of the brain for the purposes of therapy goes back as far as the oldest history of neuroscience itself, indeed going as far back as the first scientific observations that electricity could effect the human body. Franklin's early use of static electricity generated by Leyden jars in 1750 resulted in a shock from which he experienced disorientation and described memory loss. From this experience, he moved on to experimenting with electric shocks on humans with paralysis, inducing movement in limbs and claiming success in the treatment of "hysterical fits" in a patient by application of static electricity to parts of her body which were undergoing convulsion. (Bolwig and Fink 2009).

More enthusiastic investigation of the therapeutic potential of electricity came with the pioneering work of Luigi Galvani and Giovanni Aldini on what was at the time called "galvanism" - the induction of movement in muscle and nervous tissues by electric stimulation. Aldini continued this work in spite of reluctance from the scientific community to accept that animal cells had inherent electricity, demonstrating the induction of movement of limbs in dead animals and in several notable instances, the corpses of condemned prisoners. Eventually, he disproved initial objections to innate animal electricity by Volta by the induction of contractions of muscle fiber without electricity transmitted by metals. (Parent 2004).

At the same time as these demonstrations of galvanism, Aldini treated several patients with "melancholic madness" - probably better understood in modern terms as major depression. By application of static electricity from voltaic piles directly to the patients' crania, with increasing electric intensities over a period of several days to weeks. The first patient's state changed from being lethargic and non-functional to being "completely cured" over the course of weeks; the second patient had less severe depressive symptoms but similarly a cure was claimed (Bolwig and Fink 2009). Aldini later abandoned

this work, but the pioneering efforts remain remarkable.

By the twentieth century, electrotherapy had seen decades of use in the world's mental asylums, with claimed success in treating a variety of mental illnesses. The practice became truly standardized and widespread, however, with the advent of electroconvulsive therapy (ECT), starting in 1939, which uses an electrical current to induce a seizure, for the treatment of major depression and similar disorders.(Gazdag and Ungvari 2019). This treatment replaced more dangerous chemical ictogenic protocols. In the decades that followed, ECT saw widespread use in the psychiatric world and its controversial use on non-consenting patients led to it having a dark public image. Nevertheless, development and use of the therapeutic tool continued, as it continues to be effective at alleviating pharmacologically-resistant depression.

The variety and specificity of electrical brain stimulation treatments has expanded over the years: such examples would include transcranial alternating current stimulation (TACS) and transcranial direct current stimulation (TDCS), where electricity is applied to the cranial surface but not at a seizure-inducing intensity. Invasive tools like deep-brain stimulation (DBS) surgically implant an electrode deep inside the brain's volume, delivering electric current directly at a neurologically relevant treatment site.

Transcranial magnetic stimulation (TMS) continues on the success of these electrical stimulation methods, and does so non-invasively - no electrodes are required as the magnetic field is able to penetrate the patient's skull and stimulate the brain directly.

While our understanding of how and why these treatments work, and the knowledge to target and tailor them for specific ailments has certainly vastly improved in the two centuries since Aldini and Franklin, there are still significant unknowns in what brain stimulation does and how to best employ it.

TMS has been in use for a much shorter amount of time than its electrical cousins - yet because it is non-invasive and effective, it has great potential. Here we will investigate and model the physical and biophysical mechanisms by which TMS affects single cells and the brain.

1.1 Neurons: A Background

Neurons have long been considered the fundamental unit of information processing in the animal brain. Since this is the system that we will model in this work, it is important to understand its basic structure and function. The understanding that neurons were discrete units with distinct input and output is called the neuron doctrine.

In early neuroscientific research, after the revolutionary discovery of the structure of brain tissue by the Golgi staining process (Pannese 1999). This method first immerses the tissue in potassium dichromate,

followed by immersion in silver nitrate, which leads to a high-contrast dark black stain of the cell bodies and cell processes. This was one of the pioneering processes that enabled neuroscientists to visualize the intricate structure of brain tissue. However, the initial assessment of the functionality of the structure was incorrect.

The leading theory of brain structure and function in the early era, popularized by Golgi, was the so-called reticular theory (Cimino 1999). Under the reticular theory, the brain was a continuous net of brain tissue, with the net made of what would later be identified as dendrites and axons. Under the reticular theory, neural tissue would be a single large syncytium, comparable to multi-nucleus cells found in fungi.

The reticular theory was discredited by the pioneering work of Cajal (Guillery 2005). Cajal hypothesized, using an improved variant of the Golgi stain, that neural tissue was not a syncytium, but was made of discrete individual cells which were not individually connected. He did so by observing axonal growth cones, hypothesizing that these are the results of individual neurons establishing connections to other individual neurons, connecting at sites which were called synapses.

Experiments by Loewi (Borges and Garcia 2021) confirmed that the synapse was a physical barrier with chemical transmission, rather than a syncytium, by immersing nerve tissue in solution which disrupted the chemical transmission, stopping the transmission of information from one cell to the next. This was later directly observationally by the subsequent imaging of the synaptic gap by electron microscopy.

Physically, neurons are made up of three major component parts: the soma, the dendrites, and the axon. The soma contains the nucleus of the neuron, and is responsible for protein synthesis and other processes necessary for the continued function of the cell. Somata of neurons vary in size, with the smallest being those of granule cells, which are spherical on the order of $4\mu m$ in diameter. The largest somata belong to pyramidal cells, which can have somatic diameters on the order of 15-20 μm.

Dendrites and axons are collectively called neurites, as they are both protrusions from the soma; however they serve opposite purposes. Dendrites are large, branching structures that protrude from the soma. Neurons can have many dendrites, and the amount of dendrites and the structure thereof are often a key differentiating factor between different classes of neuron. Dendrites form the input mechanism of the cell; the dendrites can reach distances of up to 1mm from the soma, and many contain protrusions called dendritic spines, which are targets of synapses. Synapses can additionally target the dendritic branches; additionally a minority of synapses target the soma or the axon.

The axon is the output mechanism of the cell. It is within the axon that action potentials are generated. Axons can be sheathed in electrically insulating myelin, and nerve fibers that innervate different regions of the animal's body are principally composed of myelinated axons, as is the so-called white matter

within the brain (as contrasted with grey matter, which consists of dendrites and somata). Axons are capable of growth to make new connections; this growth is done with a structure called a growth cone, a motile structure which explores the extracellular environment, guiding extensions of the axon in the needed direction (Tamariz and Varela-Echavarria 2015; Kalil, Szebenyi, and Dent 2000). At the tips of axons are axon terminals, which contain the presynaptic connections which connect to other neurons' (or to the originating neuron in the case of recurrent connections) postsynaptic sites.

Axons thus facilitate the rapid and long-distance transmission of information throughout the nervous system. In addition to being sheathed in myelin, which aids in transmission of action potentials on account of reduced membrane capacitance relative to unmyelinated membrane, axons also have nodes of Ranvier, regions of high sodium conductance which boost the amplitude of action potentials, acting like repeaters to counter attenuation.

A schematic of the basic structure and function of a neuron is shown below in Figure 1.1.

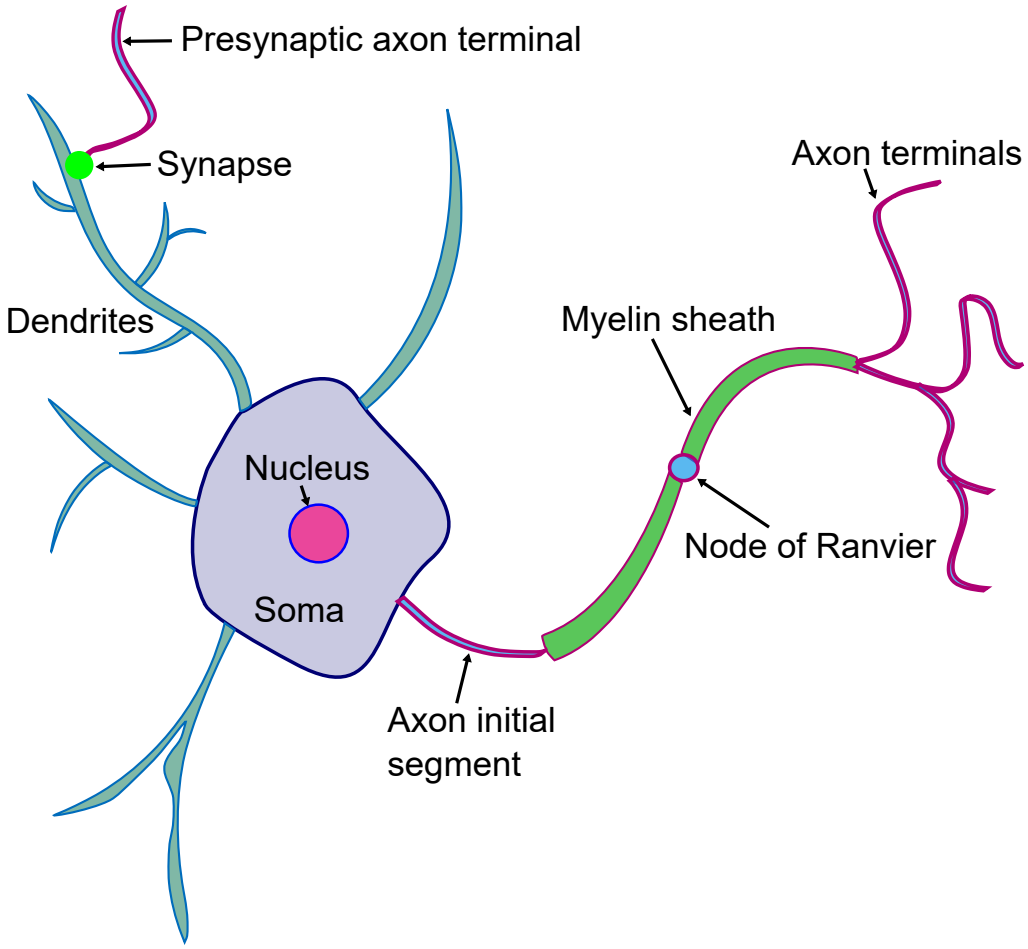

Figure 1.1. Schematic of structure of typical neuron. The neuron has several key anatomical components. The soma contains the cell nucleus, and has several neurite protrusions. Dendrites are the usual input locations where incoming axon terminals connect via synapses. Action potentials are initiated in the axon initial segment, and transmitted to the axon terminals, assisted by the insulating myelin sheath and signal-boosting nodes of Ranvier.

In addition to being divided by morphological type, neurons are also divided by function: Neurons can be excitatory, inhibitory, or modulatory, based on what neurotransmitter their axon terminals use. Each neuron only uses one kind of neurotransmitter: this rule is known as Dale's law (Barranca et al. 2022). There are a large variety of neurotransmitters in the brain.

The primary excitatory neurotransmitter in the central nervous is glutamate, whereas the primary inhibitory neurotransmitter is gaba-aminobutyric acid (GABA). Other neurotransmitters exist such as acetylcholine (the primary neurotransmitter used at the neuromuscular junction and thus responsible for all movements of muscles), and a variety of modulatory neurotransmitters which change the manner in which cells fire such as dopamine, serotonin, and noradrenaline. Acetylcholine also acts as a modulator

in the central nervous system.

Synapses which function with a given neurotransmitter are not all the same: for example, among acetylcholine receptors, there are two types, named for chemicals (aside from acetylcholine) which specifically activate them: for example, the nicotonic acetylcholine receptor (nAChR) is selectively activated by nicotine, and the muscarinic acetylcholine receptor (mAChR) is activated by the fungus-derived toxin muscarine. Each different receptor type can differ significantly in structure and function, even within those which respond to the same neurotransmitter, for example the nAChR is a ligand-gated receptor which opens when active, allowing ions to flood into the postsynaptic cell. Meanwhile, the mAChR is a G-protein coupled receiver which upon activation causes a postsynaptic signaling cascade, a type of modulating behavior. Both would, of course, be simultaneously activated in the presence of acetylcholine.

In addition to categorization by morphology and neurotransmitter type, neurons are also categorized in other ways. In the peripheral nervous system, there are three types: Sensory neurons receive direct sensory information (such as touch or light sensitive cells), motor neurons drive muscle contractions and enable the movement of the animal, and interneurons are intermediary nodes in the network. Many peripheral nervous system neurons have specialized morphologies that differ significantly from the sorts of neurons specific to the central nervous system.

In the context of the central nervous system (i.e. the brain and spinal cord), neurons are usually divided into principal cells and interneurons, with principal cells being the primary excitatory cells, and interneurons being inhibitory. Cells which have modulating effect (such as dopaminergic cells) are concentrated in specific brain regions, such as the concentration of dopaminergic neurons in the substantia nigra. In contrast to this, glutamatergic principal cells and GABAergic interneurons are found all throughout the brain.

As mentioned earlier in this section, synapses are the sites of connection between different nerve cells. The typical chemical synapse is a structure consisting of two mushroom-shaped boutons separated by a gap called the synaptic cleft, which is 20-30 nm wide. The presynaptic side of the synapse contains vesicles of neurotransmitters. When an action potential arrives at the presynapse, voltage-gated calcium channels in the presynaptic bouton open, allowing Ca^{2+} ions to enter the presynaptic membrane. The influx of these Ca^{2+} ions induces the vesicles to fuse with the membrane and disgorge their contents of neurotransmitter into the synaptic cleft in a process called exocytosis (R. C. Lin and Scheller 2000).

Although it was long thought that action potentials induced only a single synaptic vesicle to release, it is known that multi-vesicle release can and does occur widely (S. Rudolph et al. 2015). Single vs. multiple vesicle release may have implications for the subsequent strength of the postsynaptic current, since a multiple vesicle release would result in a significantly increased concentration of neurotransmitter in the

cleft.

When the cleft is filled with neurotransmitters, the receptors on the postsynaptic side of the cleft open, inducing either a postsynaptic potential in the case of ligand-gated ion channels, or a modulatory effect in the case of neuromodulators. Subsequent to the synapse's activation, the neurotransmitters are reused after being collected by neurotransmitter transport factors in a process called reuptake; subsequently they are re-incorporated into vesicles in the presynapse. This process is shown below in Figure 1.2.

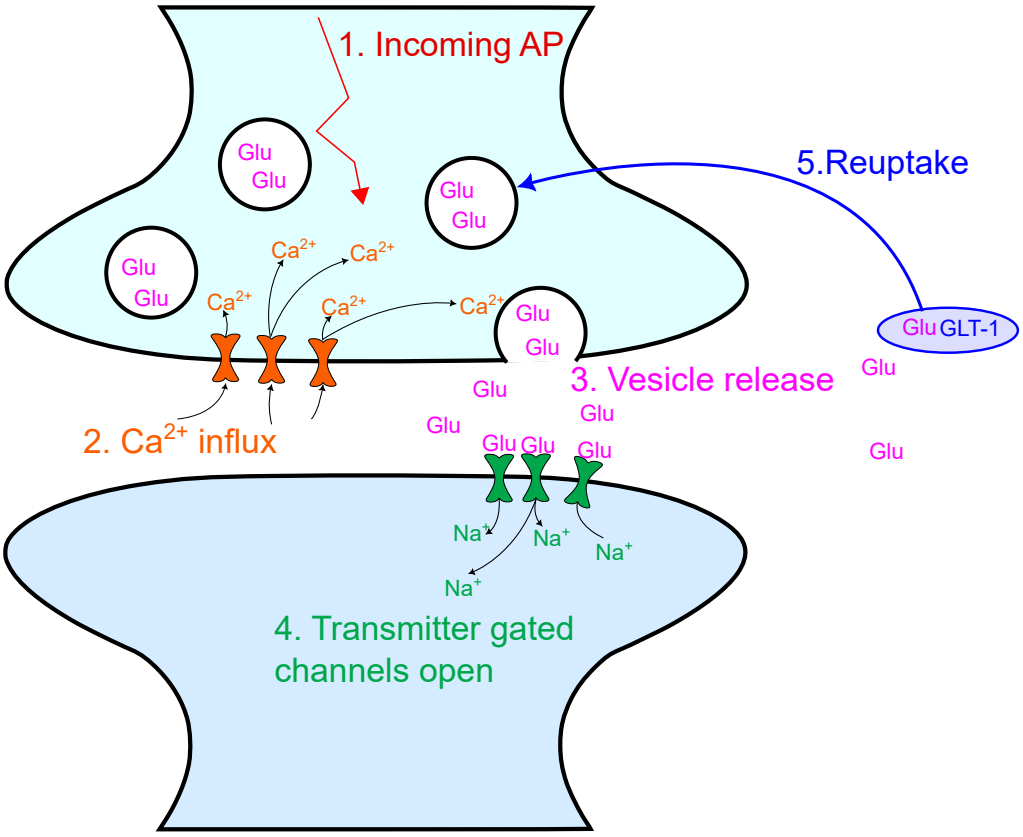

Figure 1.2. Schematic of mechanism of action of glutamatergic excitatory synapse. The chemical synapse works by activation of postsynaptic ligand-gated ion channels by a neurotransmitter, in this case glutamate. 1: The incoming action potential arrives at the presynapse. 2: The incoming action potential activates voltage-gated calcium channels in the presynapse, which allow Ca^{2+} ions to enter. 3: The action of the Ca^{2+} ions cause exocytosis of neurotransmitter vesicles, which release glutamate into the synaptic cleft. 4: The glutamate binds to glutamate-gated ion channels in the postsynapse, allowing Na^{+} ions to enter. This triggers an excitatory postsynaptic potential. 5: Transport factors (in the case of glutamate, GLT-1) absorb extracellular glutamate, and reuptake it into the presynapse for re-incorporation into vesicles.

It is worth nothing that chemical synapses are not the only type of connection between neurons. The idea of the syncytium is not completely incorrect - in many nervous systems, electrical synapses (otherwise

known as gap junctions), sites of direct contact where action potentials are able to pass from one cell to the next without any chemical transmission, do exist . These sites are points of much closer contact than chemical synapses (in an electrical synapse, the gap between the cells is on the order of 2-4nm whereas a chemical synapse's synaptic cleft is between 20-40nm, (Hormuzdi et al. 2004)), and the signals are able to cross a gap junction much faster than they can cross a chemical synapse, as transmission across a gap junction is near-instantaneous whereas there is a measurable delay for a chemical synapse to open (Bennett and Zukin 2004).

It was once thought that electrical synapses were only found in numbers in non-mammalian brains after their initial discovery in escape circuits in crayfish, however evidence has mounted that electrical synapses have an important role to play in the nervous systems of even mammals, and can have complex interactions with chemical synaptic transmission processes. (Connors and M. A. Long 2004; Pereda 2014). Because electrical synapses are freely permeable by ions, they can also allow groups of closely connected cells to fire in synchrony.

Neurons of differing types are not the only constituent cells in brain tissue. There are also a variety of glial cells which perform varying support functions. An important member of this class of cells are astrocytes, which bridge neurons and the blood vessels that permeate the brain, forming the blood-brain barrier. Other glial cells called microglia perform immune system function in the brain.

1.2 Transcranial Magnetic Stimulation

Transcranial magnetic stimulation (TMS)(Hallett 2007) is a non-invasive technique for stimulation of the brain. First commercially introduce in 1985 (Ziemann 2017), it has since been used clinically to treat a variety of neurological and psychological conditions, (Lefaucheur et al. 2020), including stroke (Hsu et al. 2012), pain and drug resistant depression (Gaynes et al. 2014; Kinjo et al. 2021), potentially also tinnitus, epilepsy, Alzheimer's (X. Wang et al. 2020), Parkinson disease (Chou et al. 2015), schizophrenia (Cole et al. 2015; Lorentzen et al. 2022), autism spectrum disorders (L. M. Oberman, Rotenberg, and Pascual-Leone 2015; Casanova et al. 2020) and other pathologies. In spite of its approval for clinical use by many national administrations, there remain significant gaps in scientific knowledge in how this relatively novel treatment methodology functions (Wassermann and Zimmermann. 2012)

TMS functions by using a magnet external to the cranium to induce magnetic fields within the neural tissue. Unlike similar non-invasive electrical protocols like electroconvulsive stimulation (ECT) and transcranial alternating/direct current stimulation (TACS/TDCS), no electrodes or other supporting equipment besides the magnetic rig is necessary. The magnet is placed above the cranium of the patient, with the magnetic flux penetrating the skull and brain tissue. A photograph of a typical TMS device is shown below in Figure 1.3.

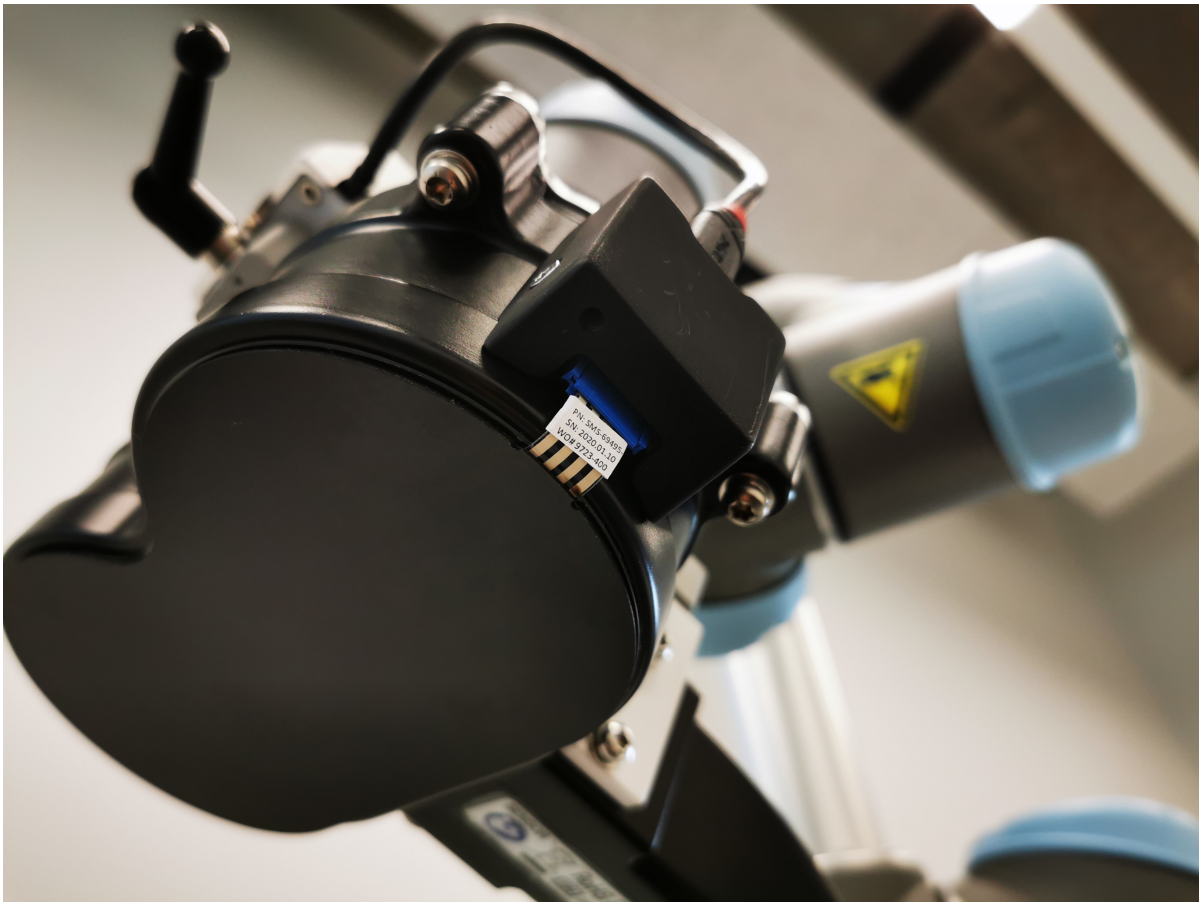

Figure 1.3. Figure-of-8 TMS coil, mounted on robotic arm. *Photograph by Zsolt Turi, private communication.*

Since brain tissue is conductive, there will be an induced electric field in the tissue every time the magnetic flux changes, because of Faraday's law, commonly written as one of Maxwell's equations in the form

$$\Delta \times \mathbf{E} = -\frac{\delta \mathbf{B}}{\delta t} \tag{1.1}$$

or, that the electric field's magnitude will be proportional to the negative rate of change of the magnetic field intensity, and it will be oriented circularly around the magnetic field direction, with the direction of the circle given by the sign of the magnetic field.

Commercial TMS machines deliver the magnetic field in pulses, so every magnetic pulse will be similarly accompanied by an electric field in the targeted area of the brain. The TMS pulse can be either monophasic (single positive pulse) or biphasic (positive followed by negative), and both pulse types are used in therapeutic protocols, and may have different therapeutic effects. (Arai et al. 2005)

There are many shapes of TMS coil. Initially, a circular coil was used, but in current practice the most typical is the figure-of-8 coil, where two current loops are placed side by side, producing a magnetic field which is perpendicular to the orientation of the coil, allowing a more focused application of the magnetic field to target a smaller region of cranium. Other designs exist; butterfly and double-cone coils conform to the shape of the head (Gutierrez et al. 2022), specialised "deep" coils focus the field to a deeper point in the brain (Harmelech, Roth, and Tendler 2021), and more exotic coils like "halo" coils where the coil surrounds the entire head exist as well (Meng et al. 2015). Each coil design represents a trade-off in penetration depth and focality, so different coil types are often used for specific targeting of specific areas of the brain to treat different conditions (Ueno and Sekino 2021). A selection of diagrams of TMS coil geometry is shown below in Figure 1.4.

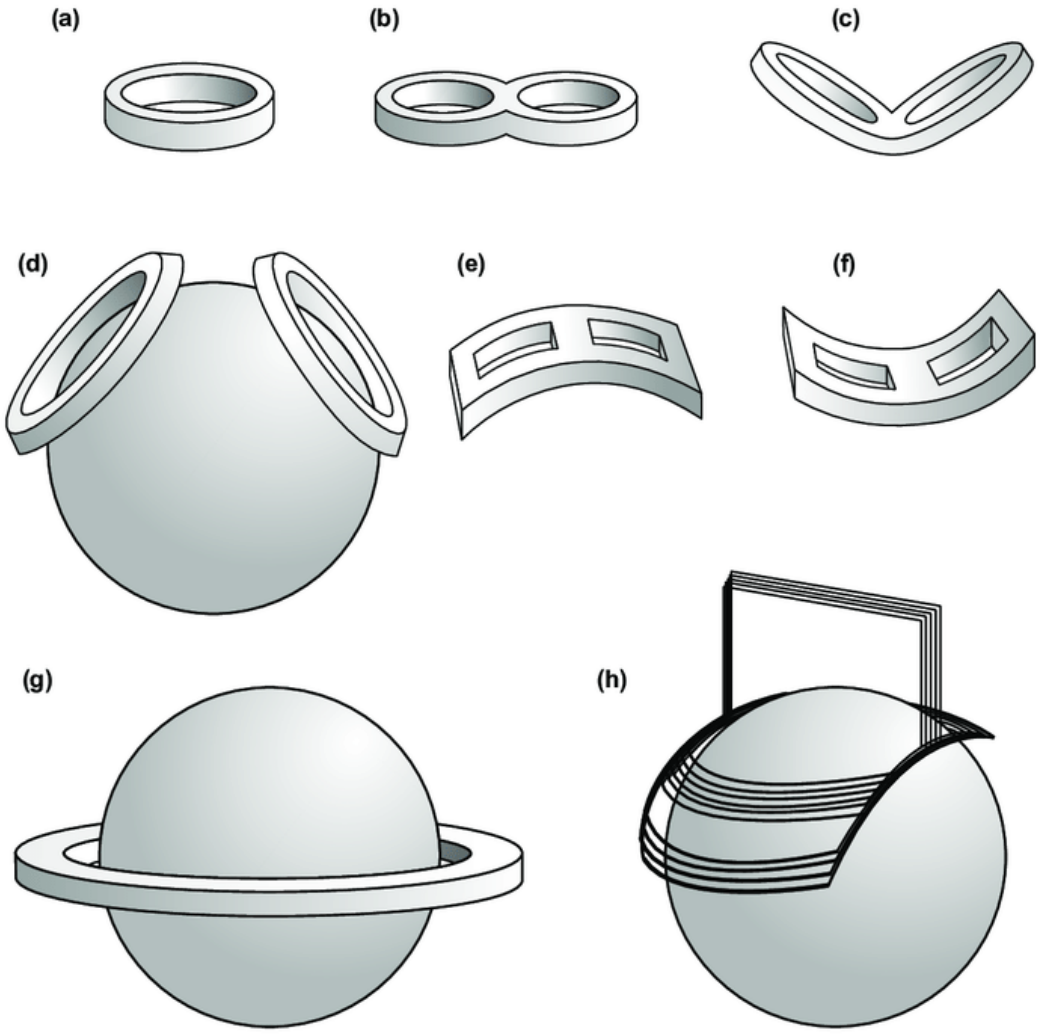

Figure 1.4. Examples of commonly used TMS coil geometries. (a): Circular coil, (b): Figure-of-eight coil, (c): Butterfly coil, (d): Cone (double circular) coil, (e): Downward-bending U-shape coil, (f): Upward-bending U-shape coil, (g): Halo coil, (h) Hesed coil (H-coil). *Source: (Gutierrez et al. 2022), Creative Commons Attribution 4.0.*

The magnetic field induced by a figure-of-8 TMS coil will be oriented perpendicular to the machine, as shown in Figure 1.5.

When neural tissue is stimulated by a TMS pulse, the induced electric field across the neurons will induce a change in the electric potential of the neuronal membrane at every point in the stimulated region. Because the axons have the highest concentration of ion channels in the cell (specifically high Na^+ and K^+ channel concentrations in the nodes of Ranvier, unmyelinated axon terminals, and axon

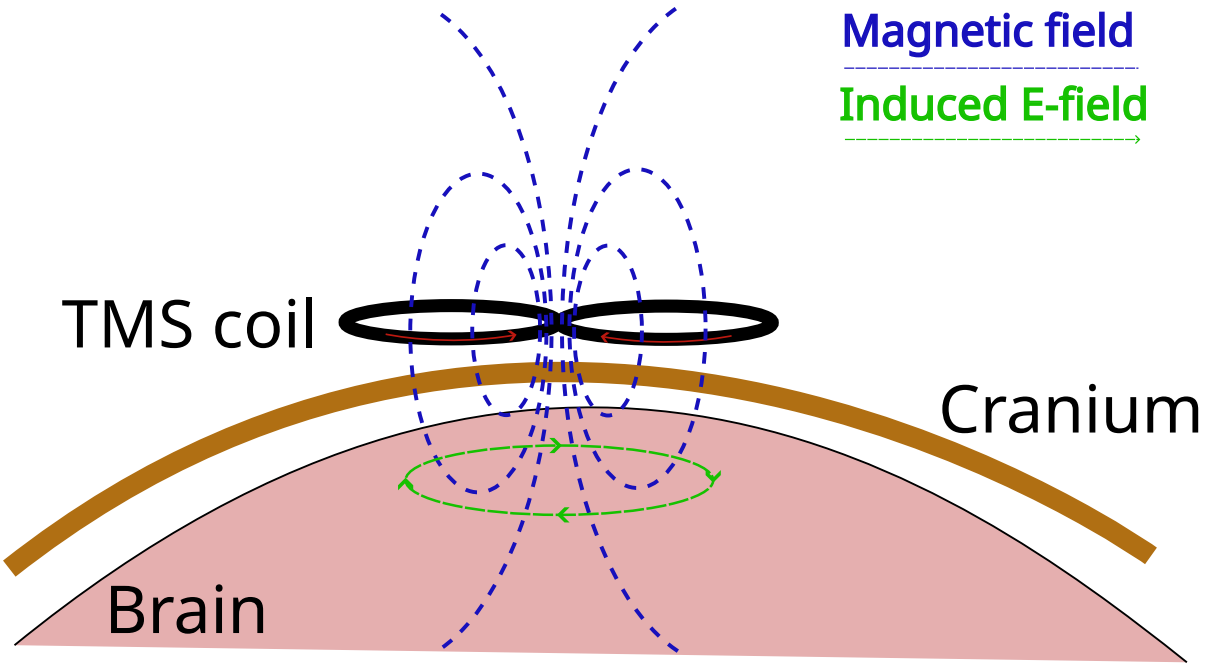

Figure 1.5. Induction of electric field in brain by transcranial magnetic stimulation

initial segment (Huerta and Volpe 2009)), these will be preferentially activated by the magnetic pulse. Within these regions of high Na^+ conductance, action potentials are initiated.

These action potentials will be both anterograde and retrograde, propagating in all directions through the axonal tree, and will ultimately stimulate both the soma and any presynaptic targets the axon has (Müller-Dahlhaus and Vlachos 2013).

When the backpropagating TMS-intiated action potentials reach the axon initial segment and soma, they may be followed by a somatic action potential, which would further back-propagate to the dendrites of the cell. This is the reverse of what is usually expected from electrical stimulation of brain tissue - in electrical stimulation targeting a cell's dendrites, the somatic action potential is generated when there is sufficient spatio-temporal summation of inputs at the soma to bring the voltage of the axon initial segment above its firing threshold.

Since axon terminals also have a high concentration of sodium channels(Suminaite, Lyons, and Livesey 2019), presynaptic terminals will be activated, and this will lead to an activation of synaptic sites in the targeted volume as well. Since synaptic plasticity (see Section 3.3) relies on coincident presynaptic and postsynaptic events, this combination of activation of multiple regions of the cell means that TMS likely can induce long-lasting changes (such as long-term potentiation or long-term depression - known

as LTP or LTD; see Section 1.4).

The amount of stimulated brain tissue is directly proportional to the size of the coil (Deng, Lisanby, and Angel V Peterchev 2013) - using a typical human-sized apparatus on a rodent will stimulate the entire brain, whereas in a larger animal, this same apparatus is capable of targeted stimulation of a single area of cranium. Since the magnetic field is emitted perpendicular to the scalp, this also means that stimulating any deeper brain areas will also necessarily stimulate any intervening areas between the cranium and the target area.

This relationship of coil size to stimulation area means that it is difficult to use animal studies to tune stimulation parameters for human clinical use, since the smaller size of the crania of typical animal models (rodents and non-human primates) often necessitates a smaller TMS coil and thus a potential for higher focal-induced electric fields (Ivan Alekseichuk et al. 2019). (Deng, Lisanby, and Angel V Peterchev 2013).

In a human, with an appropriately sized coil, the TMS pulse activates an area approximately 1cm in area and 2cm in depth, with an exponential decay of magnetic field strength with distance from the center of the target area (Huerta and Volpe 2009). Because the entire target area is stimulated, a variety of cells beyond the target area that are innervated by axons from the target area may also be activated synaptically. The limited depth of the stimulation from current TMS hardware limits the selection of areas which can be targeted by TMS.

In therapeutic use, multiple targets in the cortex are used. The most common target for actual efficacious treatment of mental illness is the dorsolateral prefrontal cortex (DLPC). This area of the brain is responsible for executive function, decision-making, and similar "higher" brain functions, and TMS targeting this area has been shown to effectively treat drug-resistant depression, memory-related issues, and anxiety disorders. (Pascual-Leone, Rubio, et al. 1996) (Balconi and Ferrari 2013).

In addition to therapeutically relevant targets, the motor cortex is also common target, since stimulation of this area will evoke involuntary movement from the patient such as a twitch of a limb. The minimum stimulation intensity at which this movement occurs is called the motor threshold, and is important for dosing of TMS treatment protocols (Turi, Lenz, et al. 2021).

TMS is also used widely as a diagnostic aid (Vucic et al. 2023). Because it is able to stimulate targeted populations of neurons non-invasively, several relatively novel technques have emerged. To diagnose the progression of degenerative diseases like myelopathies, neuropathies, and other issues with long-range transmission of information in the brain, shifts in the motor threshold over time in a patient can determine to what extent the motor neuron pathways have deteriorated (Menon et al. 2015). Similarly, mapping of motor evoked potentials can map pathways that may be affected with brain tumors, or to

determine the deterioration of patients with dementia or those recovering from a stroke (Di Lazzaro et al. 2021; Smith and Stinear 2016).

In recent years, TMS has been paired with electroencephalagrams (EEG) for the purpose of simultaneously stimulating and measuring the results of stimulation. (Tremblay et al. 2019). This is of significant importance for diagnostic use of TMS, since being able to immediately detect where, when, and how the brain activity induced by the pulse spreads makes being able to identify which pathways are activated far easier.

In the case of experiments conducted on slice cultures, which will be the primary focus of this work, the TMS (in this context however, as there is no cranium we will refer to it as repetitive magnetic stimulation or RMS) apparatus is placed at an appropriate distance from the slice such that the magnetic flux permeates perpendicular to the cells. In this case, the induced electric field will be parallel to the plane of the slice, and the direction that the induced electric field is pointing in can be accurately aimed merely by rotating the slice or the stimulator.

1.3 Computational Modelling of Neurons

Neurons can be modelled at a variety of levels of complexity. While the seminal work in mathematical modelling of neurons remains the work of Hodgkin and Huxley (Hodgkin and Huxley 1952), a variety of simpler models have been produced in the years since to cover a wide gamut of tradeoffs between detail (and attendant tuning difficulty) and computational performance.

1.3.1 Simplified neuron models

Although the focus of this work will be on more sophisticated models of neurons, simpler models do exist, and see widespread use for network modelling and other situations where computational speed is paramount.

The most common models in this class are so-called "integrate and fire" models. The earliest example of an integrate-and-fire model was the model proposed by Lapicque in 1907 (Abbott 1999). This model is given by the single equation:

$$I(t) = C\frac{dV(t)}{dt} \tag{1.2}$$

with a condition that a delta function spike is applied when the voltage reaches some firing threshold, and a reset to some resting voltage afterwards - hence the name "integrate and fire".

This is a very simple treatment, being a simple derivative of the law of capacitance, since the neural membrane is commonly treated as a capacitor.

In spite of such a model's extreme simplicity, models such as this have use when single cell level fidelity is not important.

The integrate-and-fire model can be further improved with additional perturbations, such as addition of a refractory period to prevent the cell from increasing firing rate without limit as additional current is applied, or addition of leak current terms.

The result of adding a leak term is a popular class of model called a leaky integrate-and-fire model, and can be described by the following equation:

$$C\frac{dV(t)}{dt} = I(t) - \frac{V(t)}{R} \tag{1.3}$$

Here, the membrane is not described as a perfect conductor, and has a finite resistance, which manifests as a "leak" current.

Additional terms can be added to make ever more sophisticated simplified models. The simplified model that we will use for a preliminary investigation in this work is the Izhikevich model, which is in the adaptive exponential class of simplified models, which are able to somewhat accurately reproduce the voltage trace characteristics observed in real cells.

1.3.2 Hodgkin-Huxley formulation and compartmental modelling

The cell membrane is made up of a phosopholipid bilayer, which is selectively permeable to ions by the presence of ion channels. This is modelled as a RC (resistor-capacitor) circuit. Without any active conductance, the passive membrane is given by the circuit shown in Figure 1.6.

In the Hodgkin-Huxley model, the membrane's selective permeability is modelled by breaking the membrane resistance into three components - the sodium, potassium, and leak conductances, as seen in Figure 1.7. In this context, it is generally preferred to visualize in terms of conductance rather than resistance. It is worth noting that the potassium and leak reversal potentials are the opposite sign to the sodium - sodium flows inward while potassium flows outward.

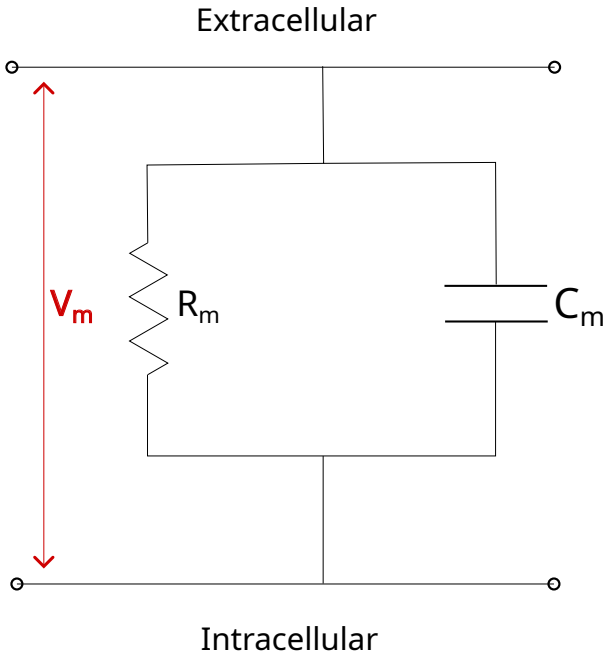

Figure 1.6. Circuit diagram of the passive cell membrane

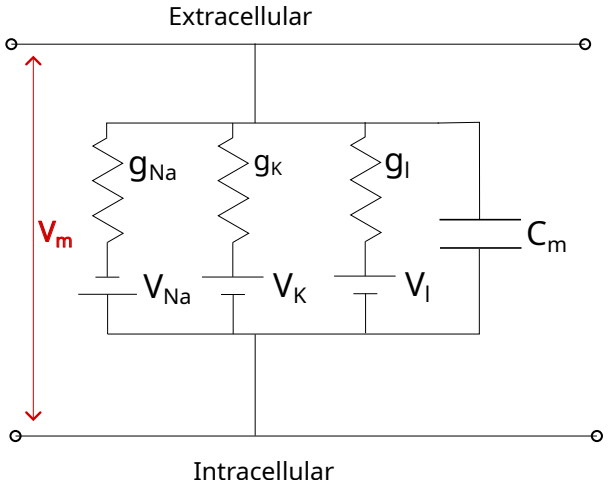

Figure 1.7. Circuit diagram of the Hodgkin-Huxley model of the cell membrane.

The Hodgkin-Huxley model of the membrane, in its original form, is given by the following equations:

$$I = C\frac{dV_m}{dt} + g_K n^4(V - V_K) + g_{Na} m^3 h(V - V_{Na}) + g_l(V - V_l) \tag{1.4}$$

$$\frac{dn}{dt} = \alpha_n(1-n) - \beta_n n \tag{1.5}$$

$$\frac{dm}{dt} = \alpha_m(1-m) - \beta_m m \tag{1.6}$$

$$\frac{dh}{dt} = \alpha_h(1-h) - \beta_h h \tag{1.7}$$

where I is the current, $g_N a$, g_K, and g_l are the sodium, potassium, and leak conductances and C is the membrane capacitance. V is the membrane voltage, defined such that zero is the resting membrane voltage, with the convention that depolarization shifts the membrane voltage in a negative direction. It is worth noting that this sign convention is the opposite of the modern convention, where zero is set as the extracellular voltage, and depolarization shifts the cell towards a more positive voltage.

The rate functions $\alpha_{n,m,h}$ and $\beta_{n,m,h}$ were defined as follows,

$$\alpha_n = \frac{0.01(V+10)}{\exp(\frac{V+10}{10}) - 1} \tag{1.8}$$

$$\alpha_m = \frac{0.1(V+25)}{\exp(\frac{V+25}{10}) - 1} \tag{1.9}$$

$$\alpha_h = 0.07\exp(\frac{V}{20}) \tag{1.10}$$

$$\beta_n = 0.125\exp(\frac{V}{80}) \tag{1.11}$$

$$\beta_m = 4\exp(\frac{V}{18}) \tag{1.12}$$

$$\beta_h = \frac{1}{\exp(\frac{V+30}{10}) + 1} \tag{1.13}$$

, with the constants set such that voltage was in units of mV, current in μA, conductances in mS, capacitance in μF, and time in ms. These values were tuned for the squid giant axon. (Hodgkin and Huxley 1952)

When implemented in the NEURON environment, these constants can be tuned to whatever sort of membrane the user desires. NEURON additionally allows the user to add additional mechanisms such as ion channels and synapses, and is backed by a robust scripting language, and can be programmed in either HOC or Python.

This model is of a single "compartment" - in a multicompartmental model, the membrane is extended such that the membrane can have spatial extent. In a multicompartmental model, the circuit diagram is shown in Figure 1.8, with R_{ax} being the axial resistance between adjacent compartments. With this framework, the Hodgkin-Huxley module can be extended spatially arbitrarily, with as much spatial

complexity as needed.

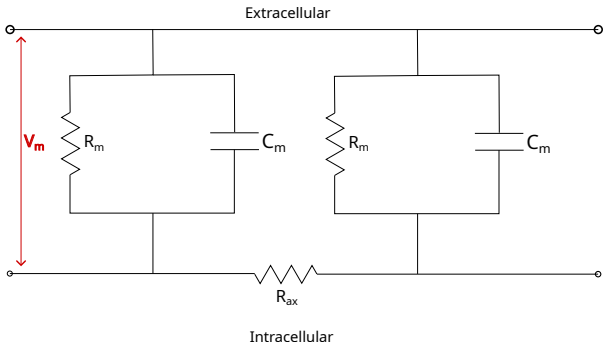

Figure 1.8. Circuit diagram of two compartments in a multicompartmental model of the cell membrane

Compartmental modelling can be further extended to model complex, realistic morphologies of arbitrary detail. This is done by visualising the neuron as a branching tree structure.

1.4 Mechanisms of neuroplasticity

The brain is capable of changing its state over time; this is obvious from the phenomenon of memory and animals' ability to interact with and react with their surroundings. These state changes happen constantly; the brain is in a constant state of flux as an animal gains new experiences. Neuroplasticity is the ability of neural networks within the nervous system to change their activity in response to extrinsic or intrinsic stimuli. Investigating the therapeutic outcomes of brain stimulation techniques thus requires an understanding of mechanisms of neuroplasticity. As there are many types of neuroplasticity, understanding what type is being evoked by a given stimulation type and protocol is of key importance.

While neuroplasticity occurs at all levels of brain organization, of particular interest to us at the cellular level are structural plasticity and synaptic plasticity.

The neuron is a dynamic entity - over the lifespan of the neuron, and indeed, the animal itself, the neuron is capable of structural change - dendrites can grow or retract in response to stimulus (Tavosanis 2012). On a smaller scale, dendritic spines, the typical postsynaptic targets for axon terminals, can change in shape or volume, and can appear or disappear as needed. This sort of change is referred to as structural plasticity. This sort of plasticity is widely assumed to be important for long-term memory. (Lamprecht and J. LeDoux 2004).

Below this level is synaptic plasticity - change in the effective strength of a synapse (expressed as the

amplitude of its excitatory or inhibitory postsynaptic potential). The most important mechanisms of synaptic plasticity are long-term potentiation and long-term depression (LTP or LTD), which are a persistent increase (LTP) or decrease (LTD) in the strength of a synapse.

The overwhelming bulk of excitatory neurons in the mammalian brain use glutamate as a neurotransmitter (Petroff 2002). There are three ionotropic (when activated, they open an ion channel) glutamate receptors, named for chemicals which are their specific agonists. These are the AMPA (α-amino-3-hydroxy-5-methyl-4-isoxazolepropionic acid) receptor, the NMDA (N-methyl-D-aspartate) receptor, and the kainate receptor.

Interplay between NMDA and non-NMDA receptors is responsible for a major component of synaptic plasticity - NMDA-receptor mediated LTP/LTD. Although both NMDA and AMPA receptors are ionotropic, the AMPA receptor is much faster than the NMDA receptor, opening in tens of microseconds and closing in milliseconds, whereas the NMDA receptor opens in milliseconds and closes in tens of milliseconds. This faster response means that the AMPA receptor is able to quickly depolarize the postsynaptic membrane when the synapse is activated.

NMDA receptor trafficking does occur, and could be responsible for some mechanism of LTP and LTD independent of the aforementioned pathway(Lau and Zukin 2007). However, regulation of AMPA receptors by dynamic activation/inactivation and a change in their number remains the primary way that the strength of an individual synapse can be dynamically changed (Song and Huganir 2002), since AMPA receptors remain the primary ionotropic glutamate receptors.

The AMPA receptor contains the GluR1, GluR2, GluR3 and GluR4 (GluR A-D), and is permeable to both Na^+ and K^+ions. The NMDA receptor consists of are comprised of mixes of NR1 and NR2A-D sub-units, and is a permeable to Na^+ and Ca^{2+} ions. The NMDA receptor additionally needs both glycine and glutamate to bind to it to open, with the glycine site needing to be occupied before the glutamate site can be occupied. Some AMPA receptors lack the GluR2 channel, with this change being made after transcription. This subtype of AMPA receptor is also permeable to Ca2+ as well as Na+. However, since hippocampal neurons have high GluR2 levels, the calcium-impermeable AMPA receptor dominates.

The NMDA receptor's permeability to Ca^{2+} is responsible for synaptic plasticity. The NMDA receptor's opening is blocked by a Mg^{2+} ion, which prevents the crossing of ions, even when the receptor is activated by glutamate - the NMDA receptor is inoperable at resting potentials. When the postsynaptic voltage is increased, either by a backpropagating action potential from the soma or from large depolarization from AMPA receptors, the Mg^{2+} ion is expelled, allowing passage of ions.

This allows the NMDA receptor to function as a Hebbian(Hebb 1949) (increase in synaptic strength

when two connected cells are active at the same time) co-incidence detector - for calcium to enter the cell, the NMDA receptor must both be presynaptically activated by glutamate, and the cell must have some level of postsynaptic activity for the blocking Mg^{2+} ion to be removed. (Lüscher and Malenka 2012).

Consistent calcium influx will cause activation of Ca^{2+}/calmodulin-dependent protein kinase II (CaMKII), a protein kinase which is responsible for adding phosphorus to other biomolecules. This will cause, in the immediate term, phosphorylation and activation of dormant AMPA receptors, as well as triggering a second messenger cascade that will eventually cause more AMPA receptors to be sent to the synapse. (Malinow 2003). Phosphorylation of the AMPA receptors happens at the GluR1 subunit; this unit is essential for classical LTP (H.-K. Lee, Takamiya, et al. 2003), and a deficit of the GluR1 subunit leads to impaired memory and reasoning tasks. When the GluR1 subunit phosphorylated, the AMPA receptor's conductance increases (J. Q. Wang et al. 2005).

Conversely, a persistent low level of calcium influx, which would be caused by the activation of AMPA but not NMDA receptors (i.e. presynaptic stimulation of the cell which does not lead to as sustained increase in postsynaptic membrane voltage), triggers a dephosphorylation of AMPA receptors by the activation of protein phosphatases and calcineurin (Isaac 2001), rendering them dormant. Curiously, this is not necessarily the "reverse" process of LTP - the dephosphorylation triggered by this process can occur at different binding sites on the GluR1 subunit (H.-K. Lee, Barbarosie, et al. 2000).

There are additional mechanisms of LTP and LTD at play in the postsynapse - in addition to these ionotropic receptors, there are a variety of metabotropic glutamate receptors which can trigger protein signals which can mediate plasticity on the presynaptic side. (Ebner et al. 2019). Sustained LTP or LTD can also eventually trigger structural plasticity events via gene transcription events in the cell nucleus.

The main putative mechanisms of action for TMS are assumed to be long-term potentiation and long-term depression (LTP and LTD) (Pascual-Leone, Valls-Sole, et al. 1994), and findings that NMDA blockade suppresses the effects of TMS strongly suggest that NMDA-mediated LTP is a primary mechanism of action. (Huang et al. 2007). However, there is still ample room for other forms of neuroplasticity including sub-cellular effects to be implicated as mechanisms of action in TMS. (Chervyakov et al. 2015).

1.5 Models of neuroplasticity

Knowledge of the existence of neuroplasticity predates any understanding of its biochemical and biophysical pathways, and studies of the ways that brains and neurons respond to inputs have been a key topic of interest for as long as there has been study of neuroscience.

1.5.1 Hebbian theory

Although there had been prior work exploring the neurological foundations in memory (Brown, Bligh, and Garden 2021), with the understanding of an engram (Josselyn, Köhler, and Frankland 2017) as a neural correlate for memory, as well as the Pavlovian understanding of conditioning wherein repeating a stimulus/response pairing could lead to a stronger future response to a stimulus, as well as very early work by McDougall (McDougall 1901) identifying the connection between neurons as the seat of memory, the theory of Hebb (Hebb 1949) is considered the early seminal work for a cellular model of neuroplasticity.

Hebbian theory focused on several key observations. Hebb identified a unit of neural processing called a "cell assembly" - that is, a group of cells which together tend to fire in concert during certain processes. In the Hebbian understanding, this cell assembly, which tends to continue firing together after the triggering events, was considered a neural correlate of the engram.

These assemblies were proposed by Hebb to be maintained by what has been termed the "Hebb synapse", which, to directly quote Hebb, can be summarized as follows: "When an axon of cell A is near enough to excite B and repeatedly or persistently takes part in firing it, some growth process or metabolic change takes place in one or both cells such that A's efficiency, as one of the cells firing B, is increased" (Hebb 1949, p.62).

This is often referred to by the shorthand "Neurons that fire together wire together", although it is important to note that under Hebbian theory, for the connection strength to increase, the presynaptic cell must have contributed to the firing of the postsynaptic cell - the theory requires co-operative, not merely coincident, activation.

In computational neuroscience, this is often expressed as a simple learning algorithm called the Hebb rule (Equation 1.14).

$$\frac{dw_{ij}}{dt} \propto x_i x_j \tag{1.14}$$

where w_{ij} is the synaptic weight from neuron j to neuron i, x_i is the activity of neuron i, and x_j is the activity of neuron j.

This activity can be interpreted as either a binary switch (where simultaneous activation of both connected cells leads to a weight increase), or if a larger time window is being considered, the activity can be interpreted as a firing rate.

As a learning algorithm, the Hebb rule is extremely simple - weights can only increase, never decrease, and there is no homeostatic mechanism to prevent continuing increases of weights in strongly connected

pairs of neurons.

This Hebb synapse would later be found to have direct physical existence with the subsequent discovery of long-term potentiation.

1.5.2 BCM theory

Subsequent study of synaptic plasticity moved beyond the initial groundwork laid by Hebb, and worked to explain phenomena which were unexplainable by the Hebb postulate, such as long-term depression, which cannot be explained by Hebbian models alone. One such early theory is BCM theory. BCM theory is named for the authors of the original paper postulating it: Bienenstock, Cooper, and Munro (Bienenstock, L. N. Cooper, and Munro 1982), and is one of the earliest theories of synaptic plasticity.

BCM proposes a threshold level of postsynaptic activity, θ_M, below which LTD will occur, and above which LTP will occur. This modification threshold changes over time based on the overall activity of the neuron. This phenomenon can be referred to as metaplasticity (Abraham 2008).

Under BCM theory, if the cell has a high level of activity, usually expressed as a firing rate over time, the modification threshold will increase, making further LTP more and more difficult, and vice-versa for a low activity cell. This manifests as suppressing plasticity in times of high activity, and facilitating it in times of low activity.

This effect can be seen in an experiment (Kirkwood, Rioult, and Bear 1996), in which the visual cortices of kittens raised in a dark environment were compared to those of kittens raised in a normal environment. The dark-reared kittens showed more potential for plasticity in their visual cortex than those raised in a normal environment, providing credence to the BCM theory - under BCM, the visual cortex neurons of the dark-reared kittens would have a significantly lower modification threshold.

BCM theory can be expressed as the following equations, where y is the postsynaptic activity, w_i is the weight of the ith synapse to the cell, x_i is the presynaptic activity at the ith synapse, $p = 2$, and θ_0 is a scaling constant, and <> is a temporal average:

$$y = \sum_i w_i x_i \tag{1.15}$$

$$\frac{dw_i}{dt} = \phi x_i = y(y - \theta_M)x_i \tag{1.16}$$

$$\theta_M = \theta_0 \langle y^p \rangle \tag{1.17}$$

The weight modification function ϕ for the synaptic weight update is a parabolic function that intersects with the postsynaptic activity axis y at θ_M before ceasing resemblance to a parabola as y increases further

past θ_M (Figure 1.9).

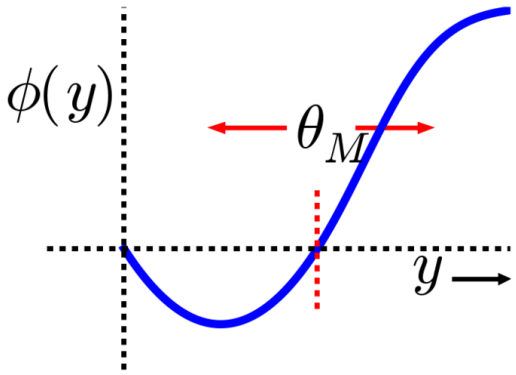

Figure 1.9. BCM modification curve; y is postsynaptic activity, ϕ is the weight modification function, and θ_M is the modification threshold. *Source: Scholarpedia on BCM theory (Blais and L. Cooper 2008), Brian S. Blais and Leon Cooper (2008) BCM theory. Scholarpedia, 3(3):1570; http://www.scholarpedia.org/article/BCM_theory, Creative Commons BY-NC-ND 3.0.*

In an implementation of BCM-inspired plasticity, the dynamically changing threshold acts as a homeostatic limit on synaptic weight - as the weights increase and the cell becomes more active, the BCM threshold will increase, leading the model to favor LTD. This overcomes one of the original problems with the Hebbian theory, in that under Hebbian theory, the weight will forever increase as pairs of connected cells fire more and more frequently from their ever-increasing connection strength.

However, like Hebbian theory, BCM does not consider the precise timing of synaptic events - it is a firing rate based theory.

1.5.3 Spike timing dependent plasticity

STDP, or spike timing dependent plasticity, is a much more recent model of synaptic plasticity (Markram et al. 1997)(Andrade-Talavera, Fisahn, and Rodriguez-Moreno 2023) that proposes a completely different framework than that of BCM. However, the theoretical foundation of STDP is fundamentally Hebbian, as under STOP, co-operative firing between two neurons results in an increase of their connection strength.

Under STDP, it is not the overall rate of activity in the postsynaptic neuron that dictates whether the weight will change, but the relative timing of spikes in the presynaptic and postsynaptic cells (Feldman 2012). If a presynaptic spike occurs before a postsynaptic spike, LTP of the synapse will occur, and LTD

will occur if the postsynaptic spike occurs before the presynaptic spike. If two spikes are simultaneous, there is no effect. This is expressed with the equations (Bi and Poo 1998):

$$\Delta w_+ = A_+ \exp \frac{-x}{\tau_+} \text{ if } x > 0 \tag{1.18}$$

$$\Delta w_- = A_- \exp \frac{x}{\tau_-} \text{ if } x < 0 \tag{1.19}$$

where $W(x)$ is the overall weight change, A_+ is the LTP scaling constant, A_- is the LTD scaling constant, τ_+ and τ_- are the LTP and LTD time constants, and x is the time between a presynaptic and a postsynaptic spike.

This allows for a theoretical framework that can explain the existence of long-term depression without BCM-type metaplasticity. Under STDP theory, synaptic inputs that do not result in activity in the postsynaptic cell result in reduction of those synaptic weights; this explains why low-frequency inputs to cells reduce weights, as these low frequency inputs may not be strong enough to induce postsynaptic firing, and when a spike from another source occurs, depressive post-before-pre spike pairings become more likely.

Spike-timing dependent plasticity has strong experimental backing (Markram et al. 1997)(Bi and Poo 1998), and computer models based on it are well fit to experiment(J. Sjöström and W. Gerstner 2010).

Broadly speaking, STDP-based theories of plasticity fall into a class of theories known as timing-based theories.

Further refinements on the theory have since been made, such as the consideration of triplets, rather than pairs of spikes (Pfister and Wulfram Gerstner 2006) or inclusion of membrane voltage as a contributing factor (P. J. Sjöström, Turrigiano, and Nelson 2001).

1.5.4 Biophysical theories of synaptic plasticity

In contrast to the earlier discussed theories of synaptic plasticity, which consider postsynaptic firing rate or spike timing to determine weight changes, there exist another class of models: biophysical models.

Biophysical models seek to mathematically model the chemical and physical pathways that underlie synaptic plasticity (see Section 3.3). Because there are myriad biochemical pathways involved which may interact in unforeseen ways, even the most detailed biophysical models must necessarily make simplifying assumptions.

The most basic models in this class model calcium influx into the postsynapse as a way of determining the direction and magnitude of any synaptic weight changes. This is well-grounded in experiment (See

Section 3.3, as the NMDA receptor dependent plasticity pathway relies on postsynaptic calcium levels to upregulate or downregulate the amount and efficacy of AMPA receptors. The regulation of synaptic weights by calcium levels is called the calcium control hypothesis, and has been a feature of many theories of synaptic plasticity. Earlier work (Lisman 1989) proposed it as a synthesis of the Hebbian (LTP-like) and anti-Hebbian (LTD-like) models of synaptic plasticity. The calcium control hypothesis thus states that small increases in postsynaptic calcium (as would be seen in post-before-pre LTD pairings in STDP) result in LTD, whereas large increases in postsynaptic calcium (as would be expected from pre-before-post pairings) cause LTP.

One such mathematical model of the calcium control hypothesis is that in the study of Shouval et al. (Shouval, Bear, and L. N. Cooper 2002). In this study, the calcium control hypothesis is formulated as follows in Equation 1.20

$$\dot{W}_j = \eta\Omega([Ca]_j) \tag{1.20}$$

where W_j is the weight of synapse j, η is a learning rate, and Ca_j is the calcium level at synapse j, and Ω is an omega function. This omega function is zero until a first threshold θ_d, after which is is negative, and positive after a subsequent threshold θ_p.

This simple description is subsequently modified with initial terms: a weight decay term is added to prevent indefinite increase in weight, and the learning rate η is modified into a function dependent on postsynaptic calcium, $\eta([Ca]_j)$.

$$\dot{W}_j = \eta([Ca]_j)(\Omega([Ca]_j) - W_j) \tag{1.21}$$

The learning rate function implemented is inversely proportional to a learning time constant, and is a sigmoid function that increases with increasing calcium. This results in a model that is dependent on both the total level of calcium and on the recent history of calcium concentration.

In practice, this model results in a weight modification curve that is very similar to the results predicted by spike timing dependent plasticity.

This model however assumes that NMDA receptors are the only source of postsynaptic calcium, whereas the actual glutamatergic postsynapse contains additional biochemical pathways.

In contrast to STDP theory however, some biophysical models of LTP/LTD predict not one but two windows for LTD, with a second window occurring with some post-before-pre pairings, which would, under the assumptions of STDP theory, trigger only LTP. (Shouval and Kalantzis 2005). This effect has

been observed in some parts of the brain, in seeming contradiction to the STDP hypothesis. (Wittenberg and S. S.-H. Wang 2006). It is very possible that the specifics of calcium-driven plasticity vary by brain location, and that detailed modelling of biophysical pathways may reveal specific differences based on anatomy, cell type, pathway specificity, and chemical kinetics.

Other models (Lisman 1989) model not the calcium level itself, but deeper parts of the NMDA-dependent LTP/LTD pathway - in this case the kinase Ca_{2+}/ calmodulin-dependent protein kinase 2 (CaMKII, see Section 3.3). Some more recent models extend this further, modelling further second messengers with independent variables, with kinases and phosphastases modeled as separate LTP/LTD induction pathways. More recent models (Ebner et al. 2019) model a large array of variables corresponding to various biophysical pathways.

1.6 The hippocampus

Although it is currently infeasible for this region to be targeted for therapeutic applications of TMS in the human brain on account of its depth, the hippocampus remains a popular target for in-vitro experimentation with repetitive magnetic stimulation because there exists a large body of research on plasticity in this region. The focus on the hippocampus as a plasticity target is largely motivated by its key importance in memory transcription, consolidation, and recall.

The hippocampus is a region of the mammalian brain located in the temporal lobe, with one hippocampus in each hemisphere of the brain. The location of the hippocampus in both the primate and rodent brains is shown in Figure 1.10. The hippocampus itself can be divided into six regions – the dentate gyrus, the hilus, which is sometimes referred to as CA4 (Scharfman and Myers 2013), CA3, CA2, CA1, and the subiculum. Some nomenclature also defines CA2 as a region between CA3 and CA1. Adjacent to the hippocampus is the entorhinal cortex (EC), which is also heavily involved in hippocampal processes.

(a)

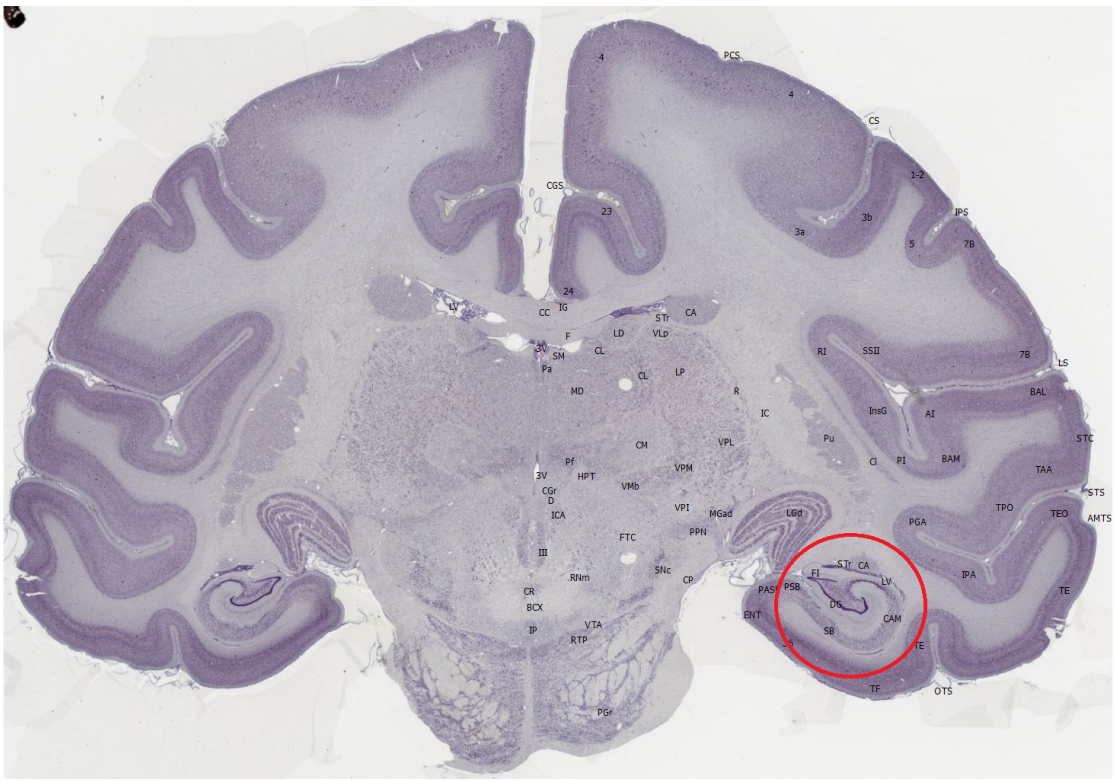

(b)

Figure 1.10. Location of hippocampus in primate and rodent brains. (a): Hippocampus highlighted in Nissl stained coronal section of macaque brain. (b): Hippocampus highlighted in Nissl stained sagittal section of rat brain. *Source: BrainMaps.org; Creative Commons Attribution.*

The hippocampus is located between two cell-free regions, the hippocampal sulcus (which separates the dentate gyrus from region CA1 of the hippocampus) and the fibriodentate sulcus. The hippocampus itself is laminated; starting from the hippocampal sulcus, the most superficial layer is the stratum moleculare, followed by the stratum lacunosum (the stratum moleculare and stratum lacunosum are often considered as one, the stratum lacunosum-moleculare), the stratum radiatum, the stratum lucidum (which is only located in CA3), the stratum pyramidale (which contains the overwhelming bulk of hippocampal cells, with their dendrites extending into the other strata), and the stratum oriens, which is superficial to the alevus, a region of white matter separating the hippocampus from the fibriodentate sulcus.

In the dentate gyrus, the input section of the hippocampus, which is situated across the hippocampal sulcus, the lamination is different – the stratum moleculare is the superficial later, the stratum granulare and the deepest layer, the hilus.

The cells in each section of the hippocampus differ. The bulk of the cells (about 85 percent) are the excitatory glutamatergic principal cells located within the stratum pyramidale and the stratum granulare, and the remaining 15 percent are a variety of GABAergic interneurons, which are much smaller and spread throughout the layers. This is true for all areas of the hippocampus except for the hilus (i.e. CA4), where approximately 50 percent of the cells are inhibitory interneurons (Cutsuridis et al. 2019).

In the dentate gyrus, the principal cells are the small, circular granule cells, which have two highly branched dendrites extending into the stratum moleculare, with their axons extending into the hilus to connect to mossy fiber cells in the hilus via multiple “en passant” synapses.

In regions CA3 and CA1, the principal cells are the pyramidal cells, named for their tapering shape with distinct apex and base. These cells have one apical dendrite and multiple (normally 3 or 4) basal dendrites. The apical dendrite extends in the superficial direction, into the stratum radiatum and stratum lacunosum-moleculare, whereas the basal dendrites extend into the stratum oriens.

The connectivity of the hippocampus can best be visualised as a loop originating in the entorhinal cortex (EC), a region of the brain adjacent to the hippocampus. Activity from layers II and III of the EC is transmitted through the perforant path to all hippocampal subfields, with the neurons in layer II projecting to the DG and CA3, and the neurons in layer III projecting to CA1 and the subiculum.

The DG granule cells then connect to the mossy cells in the region called the hilus, and from there to and CA3 via the mossy fibers, which then in turn connect to CA1 via the Schaffer collateral pathway. Outputs from the CA1 pyramidal cells then connect to the subiculum, with subicular projections in turn connecting to deep layers of the entorhinal cortex.

This connectivity from the EC - DG - CA3 - CA1 is called the trisynaptic circuit (Schematic shown below in Figure 1.11), and is one of the better-studied areas of brain connectivity, having originally been described by Cajal(Andersen 1975; Amaral 1993).

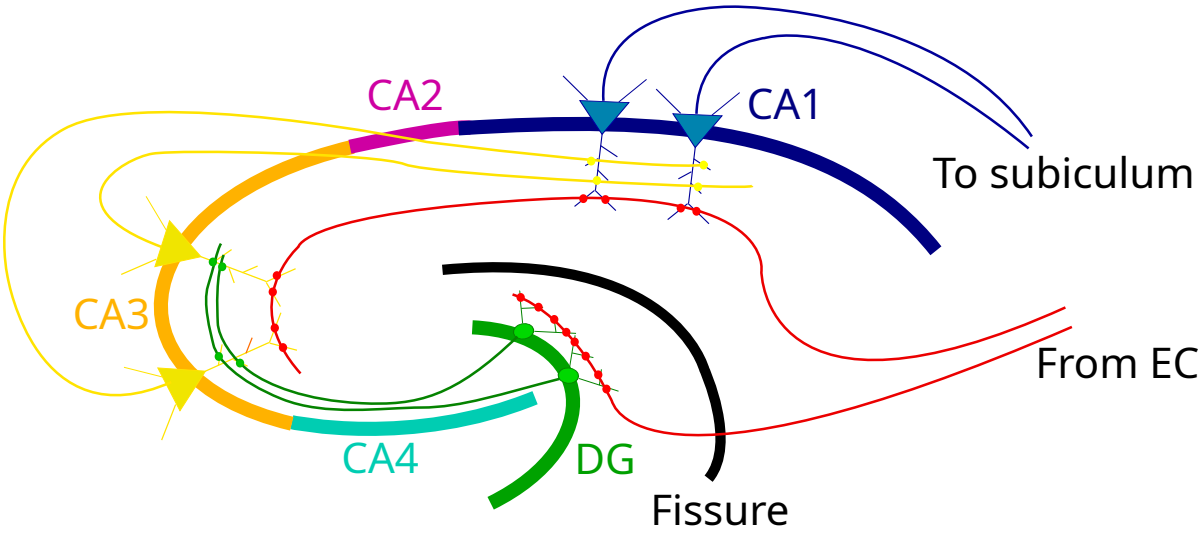

Figure 1.11. Schematic of the hippocampal trisynaptic circuit

There is also significant recurrent connectivity in CA3 and the DG-mossy area (with the CA3 neurons forming significant feedback connections with the DG granule cells) but not in CA1, and each of the hippocampal subfields also receives commissural input from the contralateral hippocampus. In addition to this there are a significant population of inhibitory interneurons which form both feed-forward and feed-back connections in all hippocampal subfields.

1.7 The CA1 pyramidal cell

Region CA1 of the hippocampus is a very common target for plasticity studies in the hippocampus. Like the adjacent CA3 and CA2 regions, the main principal cells of the CA1 region are large pyramidal cells. The CA1 pyramidal cell is a typical pyramidal cell, although smaller than the similar CA3 pyramidal cell (at 25-50 percent of the CA3 cell's surface area), is still somewhat large with a soma diameter of 15 microns.

The CA1 cell has one apical dendrite and several (2-8) basal dendrites, with the apical dendrite being larger in caliber than any of the basal dendrites. The apical dendrite extends into the stratum radiatum towards the stratum moleculare, branching off 9 or 10 times in each layer, ending with a "tuft" in the

stratum lacunosum-moleculare (Spruston, 2008). The basal dendrites bifurcate repeatedly close to the soma, with these branches extending a significant distance.

Each CA1 pyramidal cell has around 30,600 excitatory inputs, 99% of which synapse upon dendritic spines. However, in the stratum lacunosum-moleculare, 17% of excitatory inputs synapse upon the dendritic shafts. No excitatory inputs synapse upon the soma or axon of the cell, where exclusively inhibitory synapses occur (Megıas et al. 2001). In addition to the excitatory inputs, each CA1 pyramidal cell has an average of 1,700 (5.6% of total) inhibitory synapses. These synapses are concentrated close to the soma, with 7% on the soma itself, and 33% on the proximal dendrites. On the distal apical dendrites, 16% of synapses are inhibitory, whereas in the stratum radiatum and stratum oriens, only 4-5% of synapses are inhibitory. Except for in the stratum lacunosum-moleculare, where 10-20% of inhibitory synapses are on spines the remainder of synapses is almost all shaft synapses (Megıas et al. 2001).

The axon of the CA1 pyramidal cell typically emerges from the base of the soma, but may also emerge from the basal dendrites in some cases (Thome et al. 2014). The outputs connect to the fornix (to form commissural inputs on the contralateral hippocampus) and to the subiculum and EC. CA1 pyramidal cells have almost no recurrent connections - only 1% of CA1 outputs connect back to the region.

The CA1 cell has a resting potential between -84mV and -64mV, with its voltage response sagging upon a hyperpolarizing current, and changing to accommodate an action potential upon depolarizing current. These action potentials originate close to the soma and back-propagate into the dendrites in a manner that depends upon the cell's current activity – action potentials later in a spike train may fail to reach distal dendrites.

During a series of successive action potentials, the cell's sodium channels cumulatively inactivate, preventing the cell from undergoing rapid fast firing. Along with this process is a rapid inactivation of potassium currents. The decay rate of this inactivation, however, varies with location. The somatic sodium channels behave in a typical manner, whereas the channels in the dendrites have a stronger cumulative inactivation, with two components that decay in a double-exponential manner with different time constants.

The CA1 cell has multiple types of potassium channels, each mediating a different potassium current – the A current mediated by Kv4 channels, the slow delayed rectifier mediated by Kv1 channels, and the fast delayed rectifier mediated by Kv3 channels. The average respective composition of these three types of channels is 60% Kv4, 27% Kv1 and 12% Kv3, but the specific composition of potassium channels differs by location in the cell.

Calcium-gated potassium channels are unevenly distributed, with the highest density being close to the

soma, the lowest at the distal dendrites. This is in contrast to the A-mediating Kv4 channels, whose density increases with distance from the soma. Meanwhile, the Kv1 channel is only present in the soma.

The CA1 pyramidal cells receive excitatory input from three sources: the Schaffer collaterals (originating in the ipsilateral CA3), the commissural fibres (input from the contralateral CA3 cells), and the entorhinal cortex layer III via the perforant path. Each CA1 pyramidal cell receives input from around 30,600 excitatory synapses.

The Schaffer collaterals are the most significant input to the CA1 pyramidal cells, and along with their commissural fibre counterparts, synapse upon the basal dendrites in the stratum oriens and upon the medial apical dendrite in the stratum radiatum. (Cutsuridis et al. 2019). Input from the entorhinal cortex synapses upon the distal apical dendrite only, in the stratum lacunosum-moleculare (see Fig.4, where we can see LEC axons synapse upon the distal parts of the apical dendrites). The other significant excitatory input to the CA1 pyramidal cells comes from the entorhinal cortex, and synapses upon the distal apical tuft in the stratum lacunosum-moleculare.

1.8 Exploring literature in neuroplasticity induced by TMS

TMS-induced brain activity and TMS-induced plasticity induction by TMS has seen significant investigation experimentally and in theoretical and computational model;ing, with a variety of experiments conducted *in-vivo*, *ex-vivo*, and *in-vitro*. While the focus of this work will be on modelling of *in-vitro* experiments, we will overview a selection of key studies and reviews examining the induction of neuroplasticity by TMS.

Ji et al. 1998

Noting a similarity in therapeutic effects between TMS and ECT, this study(Ji et al. 1998) compares induced neural activity from both TMS and ECS (electroconvulsive stimulation) in rats. This is an *ex-vivo* study; stimulation was applied to the rats' brains while still living, and dissection made 45-60 minutes after stimulation with either TMS or ECS.

Since the actual neuronal spiking cannot be directly observed in an *ex-vivo* study, a proxy for measuring neuronal activity has to be used. The proxy chosen was *C-fos*, a proto-oncogene which is expressed within neurons following depolarization (Bullitt 1990). A radioactive probe method was used to determine levels of C-fos mRNA expression.

The authors found that ECS induced a strong increase in C-fos expression throughout the brain, but concentrated in the hippocampus and neocortex. rTMS, meanwhile, exhibited more selective increases in c-fos expression, with only the frontal and medial cerebral cortex; the hippocampus and parietal cortex showed no difference in c-fos expression from control. In contrast, TMS, induced greater amounts of

c-fos expression than CS in the paraventricular nucleus of the thalamus (PVT) and the suprachiasmic nucleus (SCN). In cortical areas, TMS produced weaker c-fos expression than ECS.

The authors also found that c-fos expression increase in all tested brain regions did not significantly depend on TMS coil orientation relative to the brain.

The authors argue that because TMS and ECS target different areas of the brain in different strengths, although both produce widespread brain activity, they may have different behavioral and therapeutic effects, with TMS's ability to target some areas unaffected by ECS (such as the PVT and SCN) may lead to it having greater efficiency in regulating specific behavior responses.

Nonetheless, TMS inducing widespread brain activity in ways that are similar to ECT without many of the negative side effects of ECT (such as the necessary seizures that ECT causes), provides a reasonable basis for explaining the therapeutic effects of the treatment.

Ziemann et al. 2004

This paper (Ziemann 2004) reviews existing literature on the induction of neuroplastic changes by rTMS focuses in the human motor cortex. In these cases, they are in-vivo measurements made on live patients during TMS treatment.

For the purposes of in-vivo human studies, it is impractical to directly measure synaptic weight changes, or direct proxies thereof. To measure the effect of the treatment, in this case, motor evoked potential (MEP) was measured. The motor-evoked potential (Bestmann and Krakauer 2015) is a measure of the effect of stimulation to the motor cortex. It is measured using an electromyograph on the targeted muscle, and is the size of evoked potential in the target muscle (usually a limb) which is elicited by stimulation to the corresponding area of the motor cortex.

The review observed multiple relationships between rTMS parameters and size of MEPs, both for measurements made during TMS treatment, and for measurements made after the treatment had concluded.

There was an observed relationship between rTMS intensity and MEP amplitude - MEP amplitude increased with TMS intensity in a sigmoid manner, with increases in MEP amplitude leveling off when the TMS intensity was well above the MEP threshold. This is accompanied by a multiple cortico-spinal volley at high TMS intensities. The authors hypothesize that this complex output is mediated by excitatory interneurons that are part of the network between the motor cortex and the target muscles.

For recordings made during TMS treatment, a clear frequency dependence was observed - for low-frequency (1Hz) rTMS, there was no change in MEP amplitude during the treatment, but for higher frequencies (more than 3 Hz), there was an increase in MEP amplitude.

The second set of cases are those observed shortly after rTMS treatment, where changes in MEP

amplitude which outlasted the rTMS train by a few seconds were observed. Here, high-frequency rTMS induced a decrease in MEP amplitude, with the authors noting one study showing an increase in MEP amplitude from very high frequency (50 Hz) rTMS below the MEP threshold.

These two result sets show that the relationship is complex Because the area targeted by TMS includes other cells such as inhibitory interneurons, a complex interplay of effects like disinhibition, short-term plasticity, and metaplasticity can produce varying effects on subtly different timescales.

The review also examined long-term changes induced by rTMS - in this case, MEP amplitude changes which outlast the rTMS stimulus train by minutes or more. In these cases, long pulse trains of more than 150 pulses were used. A consistent frequency dependence was observed - 1 Hz stimulus decreased MEP amplitude, whereas higher-frequency (5-20 Hz) stimulus led to lasting increase in MEP amplitude. In these cases, low-intensity (below MEP threshold) rTMS was less effective or ineffective in changing MEP amplitude, whereas suprathreshold stimulation resulted in changes to MEP amplitude which scaled with the amount of pulses in the rTMS train.

This result resembles classical LTP (see Section 1.4). The authors posit that the mechanisms of longer-lasting MEP amplitude change likely are different to those in the more ephemeral cases, and the cortex is the likely site for these changes to be expressed. This is because other measures of cortical excitability (the spinal short-latency stretch reflex and the trans-cortical long-latency stretch reflex) are also changed when long-lasting MEP change is evoked this way. The authors note that the general consensus is that LTP/LTD are responsible for these changes, however caution that it is not possible to prove that these changes are truly LTP/LTD due to the non-invasive nature of TMS stimulation.

They compare this long-lasting MEP change to LTP by several measures known to associate with cellular-level LTP: cooperativity (caused by activity of both presynaptic and postsynaptic locations), associativity (separate inputs can be potentiated at the same time if they are active at the same time), input specificity, NMDA receptor dependence, and $GABA_A$ disinhibition.

rTMS-induced MEP increase was seen to be cooperative, since blockers of voltage-gated sodium channels prevents MEP amplitude increase. Similarly, associativity was shown using paired pulse protocols to different cortical targets with precisely-timed convergent inputs, with one pulse source weak and the other strong - in this case, the "weak" input target exhibited strong MEP amplitude increase where otherwise it would not. This requires precise timing between the two inputs, applying an LTP-like associative relationship. Similarly, the MEP increases are input-specific; non-targeted areas do not exhibit MEP amplitude increase.

NMDA dependence was observed when the NMDA blocker dextromethorpan prevented changes in MEP amplitude. Involvement of $GABA_A$ dependent inhibition was observed with the $GABA_A$ agonist lore-

sapam, which prevented the induction of MEP increase.

The authors also note that metaplasticity (see Section 1.4 is also important in MEP increase/decrease by TMS, since priming of the cortex by subthreshold stimulus is able to enhance the subsequent MEP depression from low-frequency RMS. Priming of LTP-like MEP amplitude increase was similarly possible with cathodal transcranial direct current stimulation (TDCS).

Taken in whole, the observations made in the Ziemmann et al. review imply strongly that in the living brain, rTMS induces frequency and intensity dependent LTP/LTD, as well as possible other mechanisms such as short-term plasticity for immediate and short term changes from TMS.

Hellmann et al. 2012

The authors of this paper (Hellmann et al. 2012) used cultures human neuroblastoma cells of the SH-SY5Y line to investigate the degree to which second messengers such as cAMP (an important second messenger involved in many synaptic transmission functions including long-term potentiation and depression by activation regulation of the protein kinase A molecular cascade (Horih 1989)). These cells are able to generate action potentials and are used as an in-vitro model of human neuronal biochemical and functional properties.

These cell cultures were exposed to a 600 or 1800-pulse 5 Hz stimulus at maximum stimulation intensity from a TMS coil. The authors found that this stimulus protocol, but not a sham protocol, increased intracellular cAMP levels, as well as levels of phosphorylated CREB (cAMP response element-binding protein), a transcription factor associated with cAMP. Since CREB phosphorylation is known to be increased by antidepressant treatment in mice, the authors implicate the cAMP/CREB pathway as important for the clinical effects of TMS.

Since these second messengers are also associated with LTP, this is also suggestive of LTP's possible key role in causing the clinically relevant effects of rTMS.

Müller-Dahlhous et al. 2013

This review paper (Müller-Dahlhaus and Vlachos 2013) examines theories for the mechanisms that underlie the clinical efficacy of TMS.

First, the authors note a key difference between local electrical stimulation of a neuron (wherein an electrode is placed in a precise layer of the tissue, enabling direct stimulation of a targeted pathway) and TMS: the TMS field is comparatively indiscriminate, and may not only stimulate the axons in the targeted volume, but will also depolarize the neurons in the targeted region itself. This could lead to activation patterns that are very distinct from those induced by local electrical stimulation, the typical mechanism by which plasticity is studied.

The authors note that although axons are the primary targets of TMS, the amount of axons within the target volume that will be activated is unknown, and it is possible that complex effects could be triggered because of the amount of axons that are in a target volume: inhibitory networks and recurrent connections could also be activated, leading to complex spike patterns. Since axonal action potentials will propagate in both directions (both anterograde action potentials and backpropagating action potentials), depolarizing the dendrites of the target neuron as well as activating the presynapses of connections connected to the target axon. Other structures, such as glial cells, mitochondria, intercellular ion stores, transcription factors, and gated ion channels may also be uniquely impacted by the TMS stimulation. This suggests a very wide parameter space, and a large set of unknowns which can be investigated by experimentation and modelling.

The authors note that TMS has been seen to produce LTP-like effects, and present a hypothesis for how these LTP-like effects are induced in neurons. Since LTP can be induced by TMS at relatively low frequencies compared to those required by local electrical stimulation, the authors suggest that TMS causes a highly efficient recruitment of Hebbian-style plasticity mechanisms by the simultaneous activation of both pre and postsynaptic structures during magnetic stimulation, when backpropagating action potentials in the postsynaptic cell occur near-simultaneously with anterograde action potential induced synaptic activity. The authors refer to this as the "bAP-aAP theory", and it is this theory which we will investigate when modelling the induction of plasticity by TMS.

The authors also note that other forms of plasticity aside from LTP-like plasticity induced by TMS. The authors note that some human studies have shown effects of plasticity without changes in cortical excitability, suggesting that some form of metaplasticity may be induced by TMS. One example of this which is specifically mentioned is the possibility of TMS to "prime" the target neural network for further synaptic changes, suggesting the possibility that rTMS can also be used as a neuro-modulation tool.

Finally, the authors note the possibility for induction of structural plasticity by rTMS, wherein the dendrites or axons of target cells could be reshaped, or spine/synapse numbers changed.

Lenz et al. 2015

This study is the one which we will model extensively in this work. In this study, organotypic slice cultures of mouse hippocampi were subjected to 10Hz repetitive magnetic stimulation from a 70mm MagStim figure-of-eight coil placed 1cm above the cultures. The culture was stimulated with 900 magnetic pulses at 10 Hz, with a the pulses grouped in trains of 100, with a 30 second intertrain interval.

The authors observed strong potentiation of the synapses in the dendrites of the proximal stratum radiatum but not the more distal dendrites in the distal stratum radiatum, as shown by a 50 percent

increase in the amplitude of induced miniature excitatory postsynaptic currents (mEPSCs).

This was found to be dependent on several different biophysical pathways - voltage-gated Na^+ channels, L-type Ca^{2+} channels, and NMDA receptors, as chemical blockades of any of these pathways (by TTX for Na^+, nifedipine for L-type Ca^{2+} channels, or D-AP5 for NMDA), resulted in the attenuation of the induced increase in mEPSCs.

This strong dependence upon distance for the magnitude of RMS-induced LTP as well as the dependence on synaptically-involved biophysical mechanisms suggests a co-operative model of RMS-induced plasticity wherein synaptic transmission and postsynaptic depolarization work in concert.

Lenz et al. 2017

This study used a similar experimental setup to the authors' prior study (above), where a 10Hz rMS protocol is applied to hippocampal slice culture. In this study however, they investigated the effect on inhibitory synapses, since E/I (excitation to inhibition) balance is widely assumed to have a regulating effect on brain patterns (Sohal and Rubenstein 2019; Okun and Lampl 2009), and changes in it could be critical in understanding why TMS has a therapeutic effect, since many disorders treatable by TMS (e.g. autism spectrum disorders and some forms of schizophrenia) may be in some way inlfuenced by changes in E/I balance (Yizhar et al. 2011; Rowland et al. 2013; Fritschy 2008).

The authors found that a 900 pulse 10Hz rMS treatment caused a reduction in the amplitude but not frequency of IPSCs (inhibitory postsynaptic currents). In addition to this, cells were stained for gephyrin, a major scaffolding protein for inhibitory postsynaptic terminals. It was found that gephyrin cluster sizes, but not gephyrin expression, decreased after RMS treatment, implying that RMS induced depressive structural plasticity of inhibitory postsynapses.

The decreases in inhibitory strength were found to rely on NMDA receptors, L-type Ca^{2+} and voltage-gated Na^+ receptor activation (as, similar to the excitatory experiment, the plasticity was blocked by application of TTX or nifedipine), implying a deeper interplay between both excitatory and inhibitory plasticity pathways in response to magnetic stimulation.

This plasticity was also location-dependent: it was found that inhibitory synapses targeting the soma did not express a reduction in gephyrin cluster size, while those targeting the dendrites expressed said reduction.

Combined with the earlier work in (Lenz, Platschek, et al. 2015), this implies that the overall increase in overall cell firing rate induced by TMS is likely caused by a combination of increase in glutamatergic transmission and a decrease in GABAergic transmission.

King et al. 2022 This review (King and Tang 2022) investigates the induction of intrinsic plasticity (see

Section 3.3 by transcranial magnetic stimulation. Noting that most prior work on plasticity induction from transcranial magnetic stimulation had been focused at the synapse level, the authors identify several intrinsic properties that could be implicated in explaining changes in cell excitability in response to TMS.

The three investigated modifications of intrinsic properties are as follows. Firstly, attenuation of dendritic action potentials, which can be modulated by changes in the balance of active sodium and potassium channels, as well as amplification of postsynaptic potential propagation by deactivation of HCN channels, and vice versa. Secondly, adjustments to the resting membrane potential, which can be changed by upregulation or downregulation of the HCN channels, shown to occur in motor learning in rodents (Kida et al. 2016). Finally, alterations to the action potential threshold, i.e. the voltage at which the cell generates action potentials, which is typically adjusted by regulation of the voltage-gated sodium and potassium channels, as well as morphological changes in the axon initial segment.

The authors cite a study (Tang et al. 2016) wherein application of subthreshold intermittent TBS (iTBS) to layer 5 of the cortex of mice produced an increase in the excitability of the target neurons. There was no observed change to the resting membrane potential or input resistance, however the rate of firing frequency in response to current injections increased, and the action potential threshold decreased. In this study, the authors presume that this change came from a change in the voltage gating properties of the voltage-gated sodium channels in the axon initial segment. The change in firing frequency was thought to result from changes in the kinetics of voltage-gated potassium channels.

Chapter 2

Materials and methods

2.1 Neuron modelling

2.1.1 Point neuron modelling

In our simulations here, we started with a simple approximation of a neuron – the Izhikevich spiking neuron model (Izhikevich 2003). This is a single-compartment model - it has only one voltage measure.

Within the family of single-compartment models, the Izhikevich model is intermediate in complexity. Unlike simpler integrate-and-fire models, it features a richer mathematical description of the spike - in an integrate-and-fire model, the dynamics of the cell during the action potential are not part of the model (Burkitt 2006).

The Izkhekevich model was derived from using bifurcation analysis to reduce the parameters of the Hodgkin-Huxley model to a pair of coupled differential equations, as follows:

$$v' = 0.04v^2 + 5v + 140 - u + I \tag{2.1}$$

$$u' = a(bv - u) \tag{2.2}$$

with a reset condition which engages after the cell generates a spike,

$$\text{if } v \geq 30\text{mV, then} \begin{cases} v \leftarrow c \\ u \leftarrow u + d \end{cases} \tag{2.3}$$

In this model, v represents the voltage, u is a recovery variable, and a, b, c, and d are parameters

which specify the behavior of the cell, which can be tuned to a variety of cell types. All parameters are dimensionless, but the constants of the equations are tuned such that voltage has a scale of millivolts and time has a scale of milliseconds.

To simulate the CA1 pyramidal cell, we use Izhikevich's parameter set for an intrinsic-bursting cell, which is $a, b, c, d = 0.02, 0.2, -55, 4$.

2.1.2 Multicompartmental modelling

For more detailed treatment of the cell we are modelling, we use the NEURON simulation framework (Carnevale 2007), which implements the Hodgkin-Huxley (Hodgkin and Huxley 1952) model of the cell membrane in an extensible software environment. Although these equations were originally developed specifically for the squid giant axon, they remain the core of the overwhelming bulk of cell modelling in modern computational neuroscience.

When additional mechanisms are added in NEURON, such as additional ion channels, they are implemented as parallel-connected conductances alongside the three base conductances contained in the Hodgkin-Huxley model. Such additional mechanisms consist of things like voltage-gated channels (for example, different types of voltage-gated Na^+, K^+, Cl^- or Ca^{2+} channels), which, after a certain voltage threshold is reached, depolarize or hyperpolarize the membrane in the direction of their reversal potential.

With spatial extent, current is able to propagate across the membrane. The propagation of current across a neurite then comes to resemble the propagation of an electrical signal across a cable, so the theory within neuroscience governing such transmission is known as cable theory.

In the case of sodium and potassium channels, these reversal potentials correspond to those in Equation 1.4, where V_{Na} and V_K are the sodium and potassium reversal potentials respectively. Typical values for the reversal potentials might be $V_{Na} = 55mV$ and $V_K = -82mV$ (Kole et al. 2008; Bekkers 2000). These values may differ for individual mechanisms; a cell model might well include multiple different kinds of sodium and potassium channels with different behavior.

The reversal potential of the passive properties of the cell, as well as that of active channels which are active close to the resting potential, will dictate the resting potential of the cell, and this varies by cell type, even within the same anatomical area (Moradi Chameh et al. 2021).

A voltage-gated channel also has a threshold voltage - below this voltage the channel will not be active, and its conductance will be effectively zero. For Na^+ channels, when this threshold voltage (on the order of -55 mV) is crossed, the conductance will be nonzero, and there will be a simulated inward current (towards the positive reversal potential) which leads the cell to initiate (or sustain via active

conductance in the case of dendrites) an action potential. Similarly, voltage-gated potassium channels have a negative reversal potential, and their activation (usually at a higher threshold than sodium channels, and activated by action potentials) will terminate spikes and hyperpolarize the membrane.

Other channels can have different dynamics. For example, the HCN (Hyperpolarization-activated cyclic nucleotide–gated) channel, usually called I_h, (Benarroch 2013), activates only below a highly hyperpolarized (for example, -80 mV) voltage and has a somewhat depolarized reversal potential of around -30 mV (Kase and Imoto 2012), which pushes the cell towards action potential activation when active. Calcium channels can interact with additional calcium accumulation mechanisms, and also have positive reversal potentails, which can generate calcium-driven spikes, as is important in some classes of cell, such as human cortical cells (Hay et al. 2011). Similarly, Cl^- channels hyperpolarize the cell, with typical reversal potentials on the order of -70 mV (A. P. Morris 1999). A model can combine a great many different kinds of channel, with varying parameters and channel kinetics, to produce as complicated or as simple a model of the cell as the modeller wishes.

2.2 NeMo-TMS

For more sophisticated modelling of TMS's effect on brain tissue, we developed the NeMo-TMS (Neuron Modelling for TMS) toolbox (Sina Shirinpour et al. 2021). This toolbox integrates whole-head scale modelling of the TMS-induced electric field with single cell and sub-cellular modelling of neuronal dynamics. The NEURON framework is used for the single-cell modelling part of the toolbox.

The NeMo-TMS toolbox consists of five different modelling stages: neuron reconstruction, electric field modelling, coupling of the electric field to the neuron reconstruction, membrane voltage simulation, and calcium diffusion calculation.

2.2.1 Neuron reconstruction

To provide NeMo-TMS with a library or realistic neurons, cells taken from slice culture were reconstructed. To accomplish this, a cell is identified in the slice culture with a microscope. The cells are patched for electrophysiology recordings, and subsequently, a fluorescent dye is added to the patch solution. Confocal microscropy is then used to acquire images at multiple z-axis levels to produce a three-dimensional image stack.

Subsequently, using the Neurolucida 360 software, the shape of the neurons, including the complex axonal and dendritic branching, is manually traced. This produces a Neurolucida .ASC file, which is imported into the TREES Toolbox (Cuntz, Forstner, et al. 2010) for further processing. In the TREES toolbox, the neuron becomes visualized as a binary tree with neurites represented as cylindrical segments

with varying diameter.

TREES Toolbox allows the viewing, manipulation, and editing of neuron morphologies, as well as the subsequent export to formats which can be used by other simulation frameworks. In our case, we saved all morphologies as .SWC files after they have been processed for purpose.

Once imported to the TREES Toolbox, a quadratic diameter taper is applied to the dendrites of the cell, since fluorescence effects can lead to overestimation of dendritic diameter (Cuntz, Borst, and Segev 2007). Parameters for the quadratic taper are taken from (Lenz, Platschek, et al. 2015).

Additionally, because abrupt changes in neurite direction can cause unrealistic voltage spikes under TMS stimulation, wherein transient changes in membrane voltage induce anomalous spikes, the cell's dendritic and axonal arbor is smoothed. This is accomplished using the Laplacian smooth function of ProMesh 4. This is also a factor even absent explicit simulated TMS; in large, highly branched axons with many areas of high Na^+ channel density, without smoothing, the cell can spike spontaneously and remain depolarized indefinitely without any input at all. This effect could not be completely eliminated in all morphology combinations; in cases where a zero firing threshold exists, the simulation run is removed from the analysis.

As the axon reconstructions do not include myelination, a simple myelination algorithm is applied to the axons. Nodes of Ranvier are placed at every bifurcation point of the axonal morphology, as well at regular $100\mu m$ intervals. All internodal segments are myelinated, with a fixed thickness of 1.5 μm. The final 5 μm of each branch are left unmyelinated as axon terminals. Additionally, there is an unmyelinated axon initial segment and axon hillock where the axon connects to the soma.

2.3 Neuron model generation

The T2N extension to TREES Toolbox is used to generate the neuron models for NeMo-TMS. This extension provides an interface between the NEURON simulation environment and TREES Toolbox by translating the TREES Toolbox's morphological data into the NEURON HOC format. NeMo-TMS's models of the CA1 pyramidal cell use a generalized version of the Jarsky (Jarsky et al. 2005) model of the CA1 pyramidal cell. In addition to the dendritic parameters of that model, we additionally model the myelin as having a significantly reduced membrane capacitance of $0.01\mu Fcm^{-2}$, and tune other axonal parameters to spike in response to TMS in a large, branching axon (see Section 2.5.1). Additionally, to facilitate the modelling of TMS-induced electric fields, a variable extracellular potential is added to every compartment of the model.

For cortical simulation, we also implement two of the Aberra (Aman S. Aberra, Angel V. Peterchev, and Grill. 2018) models into NeMo-TMS. These are the human-inspired layer 2/3 and layer 5 models.

Since these models are tuned directly to their morphology, the myelination and morphological editing steps are bypassed, preserving their original characteristics.

2.3.1 FEM modelling of electric fields.

At the most macroscopic level, the electric field's spatio-temporal distribution is computed. The spatial and temporal components of the electric field are considered separately under the quasi-static approximation. With this approximation, we consider the time course of the TMS electric field to match the time course of the coil current output of the TMS stimulation equipment.

The spatial component, meanwhile, is computed using the finite element model (FEM) modelling of the electric field in the SimNIBS (Simulation of Non-Invasive Brain Stimulation) simulation software. (Saturnino, Madsen, and Thielscher 2019). This software computes the electric field induced by an external stimulator at all points within a provided head model, for a variety of possible coils.

This computed spatial component is then scaled by the amplitude of the TMS waveform at the given time point. In NeMo-TMS, two different stimulation waveforms - one monophasic and one biphasic - are used, based on recordings of the output of a TMS machine (MagPro X100 with a MCF-B70 figure-of-8 coil) in a prior study (Aman S Aberra et al. 2020). An arbitrary amount of these pulses can be combined to simulate any desired stimulation protocol, and can be scaled in amplitude to simulate differing stimulation intensities. Both of the pulse types used in NeMo-TMS are shown below in Figure 2.1.

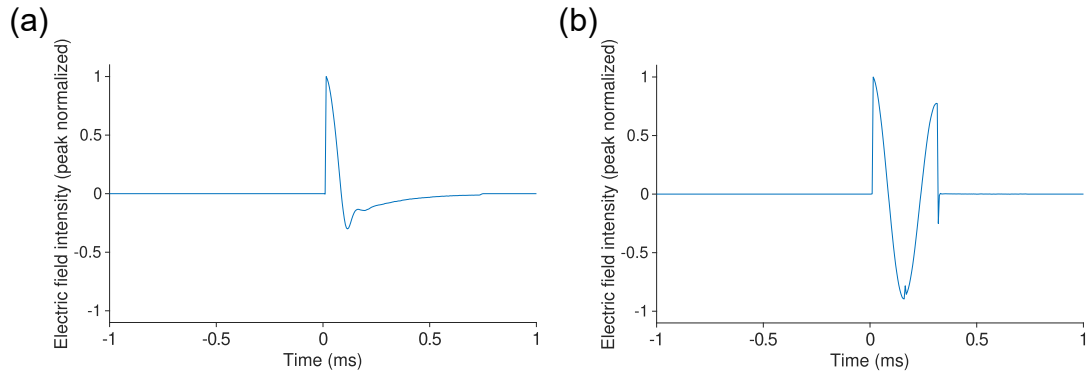

Figure 2.1. Temporal profile of both pulse types used in NeMo-TMS. *(a)*: Monophasic pulse. *(b)*: Biphasic pulse.

2.3.2 Coupling of electric field to neuron model

After the electric field is modeled as a spatial set of quasipotentials, it is coupled to the neuron model by means of an extracellular potential. This is implemented by the external membrane surface exhibiting a nonzero potential when the input electric field is nonzero.

NeMo-TMS has two options for how this is implemented; for simulations in which the electric field is considered to be spatially homogeneous (such as modelling cells in slice culture where the electric field is perpendicular to the axis of the slice), the capacity exists to model the electric field as a uniform external field of given intensity and direction, where intensity is specified as a fixed value in volts per meter, which scales the direction vector, and direction is a vector either specified as a Cartesian $[x, y, z]$ triplet, or as a polar and azimuthal angle θ and ϕ. When a more fine-grained approach is required, NeMo-TMS has a procedure for generating quasipotential files.

To accomplish this, after model generation, the toolbox has a utility which will export every neuron compartment's position in 3D space to a file. The user then specifies at what location in the simulated volume the neuron is located, and this is combined with the FEM simulations of the electric field over the simulated volume to generate electric field information for every compartment within the neuron model. This information is then supplied to NEURON, which will convert this quasipotential data into extracellular potentials for every cellular compartment in the final simulation. When the simulation is launched, each compartment's quasipotential value will be multiplied by the current scaled time value of the electric field, as shown in Figure 2.1.

2.3.3 Calcium modelling

NeMo-TMS contains a calcium modelling tool which simulates the influx of Ca^{2+} ions into the cell via voltage-gated calcium channels, and their diffusion along the membrane by reaction-diffusion methods. Since calcium modelling is usually simplified in NEURON models, a more realistic model of calcium influx and diffusion can provide insight into this important subcellular mechanism.

When the quasipotentials have been computed and the full length of the NEURON simulation has been run, a voltage trace for every location within the cell will be generated. This is combined with the locations file generated earlier, and a MATLAB script will use these in conjuction with the NeuroBox(Breit et al. 2016) simulation toolkit, which models electrical and biochemical signaling. Necessary parameters are set by default.

2.4 Plasticity modelling

To model synaptic plasticity, we choose two approaches: one for the modelling using the Izhikevich model, and one as an inclusion on top of the already robust capabilities of the NeMo-TMS toolbox.

2.4.1 mSTDP model

The model of plasticity that was used for simulations using the Izhikevich model is the mSTDP model (Benuskova and Abraham 2007), which is a synthesis of two differing theories of synaptic plasticity: BCM theory and spike timing dependent plasticity.

Both STDP and BCM theory provide alternative views of how the weight can change as a response to input, and it is possible to reconcile both into a single model. The mSTDP (metaplastic STDP) model of Benuskova and Abraham (Benuskova and Abraham 2007) accomplishes this by modifying A_+ and A_- in the classical STDP equation according to an average of the cell's activity.

Where $\langle c(t) \rangle$ is an average of recent postsynaptic activity (the length of time that is considered here functioning as a sliding window), the STDP amplitudes A_+ and A_- are modified as follows:

$$A_+(t) = \frac{A_+(0)}{\langle c(t) \rangle} \tag{2.4}$$

$$A_-(t) = A_-(0)\langle c(t) \rangle \tag{2.5}$$

The average of postsynaptic activity is calculated as follows:

$$\langle c(t) \rangle = \frac{c_0}{\tau_M} \int_{-\infty}^{t} c(t') \exp\left(\frac{-(t-t')}{\tau_M} \right) dt' \tag{2.6}$$

with scaling constants c_0 and τ_M, and c a postsynaptic spike count.

2.4.2 Four-pathway synaptic model

Because TMS induces voltage perturbations in all points of the cell, which may cause effects that activity-based models like STDP or BCM may not capture, we implemented a voltage-based model when adding plasticity to NeMo-TMS. We chose the Ebner (Ebner et al. 2019) model, which is a rich phenomenological simulation of the biophysics involved in NMDA receptor mediated LTP/LTD.

The model is an integrated synaptic and plasticity model - the synapse modelled is a combined NMDA/AMPA synapse with independent kinetics for each channel; AMPA currents have a 0.2ms rise time and 2ms decay time, while NMDA currents have 2ms rise time and 50ms decay time.

The four-pathway model models four pathways of synaptic plasticity - postsynaptic LTP, postsynaptic LTD, presynaptic LTP, and presynaptic LTD.

In the model, presynaptic LTD is presumed to arise from simultaneous activation of metabotropic gluatamate receptors and postsynaptic Ca^{2+} channels, synthesizing endocannabinoids which retrograde activate type-1 cannabinoid receptors in the presynaptic axon terminal, reducing synaptic strength. Presynaptic LTP is presumed to occur when postsynaptic L-type Ca^{2+} receptors are activated, triggering synthesis of nitric oxide, which acts retrogradely on presynaptic synapses involving a yet-unknown presynaptic coincidence detector.

Postsynaptic LTP and LTD are classical NMDA-receptor mediated LTP and LTD, with strong NMDA-driven Ca^{2+} influx activating protein kinases leading to activation of AMPA receptors, and correspondingly weak Ca^{2+} influx triggering phosphatases which decrease synapse efficacy.

Each of these biophysical processes is modeled by a variable within the model. In the case of postsynaptic plasticity, there is a presynaptic signal variable G which is multiplied by the difference of the membrane voltage and an activation threshold to generate C, which represents postsynaptic calcium levels.

If C is high, the variable K will increase based on how far above a threshold C is, corresponding to kinases. Postsynaptic LTP is calculated based on K.

Similarly, if C is low, the variable P, corresponding to phosphatases, will be elevated based on how far beneath C is the postsynaptic LTD threshold, and the variable P is used to directly calculate postsynaptic LTD.

Presynaptic LTP and LTD are handled similarly but with different trace variables. If the trace variable N, which is based on membrane voltage, is coincident with a presynaptic trace Z, the variable X is activated, representing the putative presynaptic coincidence detector. Presynaptic LTD is calculated based on the value of X. Coincidence between a presynaptic signal variable D and a membrane voltage based signal T elevates the variable E, which represents endocannabinoid synthesis, and is used to calculate the amount of presynaptic LTD.

The connections between the various model variables are shown in Figure 2.2.

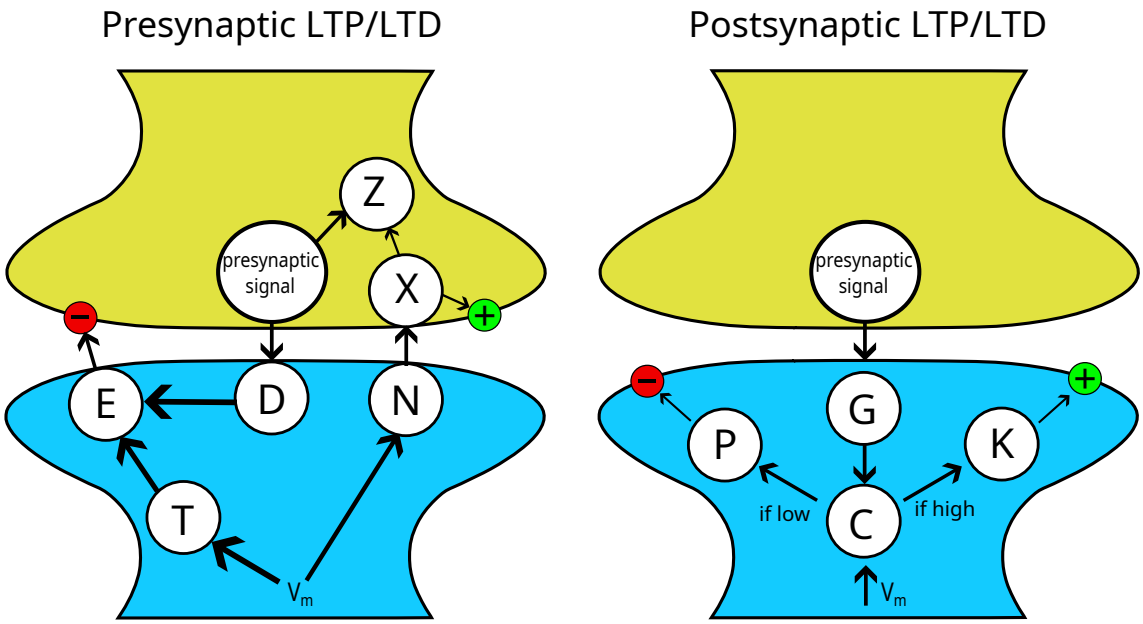

Figure 2.2. Simplified schematic of internal variables in the four-pathway plasticity model. See text in Section 2.4.2 for further details and explanation of variables.

At every time step, the synaptic weights are modified by these four separately calculated plasticity pathways. Each variable has independent activation voltages and independent decay dynamics, leading to every plasticity pathway behaving differently as membrane voltage evolves. These variables can be tuned to model relative dominance of the different LTP/LTD pathways. Additionally, all plastic changes are scaled by four amplitude variables, which enable fine-grained tuning of the plasticity model to match data. However, this does mean that there is a very large parameter space in the model - there are over 20 free parameters. The values chosen for these parameters are shown below in Table 1.

Parameter	Definition	Value	Parameter	Definition	Value
W_{MIN}	Min. weight scale factor	0.22	M_T	T saturation function slope	1.7
W_{MAX}	Max. weight scale factor	0.44	θ_U^N (mV)	u to N voltage threshold	-55
τ^A (ms)	AMPA current rise time	0.2	τ_Z^A (ms)	Z function rise time	1
τ^B (ms)	AMPA current decay time	2	τ_Z^B (ms)	Z function decay time	15
e_{Na} (mV)	Reversal potential	0	M_Z	Z saturation function slope	6
S_{AMPA}	AMPA current contribution	0.5	$\tau_{N\alpha}$ (ms)	N_α time constant	7.5
S_{NMDA}	NMDA current contribution	0.5	$\tau_{N\beta}$ (ms)	N_β time constant	20
τ_G^A (ms)	NMDA current rise time and G rise time constant	2	$M_{N\alpha}$	N_α saturation function slope	2
τ_G^B (ms)	NMDA current decay time and G decay time constant	50	$M_{N\beta}$	N_β saturation function slope	10
W_{pre}^{init}	Initial presynaptic weight	0.5	θ_N^X	N to X activation threshold	0.3
W_{post}^{init}	Initial postsynaptic weight	2.0	θ_u^C (mV)	u to C voltage threshold	-63.5
M_G	G saturation function slope	10	θ_C^-	Postsynaptic LTD threshold	8.0
A_{pre}^+	Scaling factor on presynaptic LTP amplitude	1.4e-5	θ_C^+	Postsynaptic LTP threshold	8.2
A_{pre}^-	Scaling factor on presynaptic LTD amplitude	2.25e-5	$\tau_{K\alpha}$ (ms)	K_α time constant	10
A_{post}^+	Scaling factor on presynaptic LTP amplitude	1.6e-2	$\tau_{K\gamma}$ (ms)	K_γ time constant	25
A_{post}^-	Scaling factor on presynaptic LTD amplitude	45e-5	$M_{K\alpha}$	K_α saturation function slope	1.5
τ_u^T (ms)	Filtering constant from u to T	10	$M_{K\beta}$	K_β saturation function slope	1.7
θ_u^T (mV)	u to T voltage threshold	-60	$S_{K\beta}$	K_β scale factor	100

Table 1. Parameters chosen for the Ebner four-pathway plasticity model for our plasticity simulations.

2.5 Neuron models

In this work, we will use several different compartmental models of neurons. Of particular note are the Jarsky (Jarsky et al. 2005) model, which with NeMo-TMS is generalized to arbitrary morphologies of pyramidal cell, and the Tomko (Tomko, Benuskova, and Jedlicka. 2021) reduced model of the CA1 pyramidal cell.

Both models are implemented in NeMo-TMS using the T2N(Beining et al. 2017) interface between

TREES Toolbox (Cuntz, Forstner, et al. 2011) and NEURON.

2.5.1 Jarsky model

The Jarsky model of the CA1 pyramidal cell was originally used to study propagation of postsynaptic potentials from the distal tuft synapses of the cell to the soma via enhancement from dendritic events in the apical dendrite (Jarsky et al. 2005). It is a somewhat simple model, only having four ion channels ($Na^{\cdot}$ K_{DR}, and two varieties of K_A. It does not feature any calcium channels or hyperpolarizing (I_h or HCN channel) current (Benarroch 2013), both of which are known to exist in the dendrites of the CA1 pyramidal cell (Westenbroek, Ahlijanian, and Catterall 1990; Magee 1998).

However, its simplicity makes it useful as a generalizable model. It has since seen use as a more general model of the CA1 pyramidal cell because of its combination of simplicity and varied dendritic ion channel properties (Mittag et al. 2023).

The Jarsky model features for its A-type potassium channels (it has two types of A-type potassium current; one for proximal locations and one for distal) variable channel properties based on the dendritic locations within the cell, with certain channels present or absent based on location, and some of varying strength based on distance from the soma.

We implemented a generalizable modification of a weakly propagating Jarsky model with a custom axon into NeMo-TMS. An additional variant exists; the strongly propagating variant; in this case, dendritic Na^+ conductance increases with distance from the soma. We do not implement this version. The channels and passive properties for the dendrites and soma are shown below in Table 2. Note that in the Slope calculation, M refers to the maximum dendritic path length in a cell region.

Property	**Soma**	**Proximal apical**	**Apical**	**Tuft**	**Basal**
Na (S/cm^2)	0.04 everywhere				
$K_A(prox)$ (S/cm^2)	0.048	Variable	0	0	0.048
$K_A(dist)$ (S/cm^2)	0	0	Variable	0.048	0
K_{DR} (S/cm^2)	0.04 everywhere				
C_M $(\mu F/cm^2)$	0.75 everywhere				
R_A $(\Omega \cdot cm)$	200 everywhere				
g_{pas} (S/cm^2)	2.5e-5 everywhere				
e_{pas} (mV)	-60 everywhere				

Variable property	**Equation; d is distance from soma in μm**
Slope	$\frac{6*K_A(base)-K_A(base)}{K_A(base)*M}$
$K_A(prox/dist)$ (S/cm^2)	$K_A(base)(1+d*Slope)$

Table 2. Dendritic and somatic properties of the weakly propagating variant of the Jarsky model.

We use a different axon than the default Jarsky model; the default Jarsky axonal parameters, especially the very high Na^+ conductance in the nodes and lowered K_A in the axon lead to some cell morphologies spiking without input because of transient currents in the axonal tree, or not responding at all to TMS stimulation. This is likely because the original model was designed with a short, somewhat morphologically simple axon; the large, branched axons in our reconstructions naturally have different characteristics (including, especially in highly branched axons, a much greater amount of nodes of Ranvier).

To rectify this, we tuned the axon to not spike spontaneously in any of our morphologies, and to consistently produce spikes in response to TMS pulses. To do this, we reduced the Na^+ conductance in the axonal nodes by half, removed the scaling factor on axonal K_A to make it equal to the proximal dendrites, reduced the membrane capacitance, and added the default higher Na^+ conductance to the axon initial segment, as in real cells this is the site of the action potential (Kole et al. 2008). A listing of the properties of the myelinated axon is shown below in Table 3.

Property	**Initial segment**	**Myelinated**	**Nodes**	**Unmyelinated**
Na (S/cm^2)	15	0.04	15	15
$K_A(prox)$ (S/cm^2)	0.048 everywhere			
K_{DR} (S/cm^2)	0.04 everywhere			
C_M $(\mu F/cm^2)$	0.75	0.01	0.75	0.75
R_A $(\Omega \cdot cm)$	200	200	100	200
g_{pas} (S/cm^2)	2.5e-5 everywhere			
e_{pas} (mV)	-60 everywhere			

Table 3. Properties of the custom myelinated axon implemented alongside the Jarsky soma and dendrites.

2.5.2 Morphologically reduced model of CA1 pyramidal cell

Synaptic plasticity experiments are often relatively long (a 1 Hz 900-pulse protocol takes 900 seconds, which can correspond to a large amount of computer time when simulated), and synaptic plasticity models have many parameters and will require substantial amounts of manual tuning. At the same time, however, since we intended to study the location-specific aspects of synaptic plasticity in the dendritic tree of the CA1 cell, fidelity to the cell's various properties was a necessity too. To balance these two factors, we implemented a well-validated model of the CA1 pyramidal cell with simplified but extensive morphology, and a diverse set of channels (including important ones which the Jarsky model lacks like the HCN channel and calcium channels 2.5.1).

This model (Tomko, Benuskova, and Jedlicka. 2021) has a significantly simplified morphology, replacing the complicated branching structure of a typical realistic neuron with a "reduced" morphology that nonetheless retains key features of the CA1 pyramidal cell, such as its thick apical trunk, branching basal dendrites, distal tuft, and oblique apical dendrites. A schematic of the morphology is shown below in Figure 2.3.

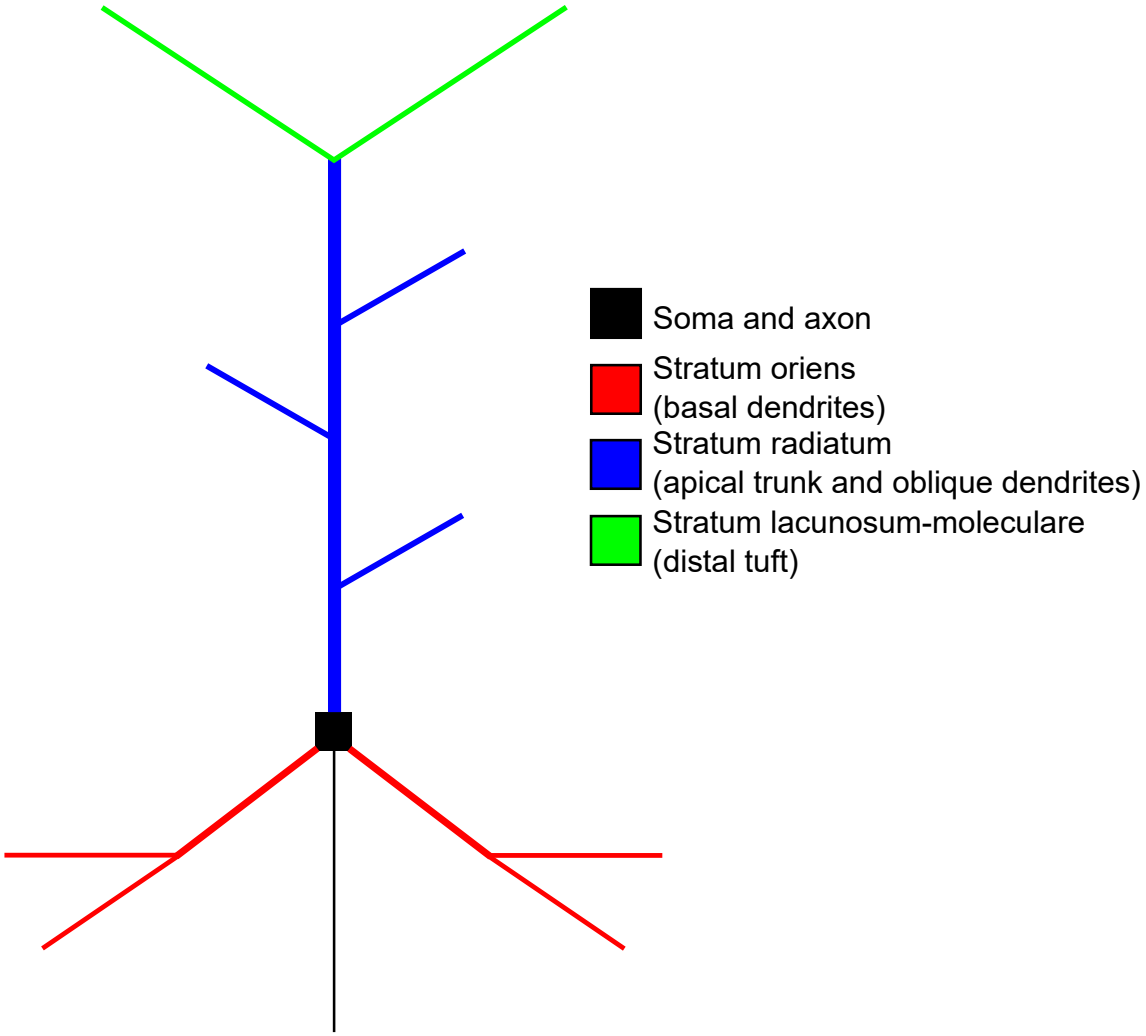

Figure 2.3. Schematic of the morphologically reduced model of the CA1 pyramidal cell. Colors indicate various model regions, and will be used to color code specific stimulation regions in Results. Distances and sizes not to scale.

One important feature of this model that sets it apart from many other models of specific neurons is that it is well-validated to produce electrophysiologically realistic output. The model was validated against the HippoUnit test battery (Sáray et al. 2021), which contains five different tests which compare the cell's output against recorded experimental values from real hippocampal cells.

The five tests present in the HippoUnit battery are as follows:

Somatic features test: The somatic features test examines both subthreshold (non-spiking) and suprathreshold (spiking) features from voltage traces recorded from a range of current injections. These features include action potential shape (e.g. its width, rise and fall rate, amplitude), and dynamic features such

as frequency and interspike interval under a sustained current injection, and from a negative current injection, subthreshold features such as voltage deflection and sag amplitude.

Depolarization block test: Depolarization block is a phenomenon wherein in response to a sustained large current injection, the cell will enter a state where it stops firing and settles on an elevated equilibrium voltage (Bianchi, Marasco, et al. 2012). The test checks the threshold current before depolarization block is entered, the maximum number of action potentials before it is entered, and the equilibrium voltage.

Backpropagating action potential test: This test generates action potentials at the soma with current injections, and examines how much they have attenuated at various distances along the apical trunk by measuring their amplitude at set points in the apical dendrite. The model we have implemented is a weakly propagating model, however the test does have alternatives here for both strongly and weakly back-propagating cells.

PSP attenuation test: Similar to the backpropagating action potential test, this test examines attenuation of post-synaptic potentials as they travel from their position in the dendrites to the soma. Artificial synapses using NEURON's default Exp2Syn synaptic model are placed at three different distances, and the attenuation of the postsynaptic potentials they generate is measured at the soma.

Oblique integration test: Oblique dendrites (i.e. the dendritic branches which extend from the apical trunk at oblique angles; the reduced model has 3 such dendrites) are known to be able to integrate subthreshold inputs by the generation of a dendritic spike which would be greater in amplitude than any combination of the postsynaptic potentials that generated it (Losonczy and Magee 2006). This test evaluates the model's oblique dendrites' ability to conduct this signal integration. To do this, the test inserts AMPA and NMDA synapses into the oblique dendrite, and stimulates them with asynchronous and synchronous input trains. Then, features such as dendritic spike initiation threshold, shape of the induced somatic postsynaptic potentials, and measures of the EPSP's nonlinearity are examined.

In order for the model to generate spikes in response to magnetic stimulation, the axon included with the model was insufficient. Spikes from TMS require a myelinated axon (Aman S. Aberra, Angel V. Peterchev, and Grill. 2018), and we included a custom axon. The axon contains 6 myelinated internodal segments of diameter 1.75 μm separated by internodal segments with length 1 μm and diameter 0.375 μm, with an unmyelinated axon terminal of length 7 μm and a tapering axon initial segment, which has elevated Na^+ and K^+ conductances. A schematic of this axon is shown in Figure 2.4.

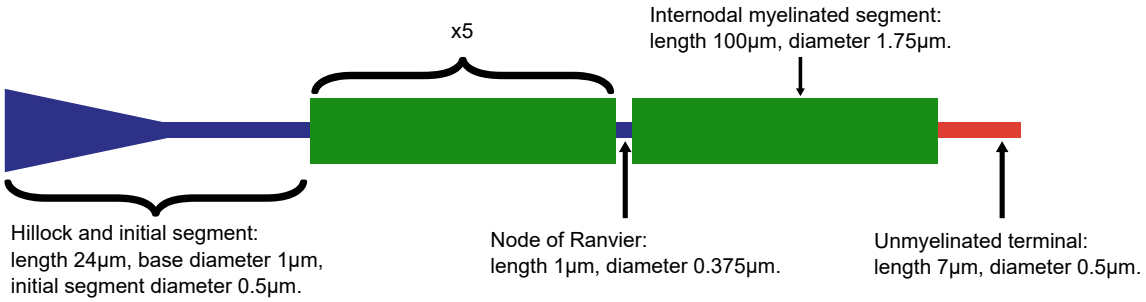

Figure 2.4. Schematic of axon added to the reduced model of the CA1 pyramidal cell.

In order for these changes to result in passing final error scores in the HippoUnit test battery, we needed to make some minor modifications to some biophysical variables in the model. A table of all channel densities and biophysical parameters is shown below in Table 4, with changes to the original shown in bold italic.

Property	**Soma**	**Apical trunk**	**Dendrites**	**AIS and nodes**	**Myelin**	**Axon terminal**
Na (S/cm^2)	0.035	***0.015-0.02***	0.03828	***0.55***		0.035
K_A (S/cm^2)	0.0075	0.1-0.2	Variable	***0.409236***		0.0163694
K_{DR} (S/cm^2)	0.0015	0.02	0.004304	***0.0291607***		0.011664
K_M (S/cm^2)	0.001			***0.0317687***		0.0264739
K_{Ca} (S/cm^2)	0.0015	9.031e-5	9.031e-5			
Cag_K (S/cm^2)	4.48e-5	4.48e-5	4.48e-5			
Ca_T (S/cm^2)	0.00005	1.185e-6	1.185e-6			
Ca_L (S/cm^2)	0.0005	8.033e-6	8.033e-6			
Ca_N (S/cm^2)	2.26e-6	2.26e-6	2.26e-6			
I_h (S/cm^2)	Variable	Variable	Variable			
C_M $(\mu F/cm^2)$	1	1	1	1	***0.01***	1
R_A $(\Omega \cdot cm)$	115	115	115	85.2	***60***	85.2
g_{pas} (S/cm^2)	9.031e-5	9.031e-5	9.031e-5	1.29e-4	***8.89e-7***	1.29e-4
e_{pas} (mV)	Variable	Variable	Variable	-79.92	-79.92	-79.92

Variable property	**Equation; d is distance from soma in μm**
I_h (S/cm^2)	$1.904e-5\frac{1+3d}{100}$
K_A (S/cm^2)	$0.0129\frac{15}{1+exp(\frac{300-d}{50})}$
e_{pas} (mV)	$-65.73-\frac{5d}{150}$

Table 4. Ion channels and membrane properties of implementation of reduced CA1 model.

Changes from the original are shown in bold italics.

The model's combination of phenomenological fidelity with replication of the basic morphological features of the cell, as well as a large reduction in computational footprint compared to the other detailed, realistic morphologies implemented in NeMo-TMS (especially those with large, heavily branched axons with many thousands of individual tree nodes) made it useful for tuning and simulating synaptic plasticity induced by repetitive magnetic stimulation.

For our synaptic plasticity simulations, we insert 130 excitatory synapses into the cell, randomly distributed in locations in the morphology in which excitatory synapses are present (Megıas et al. 2001). The random distribution of synapses within these locations provide a simple way to generate populations of models. Additionally, 18 inhibitory synapses are added, although these do not use the same four-pathway mechanism, and are non-plastic. Instead, they use the simple bi-exponential synaptic mechanism included within Neuron (Exp2Syn) with a negative reversal potential, which leads their

activation causing a reduction in local membrane voltage.

When magnetic stimulation is simulated in this model, in addition to the NeMo-TMS magnetic stimulus (which is applied to the extracellular potential of every compartment within the model), every connected synapse is activated. This is based on an assumption that magnetic stimulation will activate all (or at least a very large proportion of) axonal terminals in the target volume without necessarily inducing somatic action potentials in the presynaptic cells, leading to near-immediate activation of the connected synapses (Aman S. Aberra, Angel V. Peterchev, and Grill. 2018). The delay in the opening of the synapses is modelled by staggering the activation of the synapses from the magnetic stimulus by 1 millisecond.

Chapter 3

Results

3.1 Single-compartment modelling of rMS

Initial modelling of TMS used the single-compartment Izhikevich model, tuned to represent a CA1 pyramidal cell (intrinsic bursting cell with parameters a,b,c,d = 0.02, 0.2, -65, 8). Due to the fact that there is no spatial extent to this model, representing a TMS-induced spike required considerable simplification.

The model used has multiple synaptic inputs, which represent the activation of a synapse with a small positive current injection, which is scaled by the synaptic weight. To represent a magnetic stimulus, the synaptic input is paired with a current injection of sufficient size to cause the cell to spike.

The stimulation protocol chosen was that in Lenz et al (2015) (Lenz, Platschek, et al. 2015), consisting of 900 pulses of synaptic stimulation applied at 10 Hz. 10 Hz magnetic stimulation for 900 pulses was observed to induce substantial long-term potentiation (LTP), i.e. an increase in weight, whereas the same protocol done with pure electrical stimulation induced a decrease in weight, i.e. long-term depression (LTD).

We find that the mSTDP model is able to qualitatively produce the split between LTP and LTD when comparing 10Hz 900 pulse magnetic vs. electric stimulation (Figure 3.1), as well as showing reduced amounts of LTP magnitude for lower frequencies. However, there are also location-dependent effects observed in Lenz et al., and to reproduce these effects a more detailed model will be required, and the induced LTP amplitude we see here is far below that which was observed in Lenz. (Lenz, Platschek, et al. 2015).

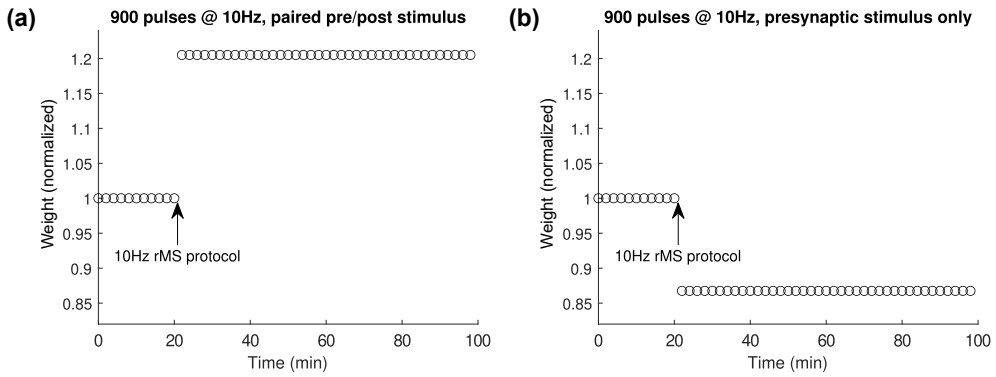

Figure 3.1. Induction of LTP and LTD by 900 pulse 10Hz protocols *(a)*: LTP induced by paired presynaptic and postsynaptic input. *(b)*: LTD induced by presynaptic input only.

Because metaplasticity could be relevant to the plasticity induced by repetitive magnetic stimulation, we tested the model's ability to produce a result dependent on it.

In this protocol, we have two pathways. Initially, one pathway is stimulated with a high-frequency synaptic input, which leads to potentiation in one, and depression in the other (heterosynaptic plasticity). This effect requires metaplasticity to reproduce (Benuskova and Abraham 2007). Then, a depression-inducing low-frequency stimulus is supplied to the second pathway, and after some delay, a high-frequency potentiating stimulus is applied to the second pathway.

With this protocol and this model and selection of parameters, we find that the second potentiating stimulus induces a greater amount of induced LTP than the stimulus to the first pathway, which implies some sort of "priming" effect from the reduction in background activity caused by the depression of that pathway (Figure 3.2). This shows that perhaps such a model of metaplasticity would be able to reproduce the "priming" effects that some TMS induction protocols rely on. (Todd, Flavel, and Ridding 2009; Cassidy, Gillick, and Carey 2014).

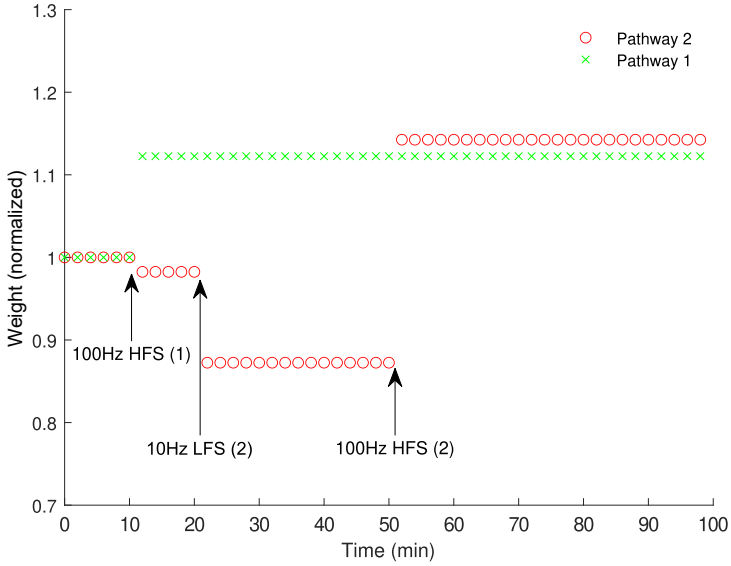

Figure 3.2. Primed induction of LTP shown in point model with metaplastic STDP model. Pathway 1 weight trace shown by green crosses, pathway 2 weight trace shown by red circles. 100Hz potentiating stimulus applied to pathway 1 at 10 minutes, 10Hz depressing stimulus applied to pathway 2 at 20 minutes, 100Hz potentiating stimulus applied to pathway 2 at 50 minutes. Note heterosynaptic LTD in pathway 2 in response to potentiating stimulus in pathway 1 and greater subsequent LTP in pathway 2.

3.2 Modelling of TMS-induced action potentials with NeMo-TMS

Publication: Multi-scale modelling toolbox for single neuron and subcellular activity under Transcranial Magnetic Stimulation, Shirinpour, Hananeia, et al, 2021

3.2.1 Reconstruction of realistic neuron morphologies for NeMo-TMS

The key advantage of NeMo-TMS (Sina Shirinpour et al. 2021) is its ability to use an arbitrary neuron morphology in simulations of magnetic stimulation. For this, we have imported a variety of different neuron morphologies into the toolbox. Each cell is reconstructed manually in Neurolucida and converted into an .ASC morphology file. Further adjustments are made (including the smoothing of sharp corners using the ProMesh4 utility, as sharp corners in the morphology cause local voltage spikes under simulated magnetic stimulation), and the cells have regions (soma, axon, basal dendrites, apical dendrites) assigned and are ready for use with the NeMo-TMS utility.

We have imported a library of 28 cells: 10 rodent pyramidal cells (5 mouse and 5 rat; included with the NeMo-TMS release for use with the Jarsky model) and 18 human pyramidal cells from layer 2 and 3 of the cortex.

The rodent cells are the most suited for highly realistic simulations, since we have access to a readily generalizable model of a rat CA1 cell in the Jarsky (Jarsky et al. 2005) model. The morphologies are shown in Figures 3.3 and 3.4.

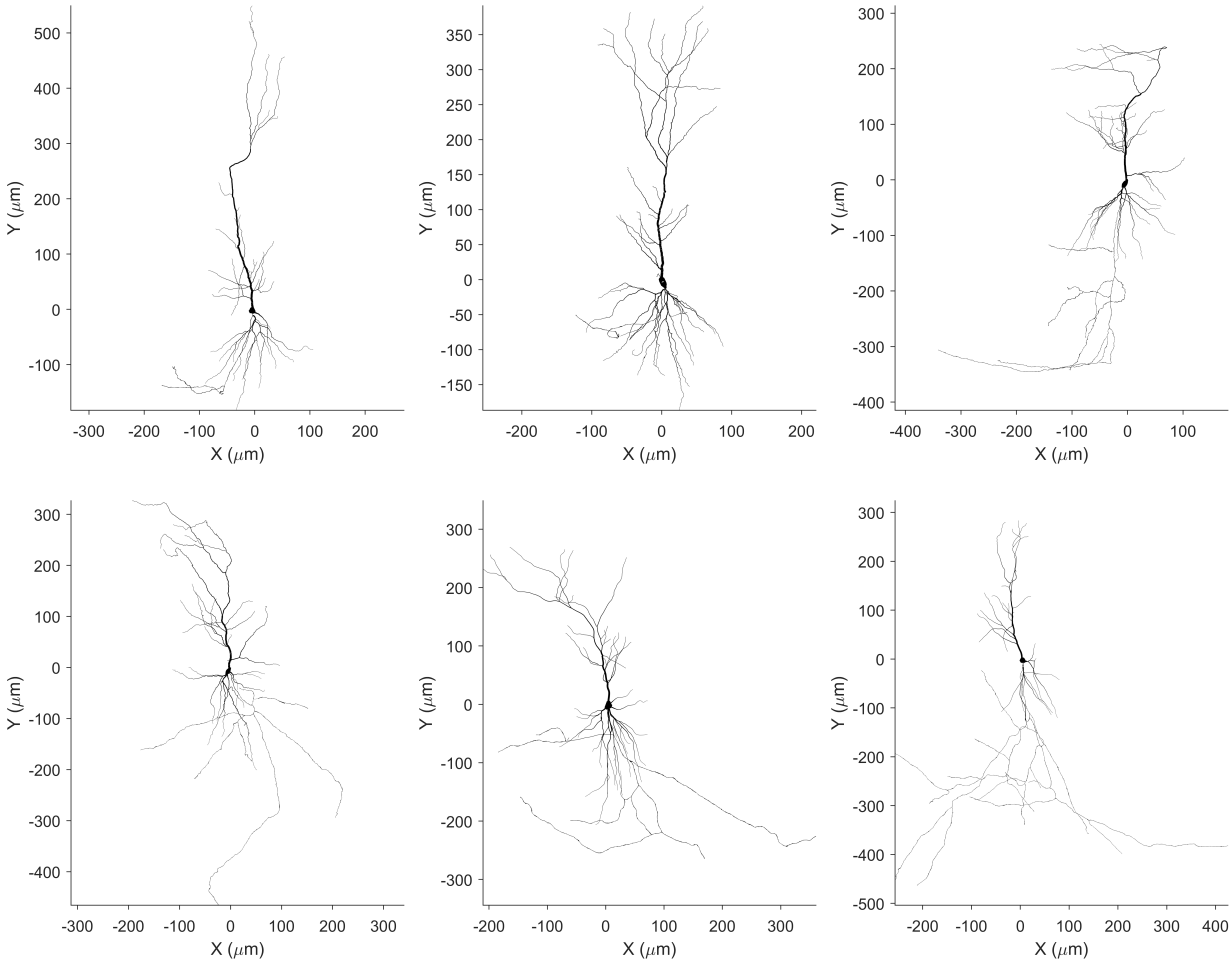

Figure 3.3. Diversity of rodent CA1 pyramidal neurons, 1/2 Set of 10 rodent CA1 pyramidal cells reconstructed for NeMo-TMS, cells 1-6. Axons vary in size from short to over 1mm in length.

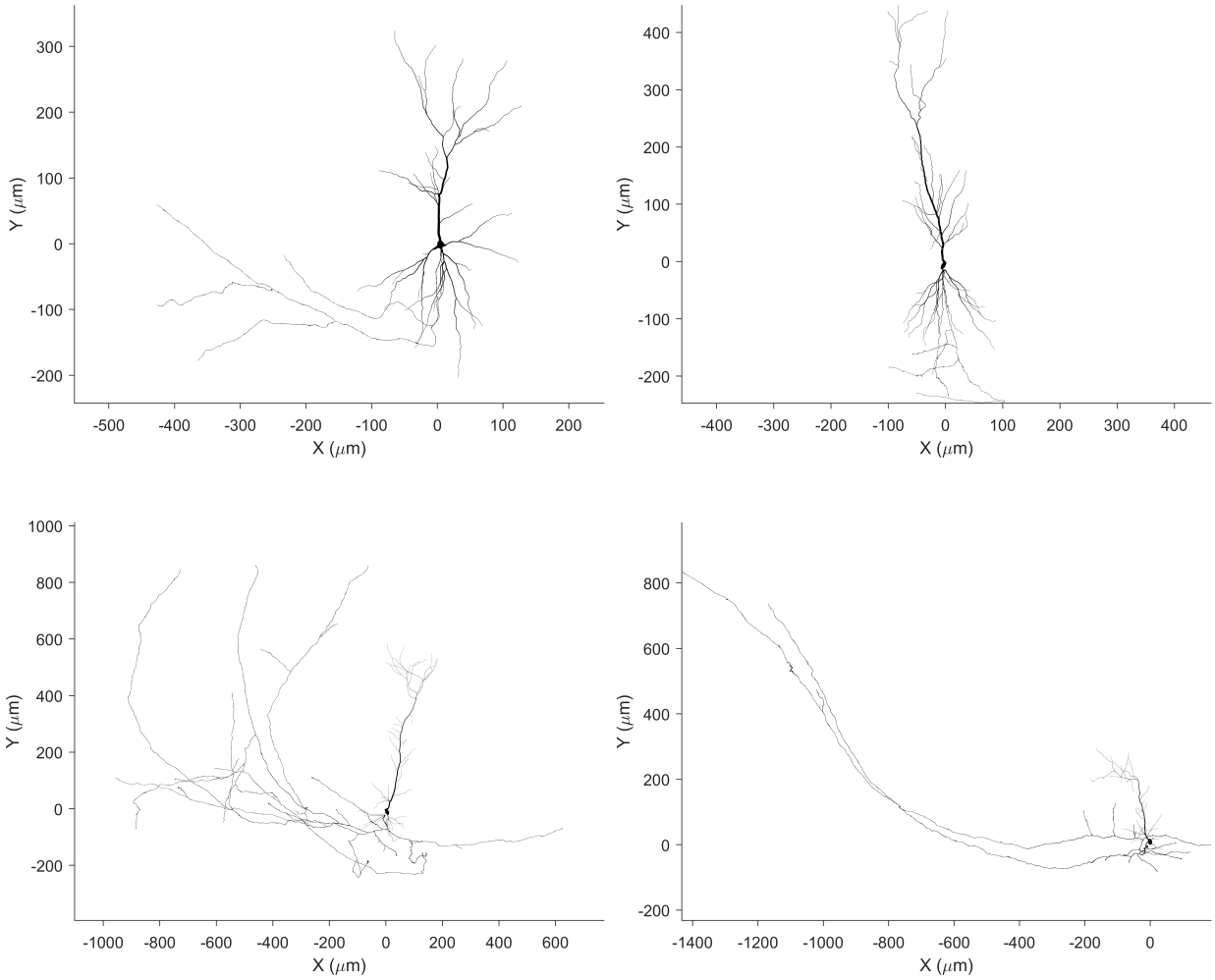

Figure 3.4. Diversity of rodent CA1 pyramidal neurons, 2/2 Set of 10 rodent CA1 pyramidal cells reconstructed for NeMo-TMS, cells 7-10. Axons vary in size from short to over 1mm in length.

We do not yet have a generalizable electrophysiological model for human cells, however we will later use them for axon propagation simulations. Some of the cells are notably considerably larger than the rodent cells (maximum apical dendrite length 500-600 microns versus the typical maximal apical dendrite length in the rodent cells of 300-400 microns) and it is worth noting that all human cortical pyramidal cell reconstructions generally have missing or cut apical tufts, due to either their large size making them vulnerable to being cut during slicing, or difficulty in perfusing the entire large cell with dye (Groden et al. 2024). Hence, the dendritic structure of cells in this set which are not considerably

larger than their rodent hippocampal counterparts should be considered with this in mind.

The morphologies of these 18 cells are shown below in figures 3.5, 3.6 and 3.7.

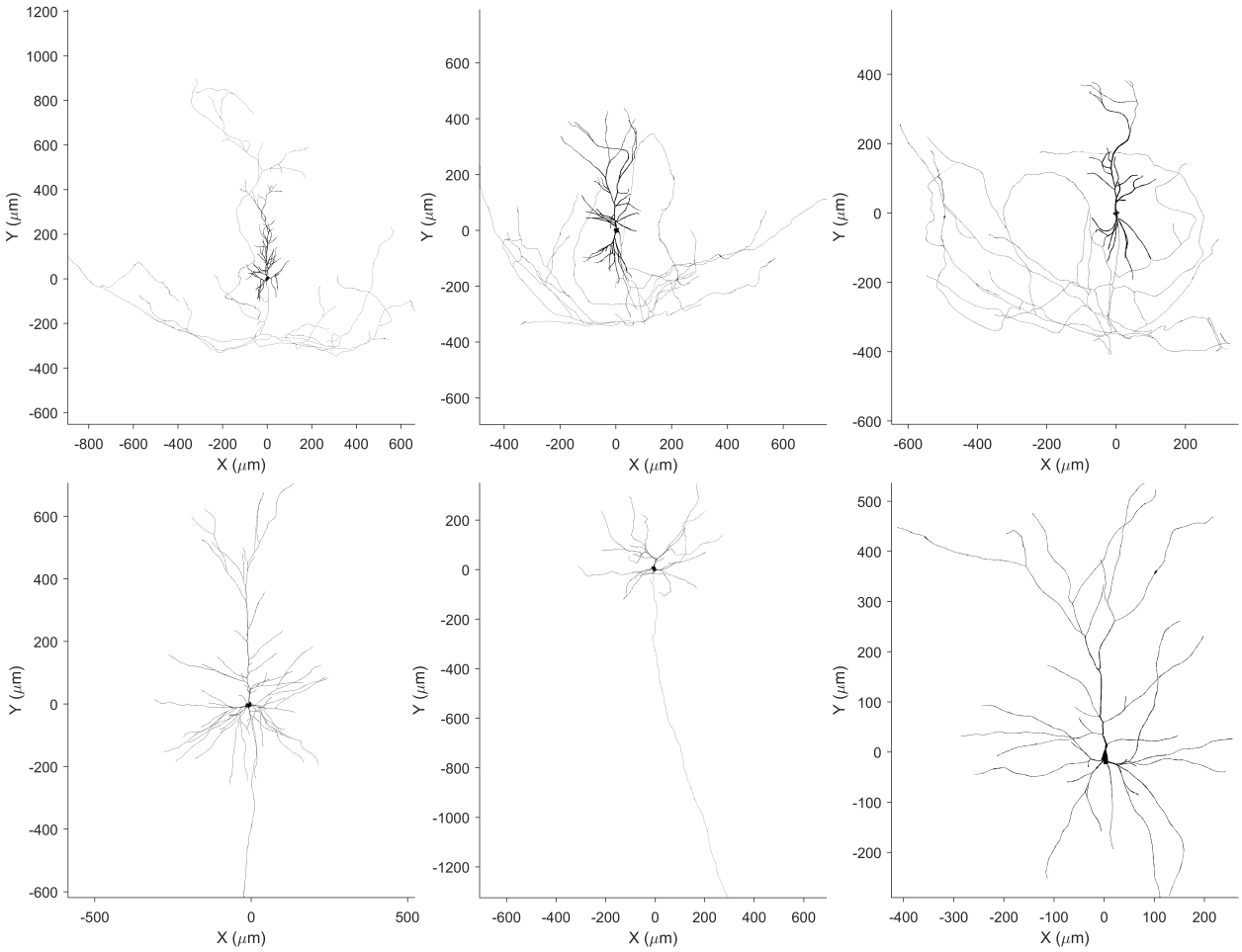

Figure 3.5. Diversity of human cortical L2/3 pyramidal neurons, 1/3 Set of 18 human cortical pyramidal cells reconstructed for NeMo-TMS, cells 1-6.

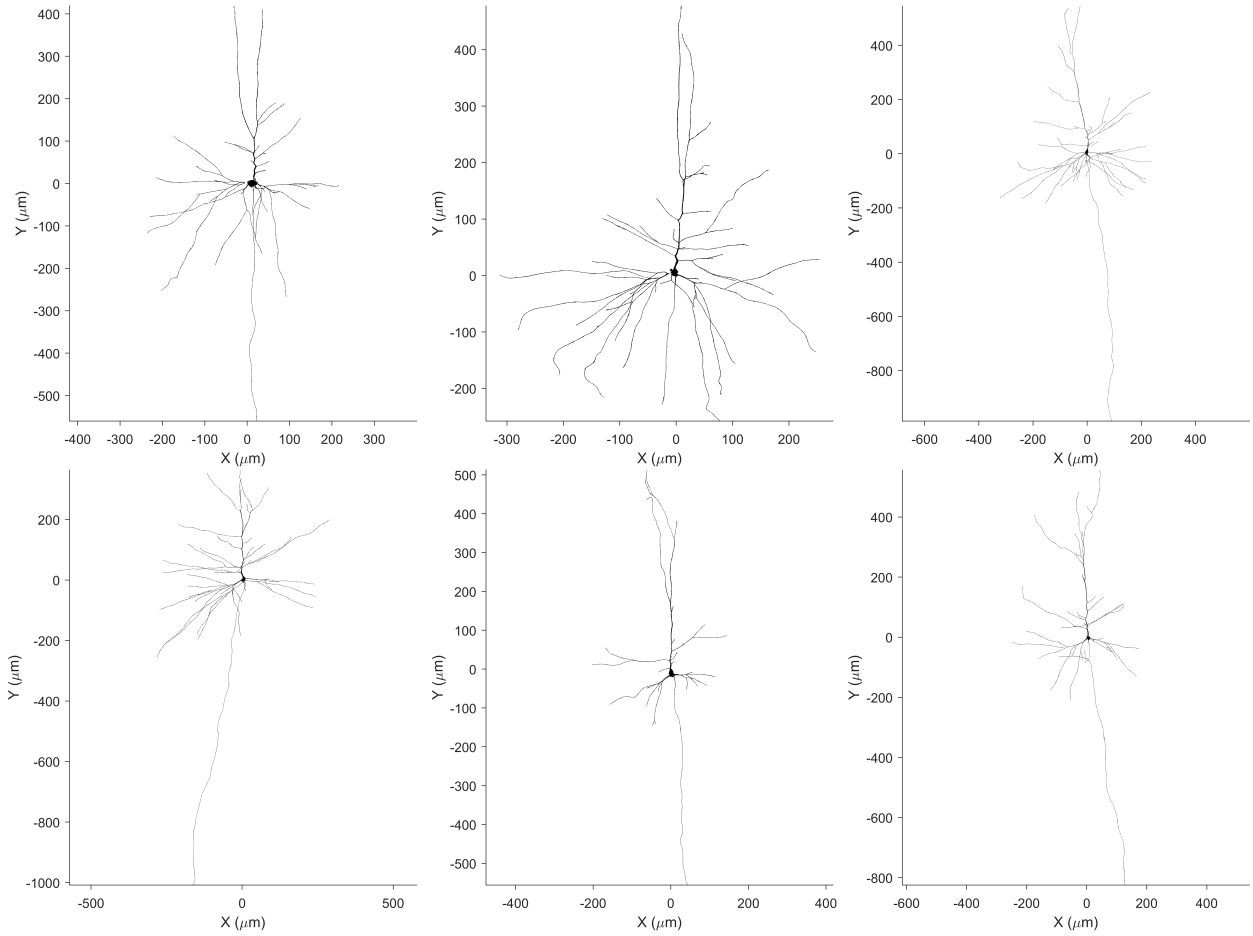

Figure 3.6. Diversity of human cortical L2/3 pyramidal neurons, 2/3 Set of 18 human cortical pyramidal cells reconstructed for NeMo-TMS, cells 7-12.

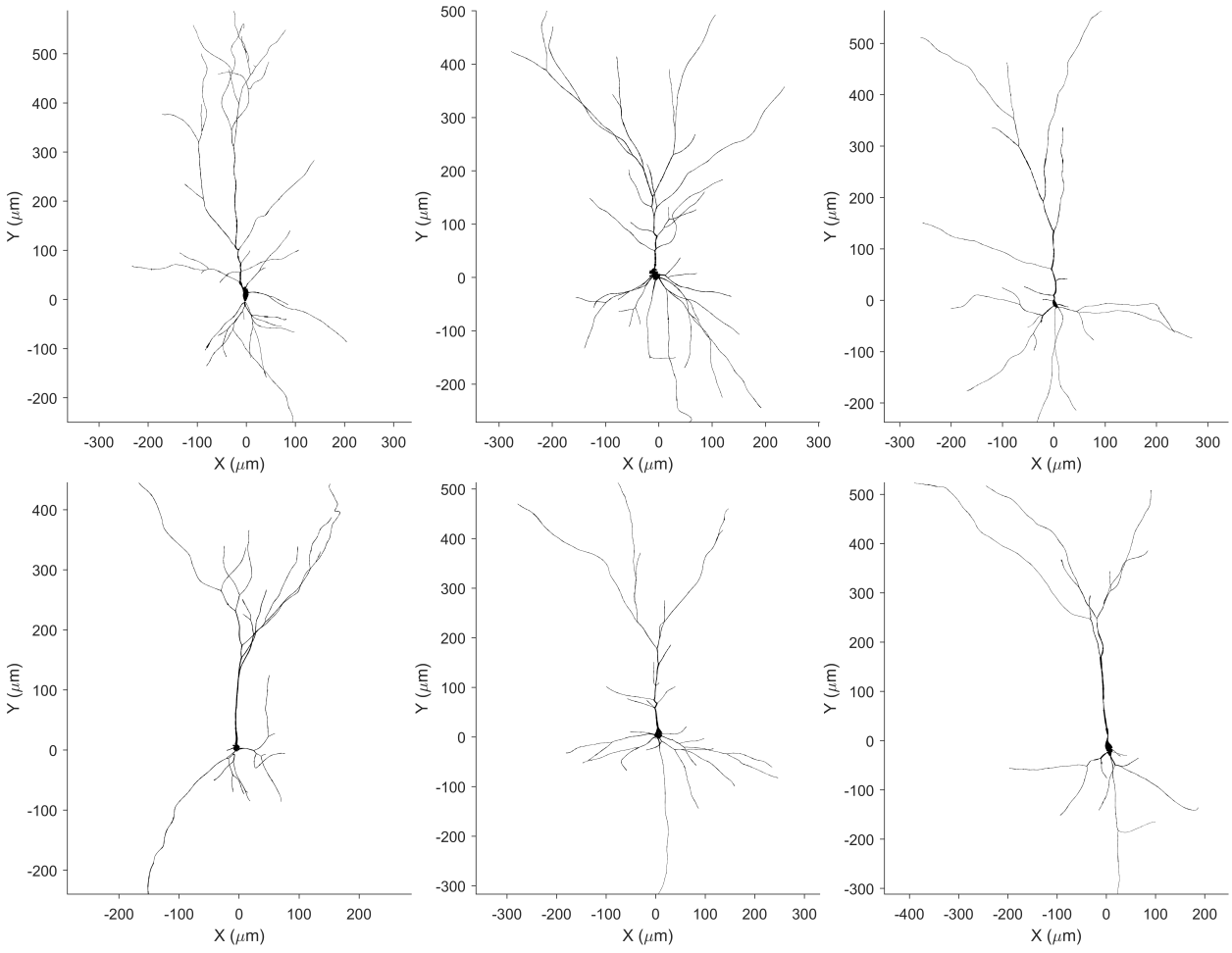

Figure 3.7. Diversity of human cortical L2/3 pyramidal neurons, 3/3 Set of 18 human cortical pyramidal cells reconstructed for NeMo-TMS, cells 13-18.

3.2.2 Realistic E-field simulation in dish model

Initially, we modelled the induction of single TMS-induced action potentials in realistic cell morphologies in the NeMo-TMS toolbox.

We use a model of a Petri dish (Alekseichuk, Shirinpour, and Opitz 2020) in SimNIBS to generate and generate the quasipotentials for a single magnetic pulse for a coil placed 4mm above the culture, as shown in Figure 3.8. This FEM simulation generates electric field vectors for every location within the simulated culture. These are subsequently used by NeMo-TMS to generate quasipotentials.

Examining the electric field lines within the simulated volume, we find that the lines are close to parallel

- this is a result of the close position of the stimulating coil to the culture, as well as uniformity of the culture itself. Discontinuity between the conductivity of the of the culture and the surrounding artificial cerebro-spinal fluid results in edge effects where the electric field becomes notably higher. This is because of the abrubt change in the conductivity of the grey matter within the culture (0.275 S/m) and that in the aCSF (1.654 S/m). For this reason, the cell was placed exactly in the geometric center of the volume when the cell's morphology was coupled to the E-field simulation.

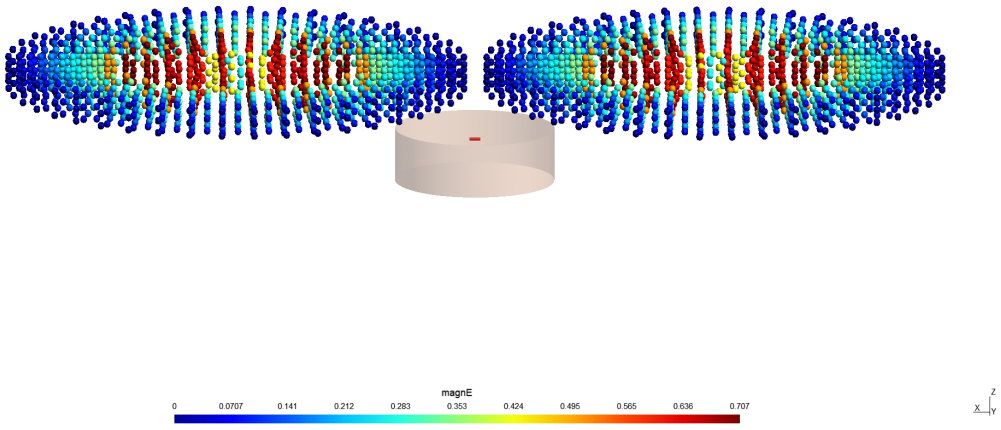

Figure 3.8. Arrangement of coil and culture in SimNIBS FEM simulation Dipoles of figure-of-eight coil (dots) positioned over simulated petri dish volume (pink) in which culture (red) is suspended.

The cell (cell number 6) generates a somatic spike when stimulated with a biphasic pulse with a field scaling factor of 270 (slightly above the firing threshold). At t = 2ms, the pulse itself is delivered, which causes a brief and small voltage deflection in both directions (since the stimulus is biphasic). After a delay, a strong somatic action potential is generated, and the cell returns to the resting voltage after a few milliseconds (Figure 3.9).

In this case, the delay is a delay between TMS stimulus onset and the induction of an axonal action potential, not the axon propagation delay.

The actual action potential itself is initiated at one of the axon terminals within the axonal tree, as shown in Figure 3.10.

At the instant the TMS pulse is delivered, there is little change in the voltage of the cell. After a short (around 1ms) delay, the action potential is initiated in an axon terminal when that terminal is sufficiently depolarized to induce a local spike. (Figure 3.10, (b)). Because the axon is myelinated, allowing rapid

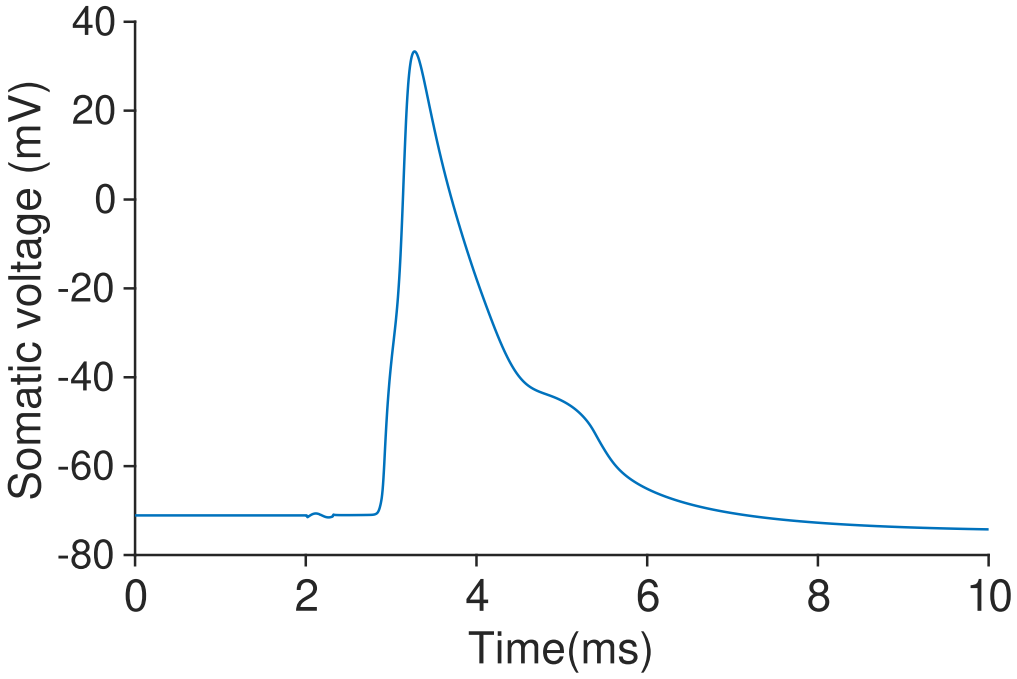

Figure 3.9. Somatic voltage trace in response to NeMo-TMS magnetic stimulus Voltage trace at soma of action potential elicited by NeMo-TMS. Stimulus onset is 2ms.

transmission with little loss, the action potential rapidly propagates across all axon branches, quickly reaching the soma (Fig 3.10 (e)). Subsequently, the soma itself spikes, and the dendrites depolarize as a result of the opening of voltage gated sodium channels and ionic diffusion. The tips of the apical dendrites take the longest to depolarize, and the rest of the cell has already begun to return to the resting potential by the time that they have depolarized. Finally, after a few more milliseconds, the cell returns to its resting potential.

It is worth noting that this delay is only observed close to the cell's TMS firing threshold, and is unrelated to the speed of propagation of the action potential along the cell's axon. When the field scaling factor is increased even modestly to 280, the somatic spike occurs nearly immediately after the application of the TMS stimulation. This is shown below in figure 3.11, where with otherwise identical parameters to the above simulation, the delay was entirely eliminated with the axonal spike being produced in exactly the same axonal terminal.

Further increases to the scaling factor do decrease the length of this delay, with the delay being reduced from 0.385ms to 0.30ms with a scaling factor of 320.

The specifics of the back-propagation through the axon, of course, depend on the axonal morphology,

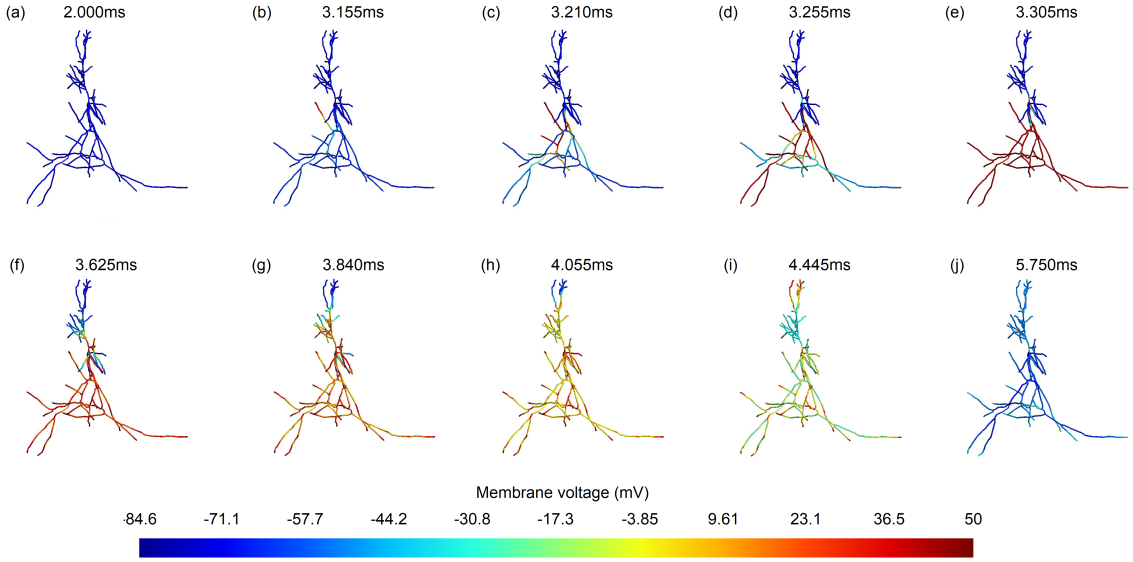

Figure 3.10. Propagation of TMS-initiated action potential through axon and dendrites Snapshots of cell voltage as action potential propagates through the cell. *(a)*: Moment of TMS stimulus onset at 2.0ms. *(b)*: Initiation of action potential at axon terminal. *(c)* - *(e)*: Action potential spreads through axon branches and arrives at soma. *(f)* - *(i)*: Action potential spreads through dendrites at much slower rate than in axon. *(j)*: Axon has returned to resting voltage.

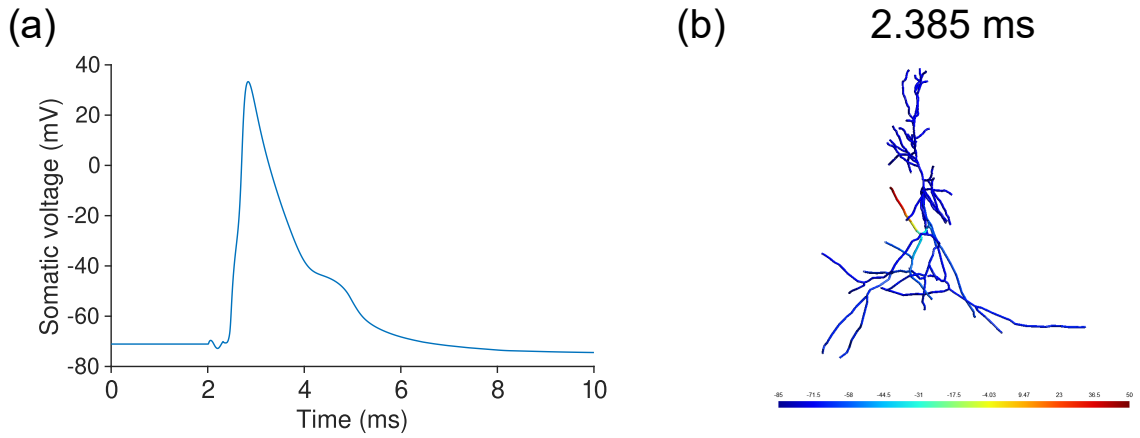

Figure 3.11. Axonal action potential delay significantly reduced by modest increase of TMS intensity above threshold *(a)* Somatic voltage trace of cell 6 stimulated by NeMo-TMS magnetic stimulus at scale factor 280. *(b)* Snapshot of initiation of axonal action potential at 0.385ms after stimulus onset.

and, although propagation through the axon is swift, more distant initiation sites will inevitably have a longer time between action potential intiation and the action potential's arrival at the soma.

3.2.3 Simulation of action potentials initiated by NeMo-TMS with uniform E-field assumption

We found from FEM simulation of electric fields (Figure 3.8) that in a slice culture with a nearby coil, the field lines in the center of the culture are close to parallel and similar in magnitude. Since a great many neuroscience experiments are performed on organotypic slice culture, the simplifying assumption of a uniform electric field (i.e. a spatially homogeneous electric field with perfectly parallel field lines and constant magnitude) could be useful, especially when precise control of the electric field direction is wanted for a simulation.

It is known (Rotem and Moses 2008; Gomez-Tames et al. 2018; Casula et al. 2022) that the orientation of the coil, and thus, the direction of the induced magnetic field, has an important role in both experimental and clinical neuroscience: different effects can be induced by changing the coil orientation on a human subject, presumably because of selective activation of certain populations of neurons.

Using uniform stimulation, we stimulate the same cell at a set of angles away from the somatodendritic axis. For this simulation, we used a from our library which has a large number of axonal branches: rodent cell 9, and determine the minimum TMS field intensity which can cause a somatic spike.

For our prior simulations, the electric field has been aligned with the somatodendritic axis of the cell, pointing in the negative Y direction, i.e. an a direction vector of [0, -1, 0]. In this simulation, we sweep across the ϕ plane in 15° increments. In the polar co-ordinate system, the original alignment corresponds to a ϕ angle of 270°.

There is a relationship between E-field angle and firing threshold, however when the electric field angle is shifted, different axon terminals become the point of initiation. When rotating through the full circle, we observed five different sites of action potential initiation. These are shown in Figure 3.12.

For monophasic stimulus is a broad trend observed - the lowest activation threshold is observed around $\phi = 90°$, which corresponds to alignment of the electric field in the positive y direction, pointing in the same direction as the terminals of sites 1 and 2, with a similar higher activation threshold for nearer to the reciprocal angle of $\phi = 270°$.

Other action potential initiation sites have associated local minima, such as site 3's at $\phi = 0°$, which corresponds to a field alignment pointing in the positive X direction, again pointing in this terminal's direction.

Biphasic stimulus causes a much less direction-sensitive excitation of the cell (the difference between the maximum and minimum firing threshold for biphasic stimulus is 55 V/m whereas the equivalent difference for monophasic stimulus is nearly twice as much at 105 V/m), and a generally lower firing threshold for most angles, with the exception of the $\phi = 90°$ orientation. There is some direction

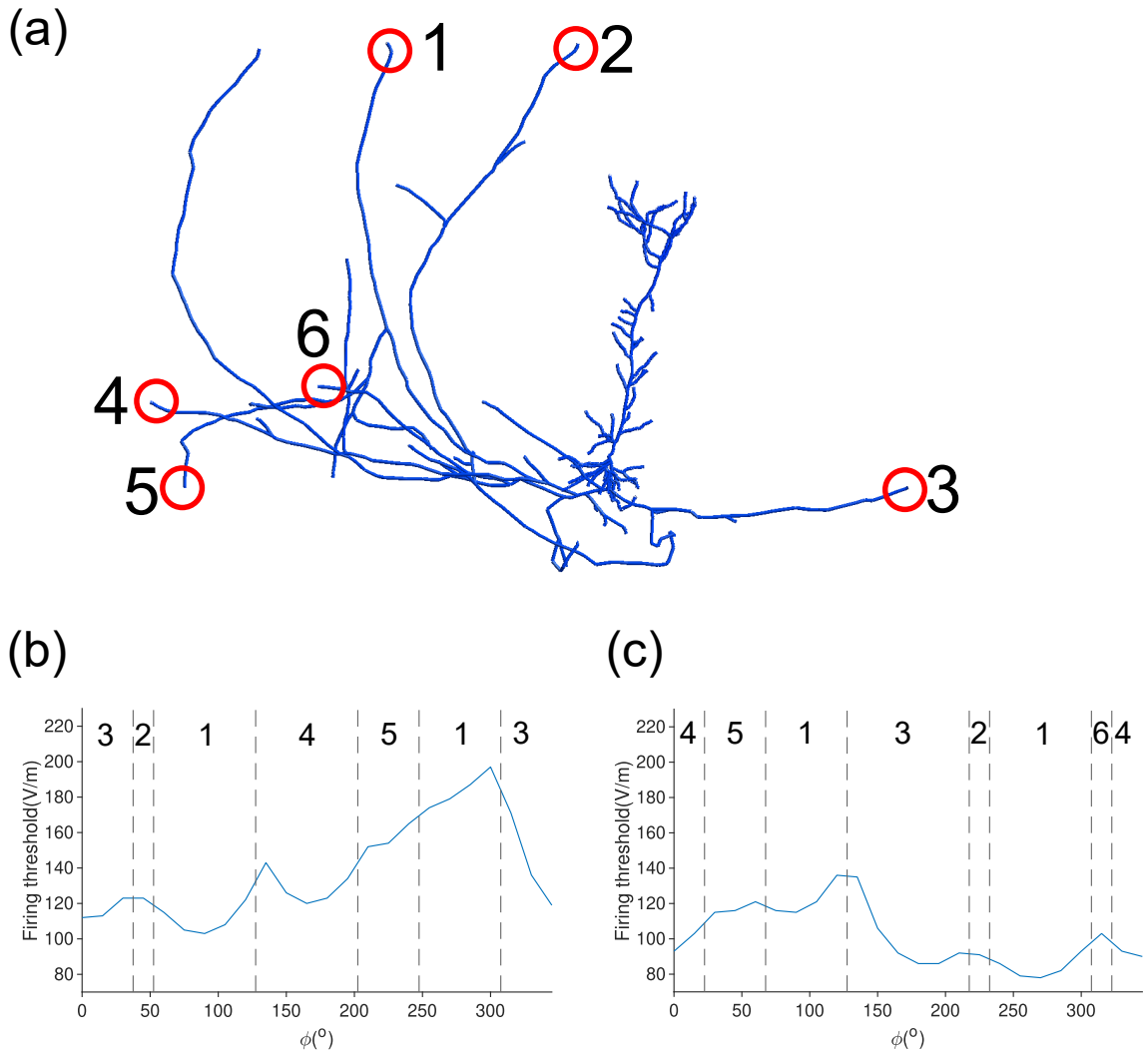

Figure 3.12. Differing action potential points and firing thresholds when electric field direction is rotated. *(a)*: Six different action potential initiation sites, circled in red and numbered 1-6, are observed when we rotate the electric field in the ϕ plane. *(b)* Cell firing threshold as a function of azimuthal angle ϕ, for a monophasic stimulus. Vertical delimiters and associated labels denote which action potential initiation site is associated with a given angle. *(c)* Cell firing threshold as a function of azimuthal angle ϕ, for a biphasic stimulus. Vertical delimiters and associated labels denote which action potential initiation site is associated with a given angle.

sensitivity - the $\phi = 270°$ orientation has a lower firing threshold than the $\phi = 90°$ orientation, which is a reversed direction preference to monophasic. This is likely because the biphasic pulse's negative phase is longer than its positive phase.

To examine the dynamics of a firing threshold with a single axon terminal, we endow one of the human cortical cells with a single, unbranching axon terminal - human cell number 11 - with the Jarsky model.

Although this model does not accurately depict the biophysics of a human cortical cell, it will be useful for the purposes of generating TMS-initiated spikes.

As expected, in this cell, all TMS-initiated action potentials began at the cell's single axon terminal. (Figure 3.13).

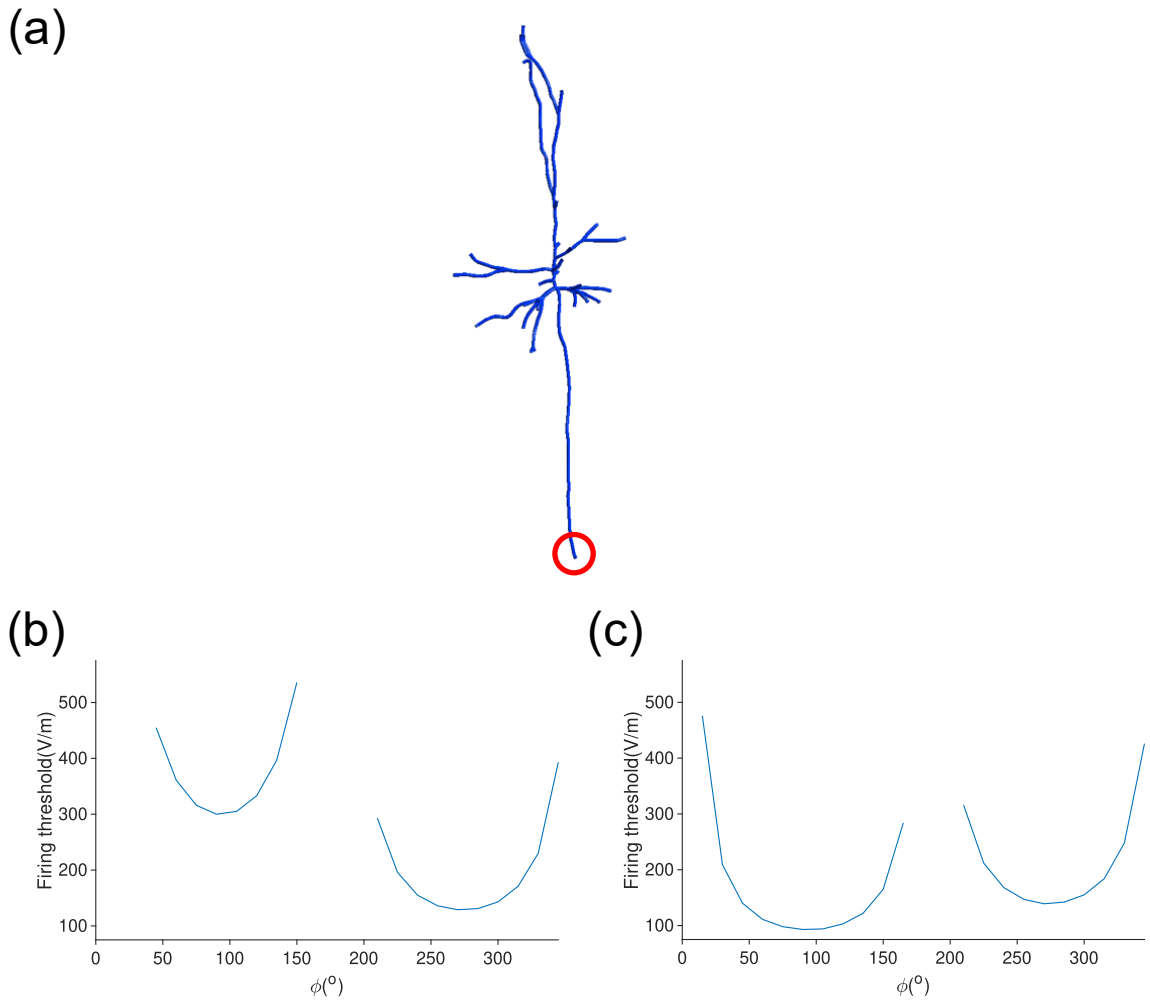

Figure 3.13. Relationship of firing threshold to electric field orientation for cell with unbranched axon. *(a)*: Single, unbranching axon has a single terminal; all TMS-initiated action potentials originate at this point (red circle). *(b)* Cell firing threshold as a function of azimuthal angle ϕ, for a monophasic stimulus. Where no line is shown, cell did not spike at this angle for any field intensity. *(c)* Cell firing threshold as a function of azimuthal angle ϕ, for a biphasic stimulus. Where no line is shown, cell did not spike at this angle for any field intensity.

We find, with this cell, a very simple and obvious angle sensitivity. As in the branched cell, the lowest activation threhsolds are found at the points where the electric field is oriented along the somatodendritic axis, with monophasic stimulus having a strong direction sensitivity, with the positive Y orientation

resulting in a much higher activation threshold. Similarly, the direction sensitivity is both minimized and reversed in the biphasic case.

When the field is oriented perpendicular to the somatodendritic axis, under both stimulation types, the cell will not fire, even with extremely large ($> 1000V/m$ was attempted before categorizing these angles as non-responsive) stimulus intensities.

In some cases in cells with many branches at certain angles, we observed that there could be more than one initiation site, in some cases with very similar firing thresholds.

For the case of the above mentioned cell 9, with an field angle of $\phi = 270°$, and a biphasic stimulus, we found that a TMS intensity of 135V/m initiated a spike in initiation point 6 as shown in figure 3.12, whereas an intensity of 137V/m initiated a spike at both site 3 and a distant seventh site.

With the same cell and orientation, we increased the TMS intensity further to determine how rapidly additional activation sites would be recruited (Figure 3.14).

With an increase of TMS intensity to 175V/m, four terminals were activated, and with an increase to 250V/m, even more were.

It is worth noting that these multi-site activations have no effect on how the somatic and dendritic propagation of the action potential occurs apart from further minimization of the activation delay (see Fig. 3.11, and possible shorter transit time if one of the additional sites is closer to the soma. The multiple colliding action potentials do not reinforce or diminish each other.

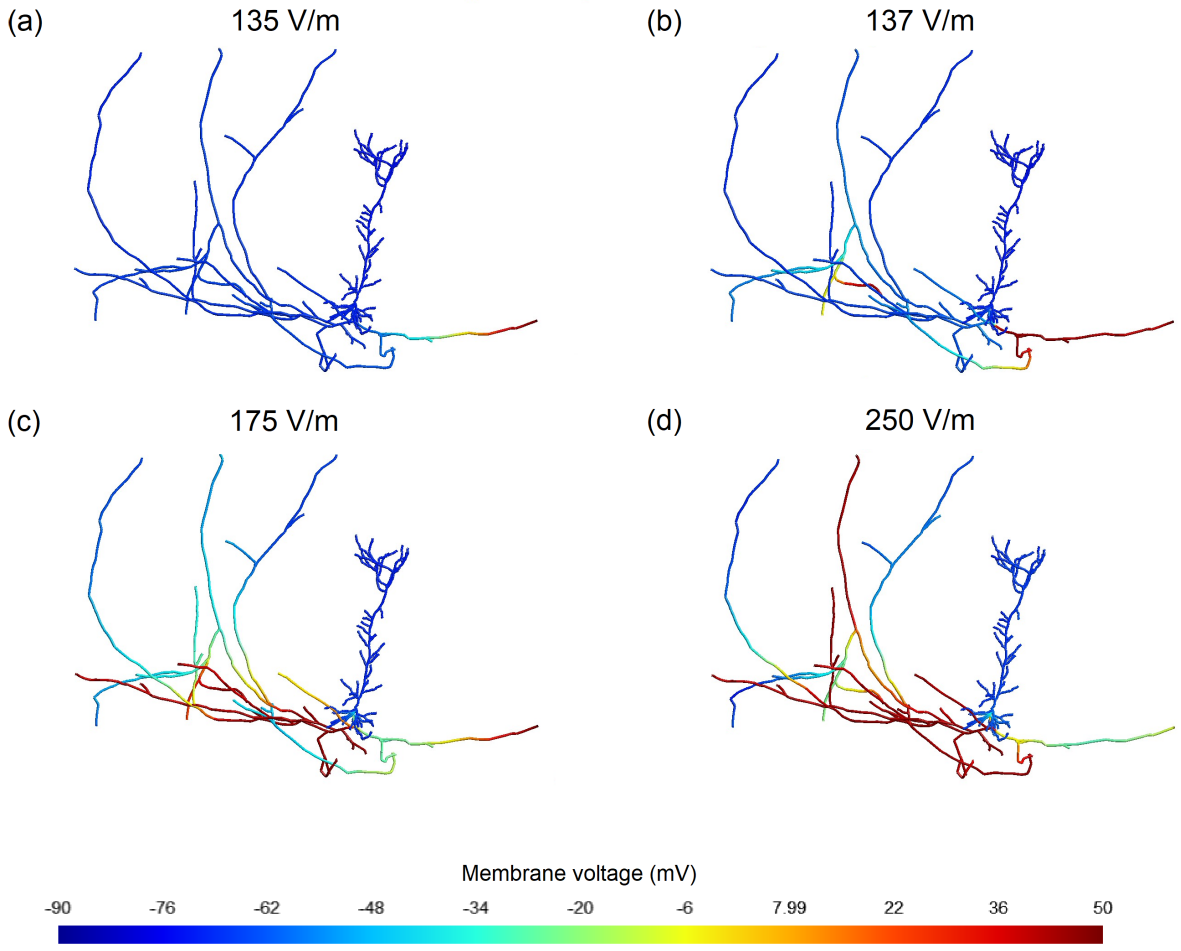

Figure 3.14. Suprathreshold stimulus can recruit additional action potential initiation sites. *(a)*: Single site initiation at cell 9 initiation site 3 (see Figure 3.12 from 135V/m stimulus. *(b)*: Additional site recruited from a marginal increase of 2 V/m to 137V/m *(c)*: Further increase to 175V/m shows four distinct activation sites. *(d)*: Increase to 250V/m activates many different axonal terminals.

Since many cells have large amounts of axon terminals, and TMS in practice will not be calibrated so closely to the minimum firing threshold, we can likely assume that a suprathreshold TMS stimulus would recruit a large amount of different axonal initiation points (as well as presynaptic terminals).

3.3 Modelling of TMS-induced synaptic plasticity

Publication: Multi-scale modelling of location- and frequency-dependent synaptic plasticity induced by transcranial magnetic stimulation in the dendrites of pyramidal neurons, Hananeia et al., 2024 ,in preparation, available as preprint.

To model induction of synaptic plasticity, we use a combination of the reduced model of the CA1 pyramidal cell and the four-pathway model of Ebner et al (Hananeia, Ebner, et al. 2024).

Since the four-pathway model has over 20 free parameters, which are by default tuned to neocortical data sets (Ebner et al. 2019), we found that the default parameter set was unsuited to our combination of models. Thus, we first wanted to determine if the four-pathway model was capable of reproducing synaptic plasticity data from electrical stimulation of CA3-CA1 Schaffer collateral synapses.

3.3.1 Reference simulation: Electrical stimulation of Schaffer collaterals

As a reference data set, we used the data of Ikegaya et al (2002) (Ikegaya, Ishizaka, and Matsuki. 2002) for frequency-dependent synaptic weight changes. In this dataset, 900 pulses of electrical stimulation were applied to the Schaffer collateral at a variety of frequencies (0.33 - 100Hz), both with and without bicuculline, a $GABA_A$ antagonist, which abolishes inhibitory synaptic currents. In the dataset, abolition of inhibition leads to an increase in the amplitude of long-term potentiation.

To model this, in addition to the 130 instances of the four-pathway synapse, we have 18 inhibitory synapses, which have their weights set to zero for simulations in which the application of bicuculline is simulated. To model the electrical stimulation, every Schaffer collateral synapse (those placed in the stratum radiatum and stratum oriens of the model) was simultaneously activated 900 times, at a varying frequency. When inhibition was enabled, the inhibitory synapses in the model were similarly activated. The distal tuft synapses were not activated, since they are activated by a different synaptic pathway.

In addition to this electrical stimulation, because slice cultures are not silent (Samoilova et al. 2008), we implement a 3 Hz random background stimulus on all synapses in the model.

Our model produced mean LTP amplitudes within standard deviation for all data points except the 1 Hz and 10 Hz inhibition-enabled simulations (Figure 3.15). As expected from the data, no meaningful LTP was observed at frequencies below 30Hz. Negligible synaptic weight change is observed at frequencies below 10Hz, which will later be contrasted to rMS results later.

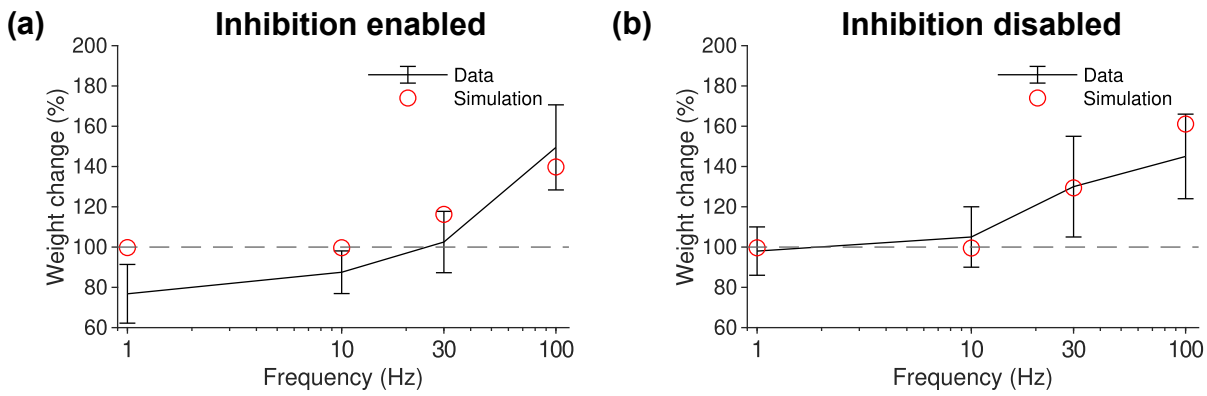

Figure 3.15. Four-pathway model of long-term synaptic plasticity reproduces frequency dependence of synaptic changes in hippocampal CA1 pyramidal cells evoked by electrical stimulation *(a)*: Stratum radiatum weight change for 900 pulses delivered at 1, 10, 30, and 100 Hz with inhibition active to simulate (red) control data (blue). *(b)*: Stratum radiatum weight change for 900 pulses delivered at 1, 10, 30, and 100 Hz with inhibition disabled to simulate (red) bicuculline data (blue).

These results show that we can reproduce realistic LTP amplitudes for typical electrical stimulation of the CA3-CA1 pathway, and as such, the parameters used for these simulations will be used for all other plasticity induction simulations.

Notably, we were unable to observe LTD in response to low-frequency synaptic stimulation in this model without synchronized background stimulation. This is likely because the asynchronous background stimulation that we use is unable to produce enough activity which is uncorrelated with the driving stimulation to induce negative (post before pre under STDP theory) pairings, which would drive LTD. We continue with the use of asynchronous background stimulation, as synchronous background stimuluation is usually considered to be a feature of in-vivo rather than in-vitro experiment.

3.3.2 Frequency and location dependence of LTP induced by repetitive magnetic stimulation

In the study by Lenz et al. (2015) (Lenz, Platschek, et al. 2015), TMS is used to evoke long-term potentiation of synaptic weights in CA1 pyramidal cell in organotypic slice culture. To study a realistic rMS protocol, we model the plasticity experiments of Lenz et al (Lenz, Platschek, et al. 2015). Here, rMS is applied to an entorhinal-hippocampal slice culture, with 900 pulses applied at 10Hz, with the electric field parallel to the somatodendritic axis of the cell. In the study, these 900 pulses were applied in 9 sets of 100 pulses with an intertrain interval of 30 seconds. The coil is placed 10mm from the center of the slice culture.

Since our plasticity model is not metaplastic, and this intertrain interval is not considered clinically relevant (it exists to prevent overheating of the TMS coil), we model this stimulus as a single 900-pulse 10Hz train. Additionally, since the coil is so close to the culture, we model the electric field as being uniform in space. The pulses are monophasic, and are delivered at 275V/m intensity, which is well above the model's spiking threshold of 210 V/m. Each magnetic stimulus corresponds to simultaneous activation of all synapses in the model, both excitatory and inhibitory.

Similarly to in the simulations with the Jarsky model in Section 3.2, the action potential is initiated at the axon terminal and propagates back to the cell, and from there spreads to the dendrites. This is shown below in Figure 3.16.

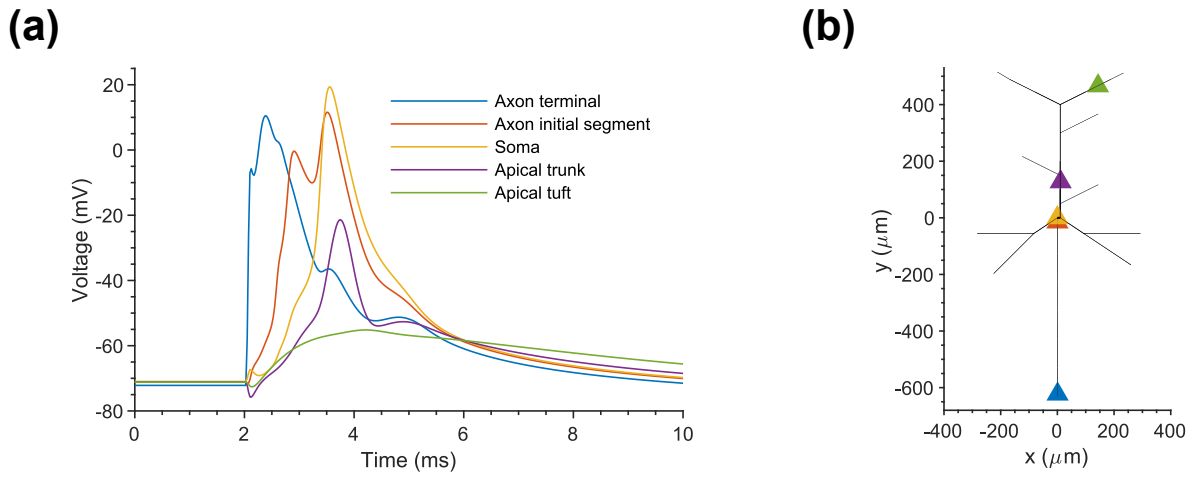

Figure 3.16. Visualization of propagation of TMS-induced action potential in morphologically reduced model

Propagation of a TMS-induced action potential in the morphologically reduced model. *(a)*: Voltage trace at various sites within the cell showing induction at axon terminal and attenuation of backpropagating action potential in the dendrites. *(b)*: Schematic of model showing recording sites.

The 10Hz stimulus caused an average increase in synaptic weights of 30 %, with the potentiation strongly concentrated in the proximal dendrites of the stratum radiatum and stratum oriens. Focusing on the proximal stratum radiatum, defining "proximal" to mean the first half of the apical dendrite and its obliques, we observed an average increase of 68%, with there being no LTP in the the apical tuft, and significantly reduced LTP in the distal stratum radiatum Figure 3.17. This is in line with observations in Lenz et al, where LTP was strongly concentrated in the proximal dendrites.

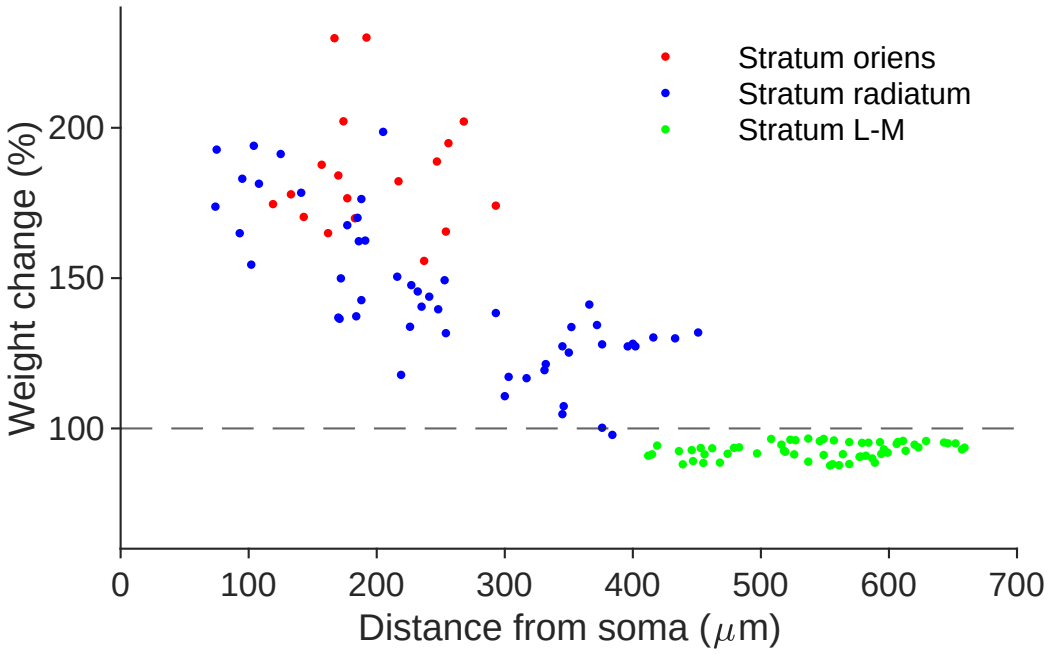

Figure 3.17. Distance profile of synaptic weight changes

Induction of LTP by 900 pulse repetitive magnetic stimulation is strongly concentrated in the proximal dendrites, with the greatest increases in the stratum oriens (red) and the proximal half of the stratum radiatum (blue). No LTP is observed in the stratum lacunosum-moleculare (green).

To model to what extent this LTP is impacted by stimulus frequency, we also administered similar 900-pulse protocols at lower frequencies (1, 5, 6, 8, and 9 Hz) (Figure 3.18).

We observe a strong correlation between induced LTP amplitude and frequency, with a rapid decline of LTP at frequencies lower than 10Hz.

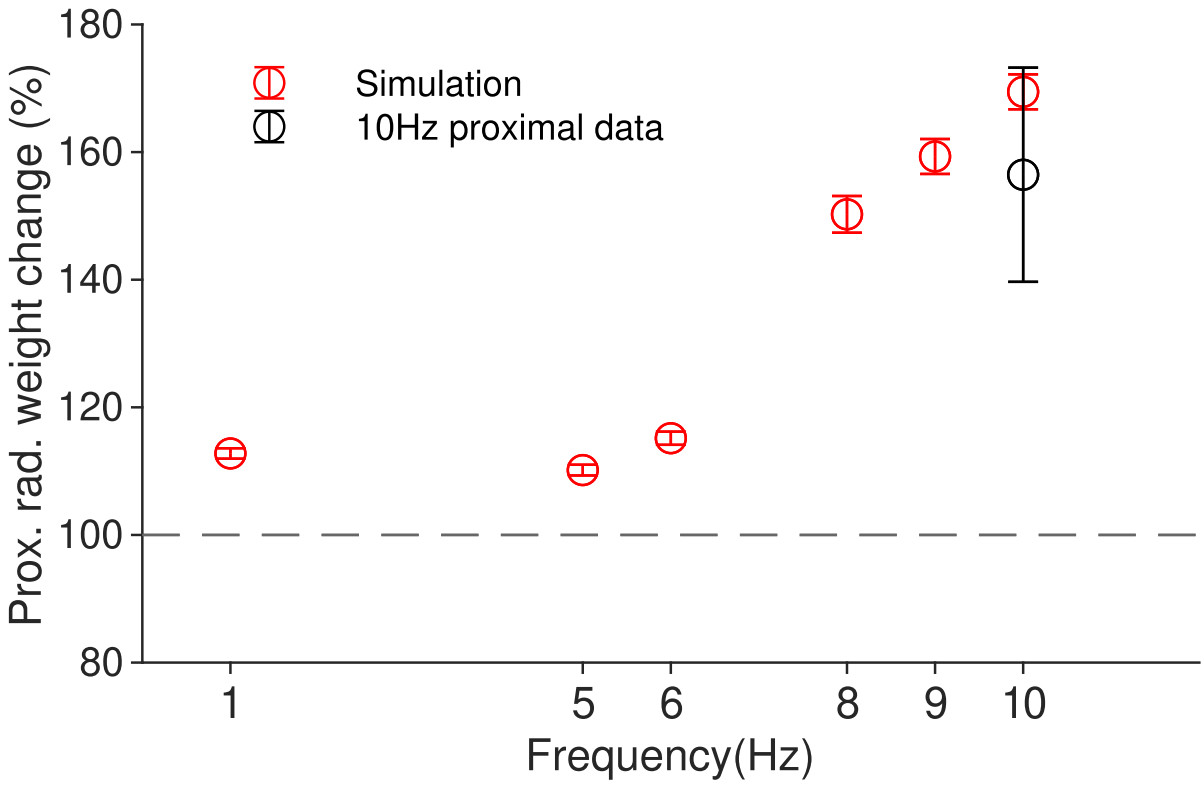

Figure 3.18. Frequency dependence of proximal synapse LTP
Mean synaptic weight increase in proximal (first half of apical trunk) stratum radiatum dendrites (red) decreases with decreasing frequency. At 10Hz, induced proximal LTP is in agreement with range of LTP induction observed in Lenz et al (blue).

Our simulations here show that with rMS, LTP can be induced at much lower frequencies than would otherwise be required with electrical stimulation (Ikegaya, Ishizaka, and Matsuki. 2002), with this LTP induction itself decreasing with lower frequencies.

3.3.3 rMS-induced LTP can be attenuated with pharmacological interventions

In the study of Lenz et al.(Lenz, Platschek, et al. 2015), the induction of LTP by rMS was compared between untreated cultures, and those that had been treated with a variety of drugs known to inhibit LTP induction. These are tetrodotoxin (TTX), a sodium channel blocker (C. H. Lee and Ruben 2008); nifedipine, an L-type calcium channel blocker(Quevedo et al. 1998) and D-AP5, which prevents glutamate binding to NMDA receptors (R. Morris 1989). Under all of these treatments, no significant increase in post-synaptic current amplitude was observed; additionally this occurred when the culture was in a medium absent of Ca^{2+}.

Each of these conditions can be modeled by modifications to the four-pathway plasticity rule and to the cell model. To simulate TTX, all dendritic sodium conductances are set to zero. To simulate nifedipine, all L-type calcium channel conductances are set to zero, and the internal variable corresponding to L-type conductance (and also presynaptic LTP) in the four-pathway model, the variable N is set to zero at every time step (which corresponds to L-type calcium driven plasticity). To simulate D-AP5, the NMDA component of the synaptic model is set to zero, and the variables corresponding to NMDA receptor activation (C) and calcium-modulated LTP (N) are set to zero at every time step. Finally, to simulate a calcium-free medium, all calcium channel conductances in the model are set to zero, and all plasticity pathways dependent on calcium (variables C and N) are zeroed at every time step.

In agreement with the experimental data, simulated TTX application, NMDA suppression, and a simulated calcium-free medium completely eliminated induced LTP from the 10Hz stimulus (Figure 3.19a, b, d), even though the cell did spike in response to the stimulus. Unlike in experiment (Lenz, Platschek, et al. 2015), simulated L-type suppression did substantially reduce the magnitude of LTP (by removing the presynaptic-LTP pathway entirely), but failed to completely extinguish induced LTP, as was observed in experiment (Figure 3.19c). In our model, this is because the postsynaptic LTP pathway is still active.

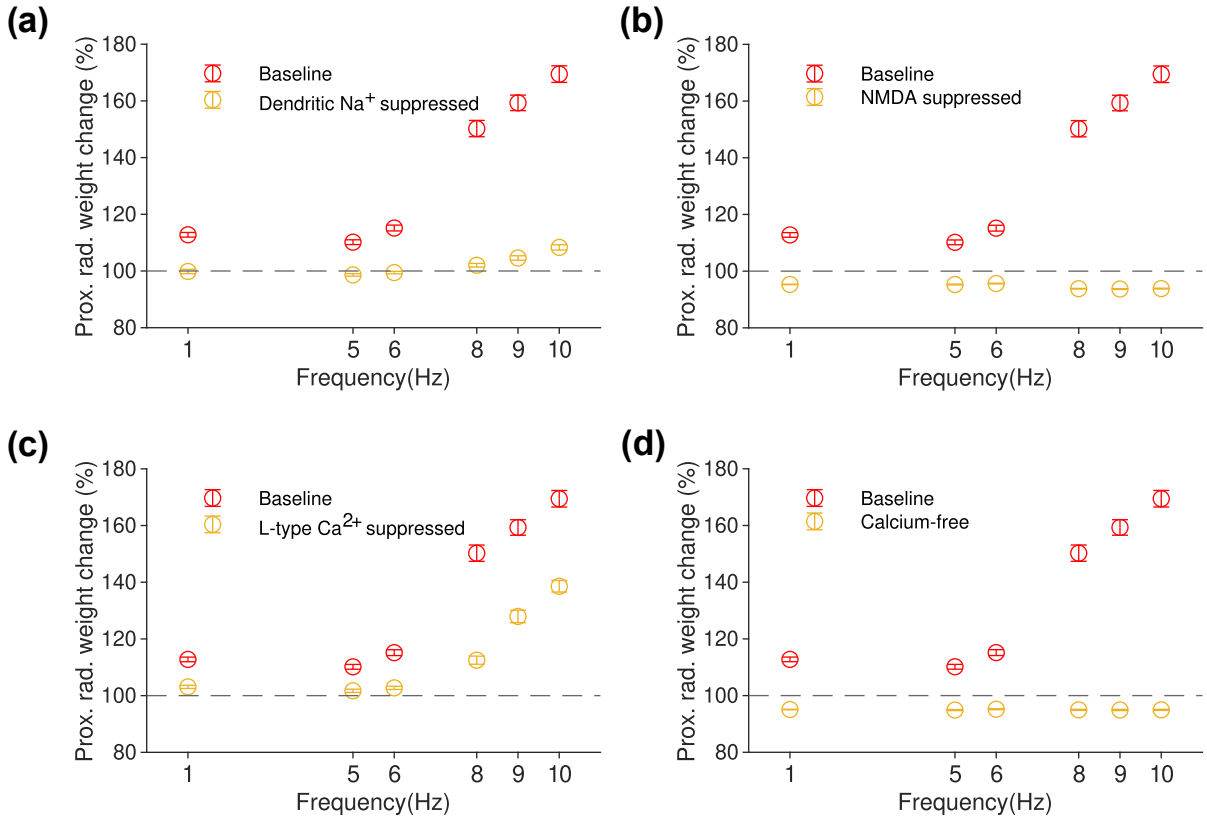

Figure 3.19. NeMo-TMS modelling can reproduce the dependence of rMS-induced LTP on dendritic sodium and calcium, as well as synaptic NMDA channels.
(a): Elimination of LTP when dendritic sodium channels are suppressed, simulating TTX application. *(b)*: Elimination of LTP when NMDA-like processes within the synaptic model are disabled. *(c)*: Large reduction of LTP induction when L-type calcium channels are suppressed. *(d)*: Elimination of LTP observed when calcium-free solution is modeled.

3.3.4 Dependence of LTP induction on TMS stimulation intensity

In most of our simulations, we delivered an rMS stimulus which was 30 percent above the firing threshold of the cell. In the case of our reduced model of the CA1 pyramidal cell, this firing threshold with a monophasic NeMo-TMS pulse was tested to be 210 V/m. We investigated the dependence of the induction of LTP by 10Hz rMS on the amplitude of induced LTP.

We found an intensity-dependence in LTP, with no change observed below the action potential threshold, but with rapid increase in LTP amplitude above the threshold, and diminishing increases with increases much more than 300V/m (Figure 3.20). This indicates that this is both co-operative and subject to a threshold - LTP induction is utterly reliant on the presence of a postsynaptic spike, however that alone is not sufficient to induce large amounts of LTP.

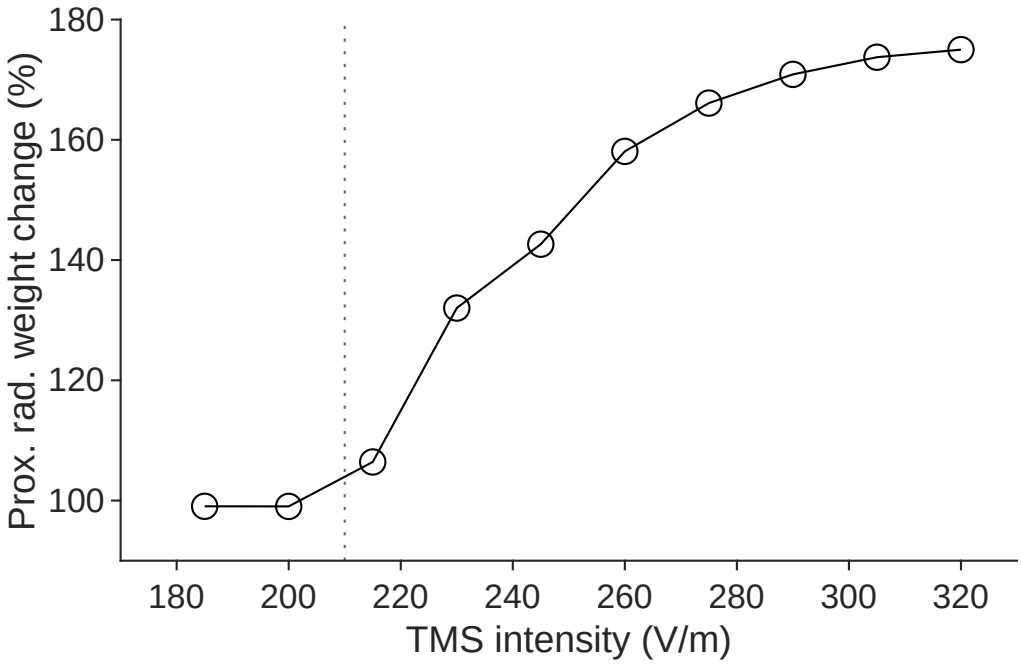

Figure 3.20. Dependence of induced proximal LTP on magnetic stimulation intensity
Below the firing threshold (vertical dotted line), no LTP is induced. Above the threshold, LTP induced by TMS increases quickly, but increases saturate at around 300V/m.

3.3.5 Dependence of LTP induction on TMS stimulation type

Commercial TMS machines are typically capable of producing three types of TMS waveform: monophasic, biphasic, and half-sine NeMo-TMS is capable of monophasic and biphasic stimulation. We compare induction of LTP by a monophasic pulse, as earlier, with that from a biphasic pulse. Monophasic stimulus is associated with larger motor-evoked potential induction than biphasic (Arai et al. 2005).

We compared induction of proximal LTP at the same spread of frequencies with monophasic and biphasic stimulus, with an identical stimulation intensity of 275 V/m. Both biphasic and monophasic stimulation have similar action potential thresholds - monophasic stimulation begins inducing action potentials in this model at 210 V/m, whereas biphasic stimulation has a threshold of 200 V/m.

We find that biphasic stimulus induces substantially less LTP than monophasic stimulus at 10 and 9 Hz, but produces similar effects at lower frequencies (Figure 3.21). Given that both stimulation types have similar action potential thresholds, this suggests that the temporal profile of the magnetic stimulation in the dendrites is important in how the synapses respond - the negative-phase component of the biphasic stimulus may be responsible.

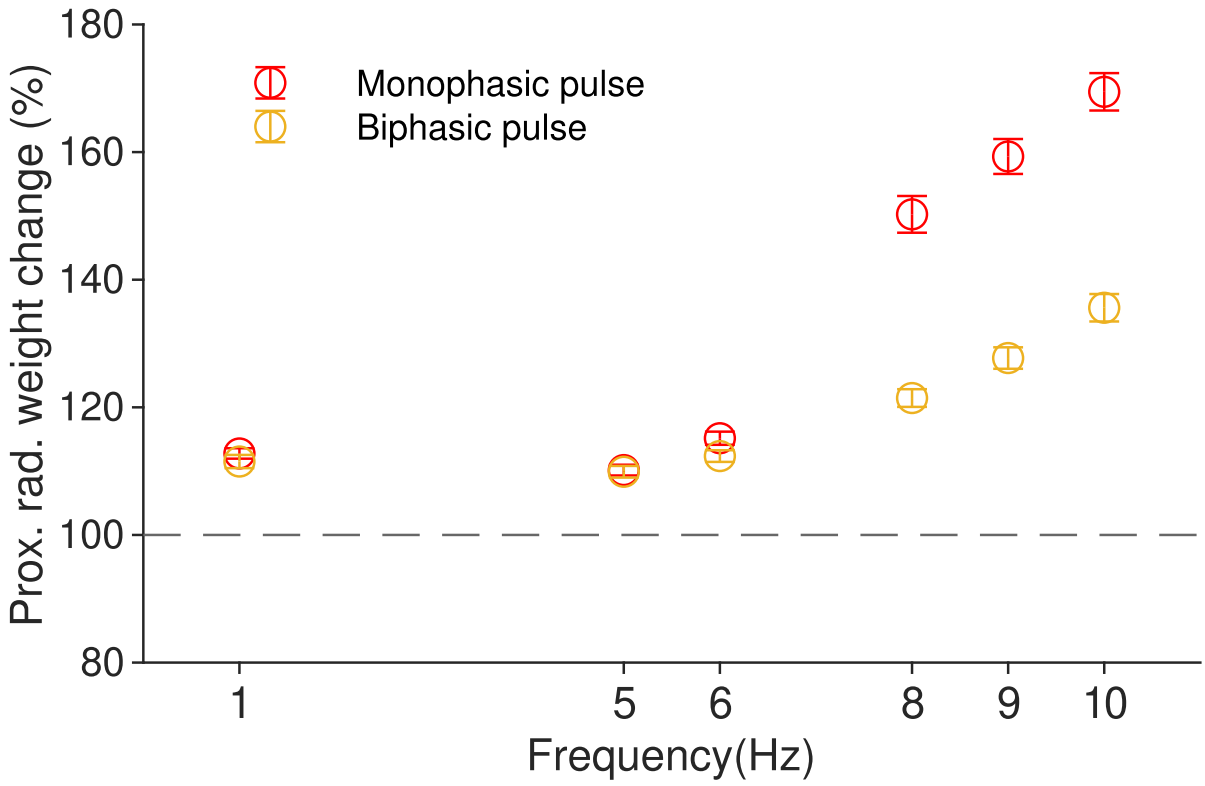

Figure 3.21. Comparison of LTP induced by monophasic and biphasic magnetic stimulation

Biphasic stimulus (red) produces substantially less proximal LTP than monophasic stimulus (blue) does at 9 and 10 Hz, but produces the same amount of LTP at lower frequencies.

3.3.6 Forced pairing protocol

We compared induction of LTP by magnetic stimulation with that of a forced electric pairing protocol. In the forced pairing protocol, we disable magnetic stimulation of the cell. Each synaptic stimulus is paired with a brief (0.5ms) current injection at the soma of sufficient intensity (4 nA) to induce a somatic spike with each stimulus, with an equivalent synaptic activation delay as with our TMS simulations.

In this, we find that the forced pairing protocol is unable to induce large amounts of LTP at any frequency we tested, with a very slight increase in the small amount of induced LTP with increasing frequency (Figure 3.22). This shows that LTP induction by rMS is dependent on the activation of the dendrites by magnetic stimulation as well as the ensuing somatic spike.

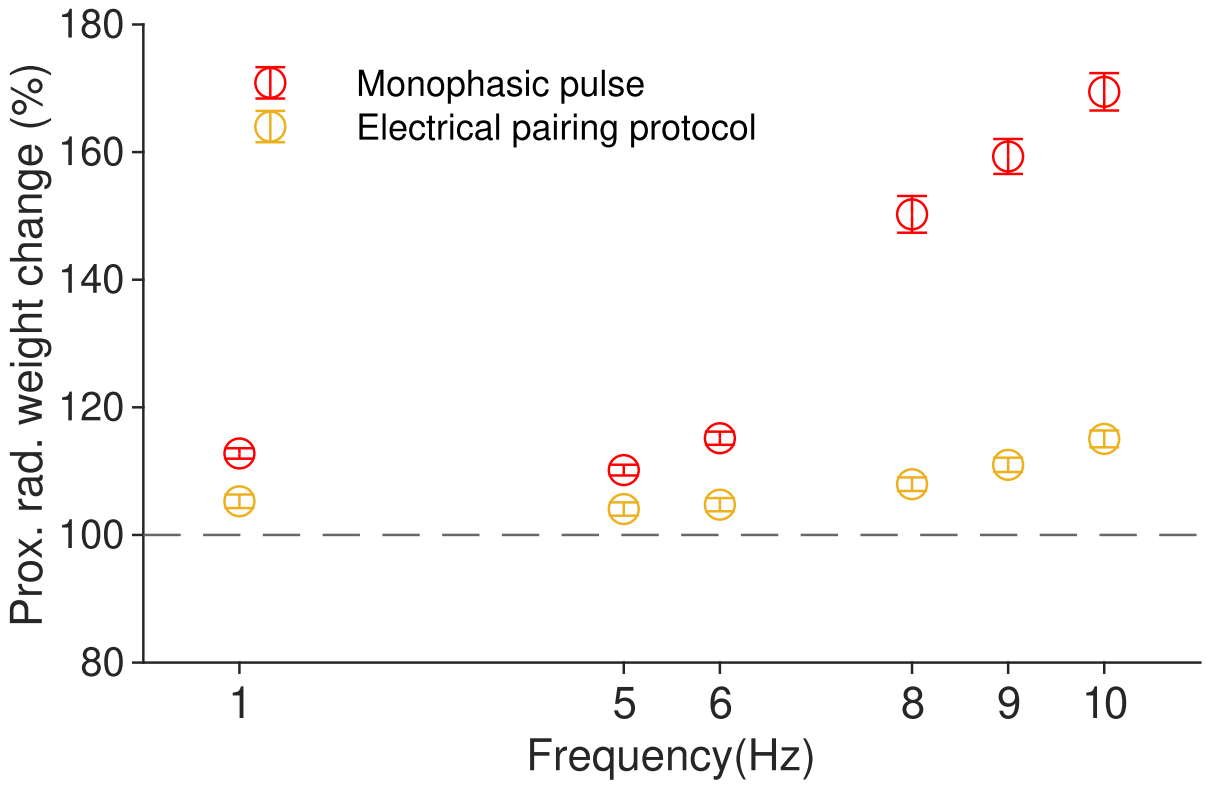

Figure 3.22. Forced pairing protocol cannot induce LTP equivalent to that induced by rMS

Forced pairing protocol fails to induce equivalent LTP to that of rMS at all tested frequencies.

3.3.7 Induction of distal LTP by theta burst protocols

Our model has so far shown that rMS can reliably induce LTP in the proximal dendritic locations of the CA1 pyramidal cell. We investigated under what conditions the distal tuft dendrites (those connected to the perforant path, originating from the entorhinal cortex) could exhibit plasticity in response to rMS.

Induction of LTP in these locations has been shown to rely on the presence of dendritic spikes (Y. Kim et al. 2015), phenomena when active voltage-gated Na^+ and K^+ channels in the dendrites produce a localized spike, rather than a typical somatic spike (which would be generated in the axon initial segment). Dendritic spikes are strongly implicated in dendritic information processing (such as spatial summation and local computation) (Spruston, Häusser, and Stuart 2013). Additionally, dendritic spikes do not necessarily result in somatic spikes, and in the CA1, usually do not unless there is additional activation of the Schaffer collaterals (Jarsky et al. 2005).

Since the four-pathway model of synaptic plasticity, unlike many other plasticity models, does not rely on somatic events for computing plasticity, it is well-suited to investigating the induction of LTP by dendritic spikes and other sub-threshold interactions. In the study of Kim et al., LTP was induced in the tuft synapses of a pyramidal cell by theta-burst stimulation (Y. Kim et al. 2015).

Theta-burst stimulation is a common type of brain stimulation, wherein the tissue is stimulated in short bursts at high frequencies (over 50 Hz), with these short bursts repeated at a frequency typical of the brain's natural theta rhythm of 5-10 Hz. A typical theta burst stimulation train might consist of bursts of four pulses delivered at 100Hz, repeated every 200ms (Larson, Wong, and Lynch 1986). In recent years, theta burst protocols for rTMS have found clinical use, as a clinically useful theta burst rTMS protocol can last only a 1-3 minutes, compared to the 20-40 minutes typical of "classical" rTMS protocols with similar effect (S. W. Chung, Hoy, and Fitzgerald 2015) (L. Oberman et al. 2011).

In the study of Kim et al., the theta burst stimulus was applied electrically to the perforant path synapses of the CA1 pyramidal cell, and consisted of 3 groups of 5 bursts. Each burst was made of 5 pulses at 100 Hz, with an inter-burst interval of 200ms, and an inter-group interval of 30s. (Y. Kim et al. 2015). Since our model is not metaplastic, and because the variables have long since reset to their baselines in the 30 second period, we model this as 15 bursts administered with a 200ms inter-burst interval, since our test simulations found no difference in if an inter-group interval was used or not.

Because the induction of LTP depended on the induction of dendritic spikes, inhibitory current was suppressed by use of GABA antagonists. In the experiments, the soma was prevented from firing; in our simulations we did not find this necessary, as the somatic voltage deflections from the incoming synaptic current are very small, on the order of 2mV, which never produced a somatic spike. For these simulations, the amount of excitatory and inhibitory synapses in the distal tuft region of the model was increased to a level where dendritic spikes were reliably observed.

Because theta burst protocols have found widespread use in rTMS treatments, we additionally simulated magnetic theta burst protocols, both with and without inhibition, to compare and contrast them with LTP induction from electrical-only protocols. In the case of rTMS protocols, we model the theta burst stimulus as a spatially homogeneous biphasic pulse at 275 V/m, along with coincident activation of all synapses in the cell.

We compared the LTP/LTD distance dependence in all four cases: electrical TBS with and without inhibition, and magnetic TBS with and without inhibition (Fig. 3.23).

With purely electrical TBS and no inhibition, LTP was observed in the distal tuft, increasing in magnitude with greater distance.(Fig. 3.23b). This LTP was strongly attenuated by the presence of inhibition. (Fig. 3.23a). In contrast to electrical TBS, we observed LTP in the distal tuft under a theta burst rMS

protocol, both with and without inhibition. (Fig. 3.23c, 3.23d). Similar to the 10 Hz rMS protocol, LTP induction was also observed in more proximal synapses, to a similar extent as in the distal tuft.

Our simulations thus predict distal strengthening of synapses by magnetic theta burst stimulus, of similar magnitude to that induced by a comparable electrical protocol.

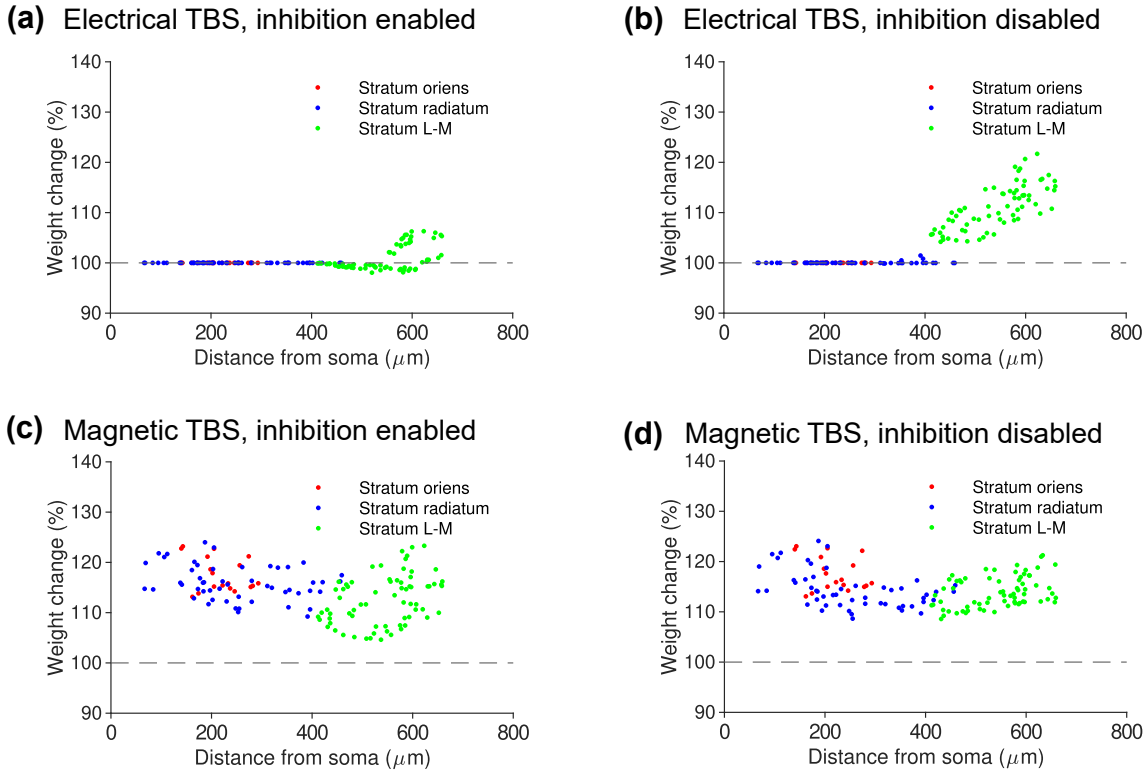

Figure 3.23. The synaptic plasticity model used in NeMo-TMS reproduces and predicts that electric and magnetic TBS are each capable of inducing LTP in the distal tuft.
Induction of LTP by electrical TBS to the perforant path. *(a)*: Negligible plasticity observed when inhibition is present. *(b)*: Distal LTP observed when inhibition is absent. *(c)* LTP in both distal and proximal synapses when magnetic stimulation is used. Unlike electrical TBS, magnetic TBS is able to induce large LTP when inhibition is present. *(d)*: LTP in both distal and proximal synapses when magnetic stimulation is used and inhibition is disabled.

We observed dendritic spikes in the distal tuft of the model when electrical stimulation was delivered in the absence of inhibition. These dendritic spikes only generate small somatic voltage deflections, however the deflections are much larger at the tuft (Figure 3.24). In the presence of inhibition, the dendritic spikes are extinguished.

With magnetic TBS, both somatic and dendritic spikes are induced both in the presence and in the absence of inhibition, explaining why there was no difference in the mean LTP amplitude between when inhibition was enabled and when it was suppressed under magnetic stimulation.

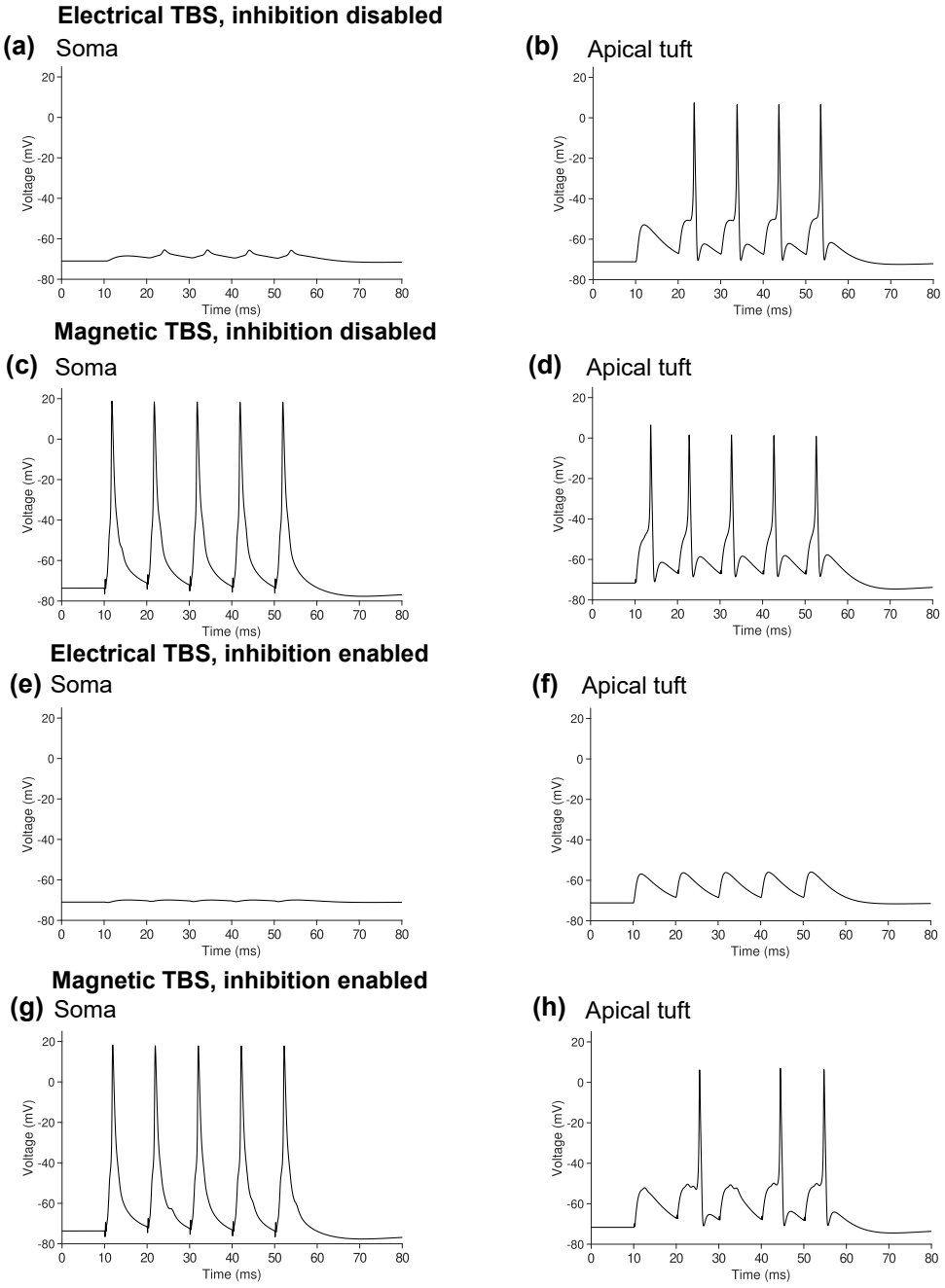

Figure 3.24. Voltage traces from electrical and magnetic TBS, recorded at the soma and apical tuft, account for the outcomes of synaptic plasticity.

(a): 100 Hz electrical TBS only causes small somatic voltage deflections when inhibition is disabled. *(b)*:100 Hz electrical TBS induces dendritic spikes when inhibition is disabled. *(c)*: 100 Hz magnetic TBS causes multiple somatic spikes. *(d)*: 100 Hz magnetic TBS induces dendritic spikes when inhibition is disabled. *(e)*:100 Hz electrical TBS causes almost no somatic voltage deflection when inhibition is enabled. *(f)*: 100 Hz electrical TBS does not induce dendritic spikes when inhibition is enabled. *(g)*: 100 Hz magnetic TBS causes multiple somatic spikes with inhibition enabled. *(h)*: 100 Hz magnetic TBS induces dendritic spikes even when inhibition is enabled.

The study of Kim et al. confirmed the reliance of electrical LTP induction on the presence of dendritic spikes by the application of TTX. Similarly, our model was able to reproduce this result - simulated application of TTX by zeroing of dendritic sodium conductances extinguished the spikes, leading to eliminating plasticity both for electric and magnetic stimulation, although without inhibition, a small amount of LTP is observed when dendritic sodium conductances are zeroed (Figure 3.25).

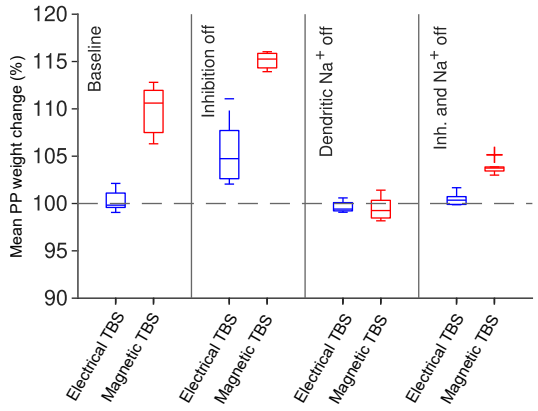

Figure 3.25. Distal LTP induced by magnetic stimulation is less dependent on sodium dendritic spikes and inhibition than electrical stimulation.
Magnetic TBS (red) generates LTP even when electrical-only TBS (blue) does not. In the presence of simulated inhibition, magnetic stimulation induces LTP comparable to electrical stimulation without inhibition (i.e. simulation of bicuculline application). When sodium dendritic spikes are blocked (i.e. simulation of local TTX application), neither of the two stimulation protocols we tested was able to induce LTP in the dendritic tuft. Sample of 10 models with different randomized synapse locations.

3.4 Dependence of cell firing threshold on dendritic and axonal morphology as well as intrinsic cell properties

Publication: Axon morphology and intrinsic cellular properties determine repetitive transcranial magnetic stimulation threshold for plasticity, Galanis et al., 2024

We have observed the magnetic induced action potential to always originate in the terminal of a myelinated axon when simulated in NeMo-TMS (Figure 3.10).

While it is clear that axons and their terminals play a vital and determining role in the initiation of action potentials by TMS (Aman S. Aberra, Angel V. Peterchev, and Grill. 2018)(Aman S Aberra et al. 2020), Figure 3.12, we sought to determine just how determinative this role is.

3.4.1 Axon swapping

To do this, we made use of the TREES Toolbox. TREES Toolbox's ability to quickly import and edit neuronal morphologies is ideal for this task. While the axons and their diverse have an important role, the cells we have access to also have a wide diversity of dendritic morphology.

We imported all 28 cells in our library into TREES Toolbox, and performed morphology edits. Every cell was stripped of its axon, and then the resulting bare dendrite/soma morphology was combined with every other cell's axon, connected at the same place that the original axon emanated from. This connection point can be either the soma or a basal dendrite; almost half of pyramidal cells have their axons emanate from a basal dendrite (Thome et al. 2014), so this morphological quirk was preserved whenever it occurred.

The result was a set of 28x27 = 756 combination morphologies, with the originals included in the set to make an expanded library of 784 cells. Each of these was denoted as "cell x with axon y", with "cell 1 with 1" being the original cell 1, and "cell 1 with 3" being cell 1 with cell 3's axon appended.

We then used NeMo-TMS to endow each of these combination morphologies with the Jarsky model of the CA1 cell, and applied the same myelination that was used in prior simulations. While many of these cells are not hippocampal cells, keeping the biophysics constant will allow us to see the influence of morphology alone. We then assessed the firing threshold of each combination morphology in response to a uniform monophasic TMS stimulus applied in the direction of the somatodendritic axis.

The firing thresholds are shown below, in Figure 3.26.

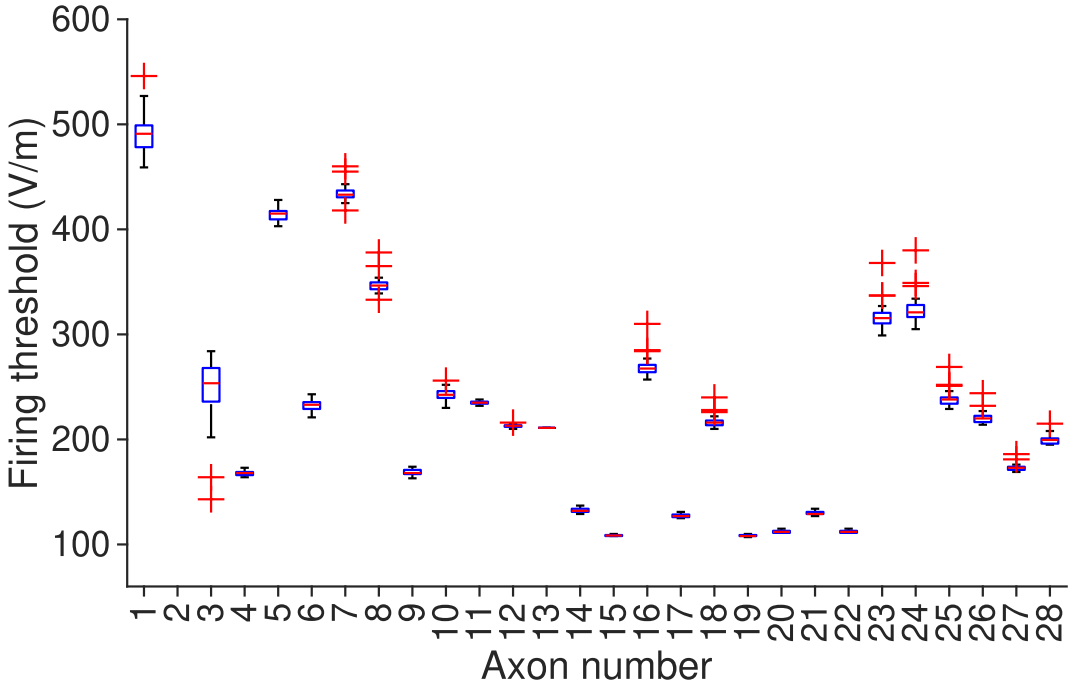

Figure 3.26. Axon morphology is strongly determining of firing threshold.
Magnetic stimulation firing thresholds of a set of 28 different cells with swapped axons, plotted by axon number. While cells with the same axon number have similar firing thresholds, there is still a variance between cells with the same axon.

We found that axon morphology strongly drives the overall cell firing threshold, however it is not entirely determinant - for many of these axon/cell combinations there is a spread of activation threshold values corresponding to different dendrites. Whether or not there is a sizeable spread is dependent on the axon - some of these axons have wide spreads, whereas others have extremely narrow ones.

In the case of axon 2, no combination of axon and dendrites yielded a firing threshold for the range of values we scanned.

The existence of the spread, however, implies that whether or not the cell generates a somatic spike depends somewhat on the properties of the soma and dendrites.

3.4.2 Rat vs. mouse cells

Both rats and mice are widespread animal models for neuroscientific experiments, and rat and mouse hippocampal slice cultures have been widely used (Vlachos, Müller-Dahlhaus, et al. 2012; Ma et al. 2013; Lenz, Platschek, et al. 2015; Lenz, Galanis, et al. 2016; Tokay et al. 2009; Weiler et al. 2023)as targets for investigating many different effects of repetitive magnetic stimulation. Due to the widespread use of

rodent models, understanding the difference in reaction between species is important.

It has been observed (Galanis et al. 2024) that a 10% greater stimulus intensity was required to induce LTP in rat neurons, compared to their mouse counterparts. Below this intensity, no LTP was observed in the rat cells, whereas LTP was observed in the mouse cells.

Since LTP is not only determined by TMS stimulation intensity, our colleagues investigated several other possibilities for the difference. There was also no difference observed between the background network activity between the two species, no major differences in structure (like total dendritic length), and no difference in inhibitory synaptic strength was observed.

We have previously found (Figure 3.20) that LTP induced by TMS, in our simulations, requires a stimulus intensity that is well above the firing threshold of the cell. It is thus reasonable to presume that this difference between rat and mouse cells is caused by a difference in TMS firing threshold.

As the cells are in slice culture, any effects from the difference in brain anatomy between rat and mouse (e.g. from the rat's substantially larger head) will not be relevant. To identify what could cause the difference in firing threshold between rat and mouse cells, we imported ten new cells into NeMo-TMS and endowed them with the Jarsky model - 6 rat cells, and 6 mouse cells, all with detailed reconstructions of their axonal structure. All 12 of these cells have highly branched, realistic axons, as shown in Figures 3.27, 3.28, and 3.29. The cells notably do not have any specific morphological features that would readily explain why the rat cells have higher LTP induction (and presumably firing) thresholds.

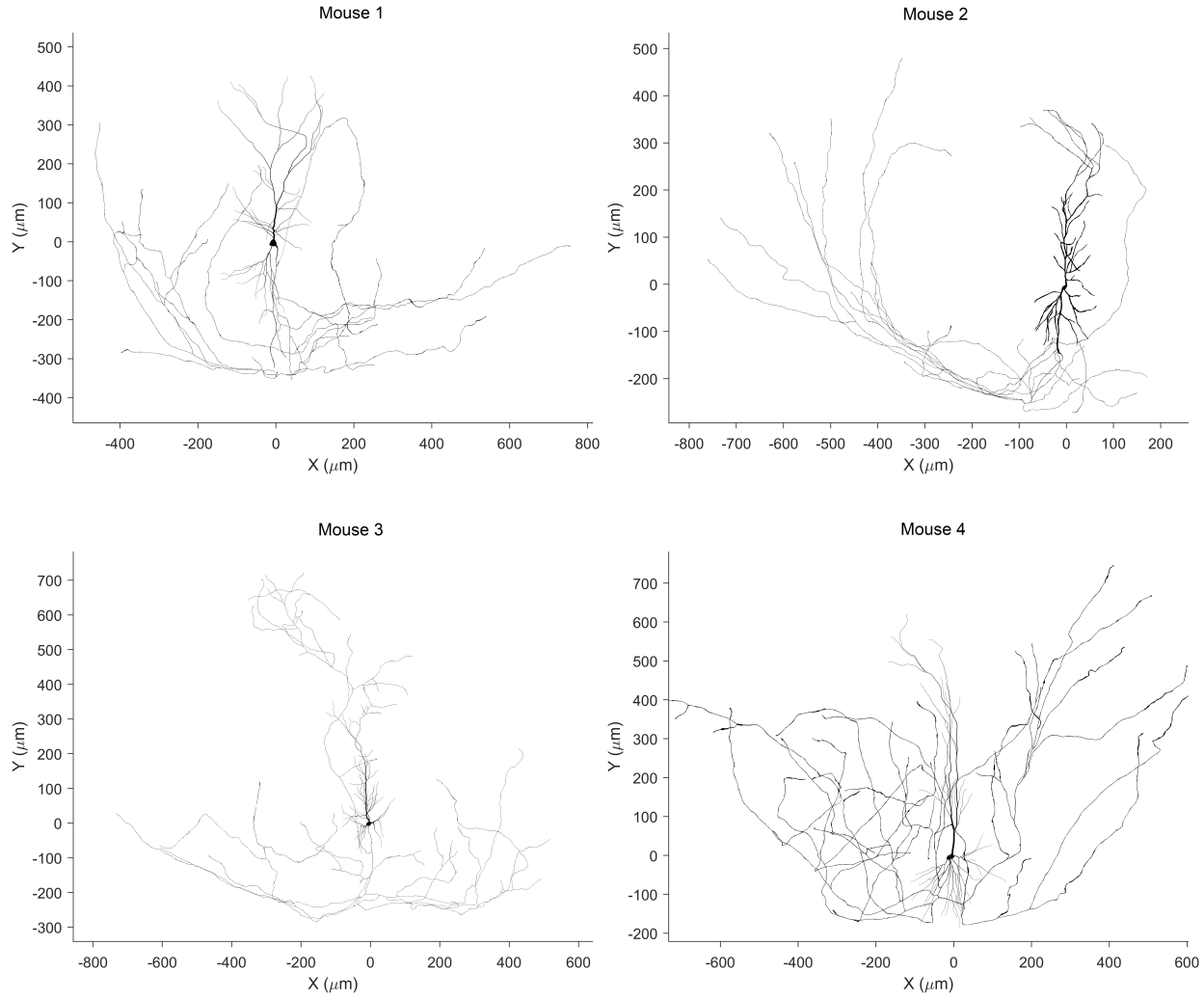

Figure 3.27. Morphologies of mouse and rat CA1 pyramidal cells with highly detailed axons, 1/3.

These mouse and rat cells do not have noticeably divergent morphological features that would explain the systematic difference in TMS induction threshold.

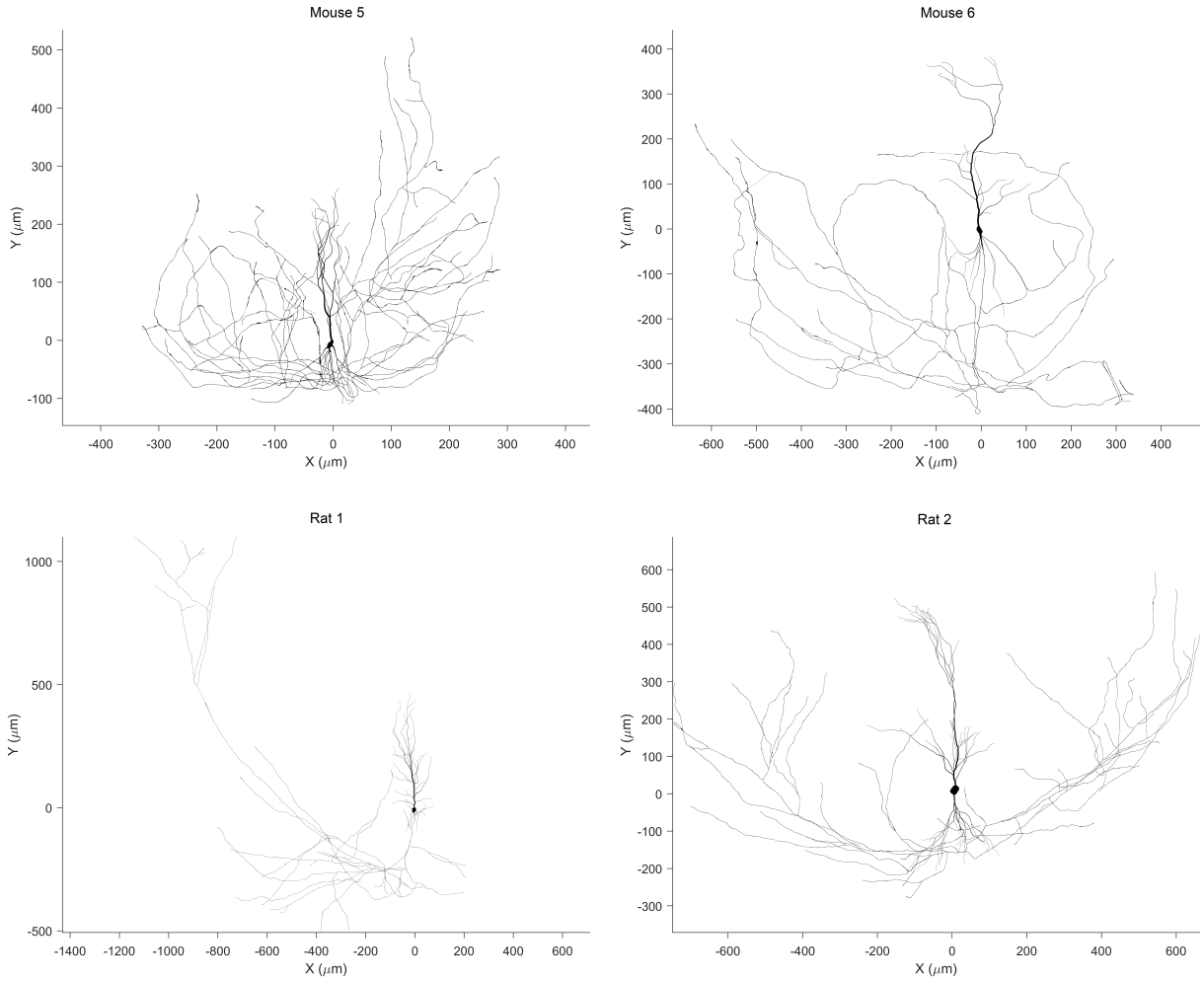

Figure 3.28. Morphologies of mouse and rat CA1 pyramidal cells with highly detailed axons, 2/3.

These mouse and rat cells do not have noticeably divergent morphological features that would explain the systematic difference in TMS induction threshold.

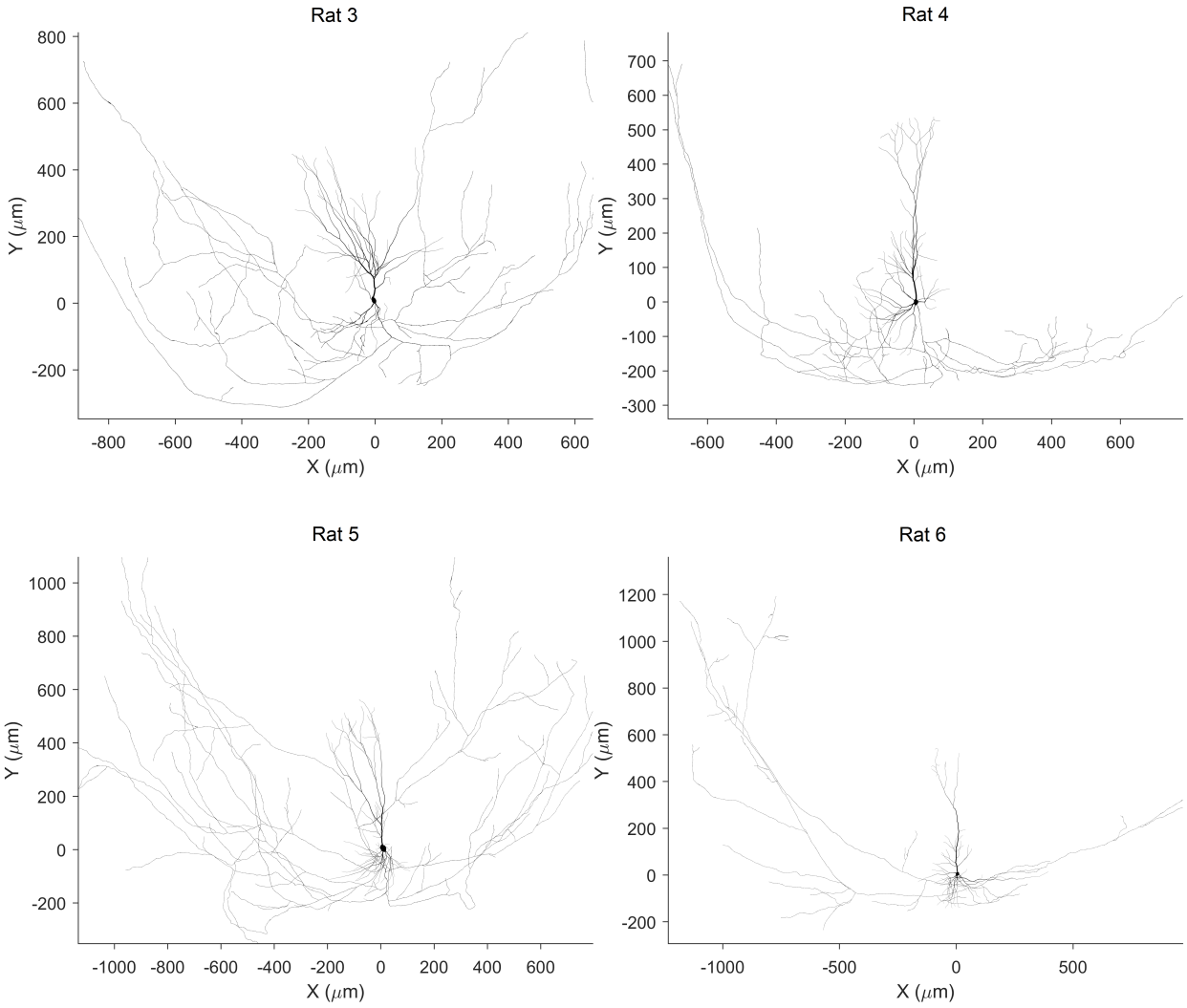

Figure 3.29. Morphologies of mouse and rat CA1 pyramidal cells with highly detailed axons, 3/3.

These mouse and rat cells do not have noticeably divergent morphological features that would explain the systematic difference in TMS induction threshold.

We measured the firing thresholds of these cells and found substantial overlap between the ranges of firing thresholds for the mouse and the rat cells, with the average firing threshold for the rat cells being in fact lower (Figure 3.30).To control for possible dendritic effect, we also endowed all 12 cells with a straight "stick" axon from Figure 2.4.

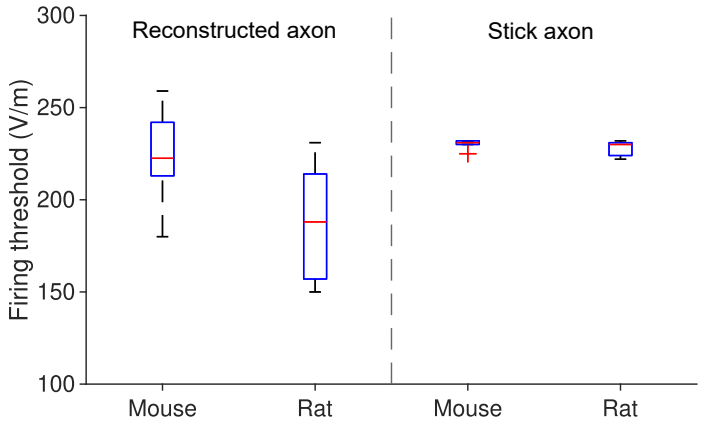

Figure 3.30. Morphology does not explain difference in firing threshold between mice and rats

Firing thresholds of 6 mouse and 6 rat cells under uniform monophasic stimulus. The range of firing thresholds for mouse and rat cells overlap, and there is no difference between the thresholds of mouse and rat cells when they have a simplified "stick" axon.

As expected from our prior investigation into axon swapping, there is no difference in firing threshold between the two groups when they all have the stick axon, showing that any differences in dendritic morphology are also insufficient to explain the increased LTP threshold of rat cells over mouse cells.

Additionally, we repeated an axon swapping analysis with these 12 cells, again measuring for their firing threshold with a uniform monophasic stimulus along the somatodendritic axis. This is shown below in figure 3.31.

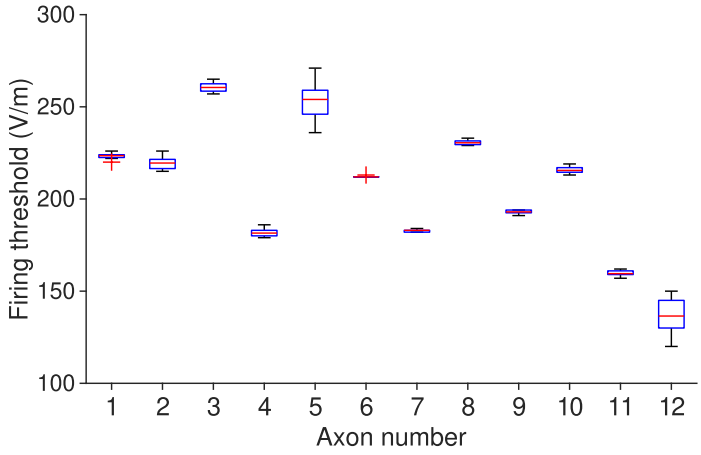

Figure 3.31. Axon swapping with set of detailed rat and mouse morphologies

Axon swapping simulation repeated for set of 12 detailed rat and mouse morphologies; axons 1-6 are mouse and 6-12 are rat.

As with before, axon morphology remains strongly determinant of firing threshold, and the observation of overlap in the thresholds of these two data sets remains.

3.4.3 Difference in intrinsic properties of cells explains difference in TMS LTP induction threshold

With differences in axonal and dendritic morphology ruled out as possible causes for the higher LTP threshold in rat cells, we investigated whether differences in the intrinsic properties of the cells could explain the difference. So far, all cells we have investigated have had identical biophysical properties so that we could isolate any difference caused by morphology.

It is known that mouse CA1 pyramidal cells have higher input resistance than mouse cells. (Bianchi, Migliore, et al. 2022; Migliore et al. 2018; Staff et al. 2000). Input resistance is a measure of a cell's response to a current injection. It is typically measured by injecting hyperpolarizing currents of varying known currents, measuring the steady state voltage after current injection, and defining input resistance by Ohm's law as the slope of the curve of injected current and measured voltage deflection, i.e.

$$R_{in} = \frac{\Delta V}{I} \tag{3.1}$$

Our colleagues measured the average input resistance of the mouse cells to be $148 \pm 10 M\Omega$ and the input resistance of the rat cells to be $67.27 \pm 4.33 M\Omega$. We tuned our 12 cells to these values, giving four sets of resulting models - mouse cells with mouse-like R_{in}, mouse cells with rat-like R_{in}, rat cells with mouse-like R_{in}, and rat cells with rat-like R_{in}.

To accomplish this, we modified the Jarsky model. Input resistance is influenced by, among other factors, the passive membrane conductance (see g_l in Figure 1.7), and potassium channels like the K_A (or KV4) channel (J. Kim, Wei, and Hoffman 2005). Three properties in the Jarsky model were adjusted with a scaling constant - the passive conductance (gpas), the A-type potassium channel, and the delayed-rectifier (Manis 2022) potassium channel.

Additionally, to enable us to explore the high-resistance (low axonal potassium) parameter regime, for all of this set of simulations, to prevent issues we encountered with spontaneous firing, the sodium conductance in the axon terminals was lowered by 50% of its value in all other simulations.

This enabled us to individually calibrate each cell to both the mouse-like (a target of $150 M\Omega$) and rat-like (a target of $70 M\Omega$) cell properties. Because the input resistance depends on, among other things, dendritic morphology, each cell needed to be individually tuned and have its input resistance measured.

For almost all of these morpologies, the base observed input resistance fell between the targets of $70 M\Omega$

for low input resistance, with the only exception being cell 11, which had a very low base input resistance. In every other case, low input resistance cases required upscaling of the three chosen parameters and high input resistance required downscaling them.

Even with the modifications made, we still observed spontaneous firing in 3 models - these were cell 4, cell 9, and cell 11. For the high input resistance case for these three cells, we increased the input resistance as high as it could be reached without spontaneous firing happening. In the case of cell 4, this was $118M\Omega$, for cell 9, this was $129M\Omega$, and for cell 11 it was $88M\Omega$.

With this new set of 24 models, we determined the TMS activation threshold for each, as shown below in Figure 3.32.

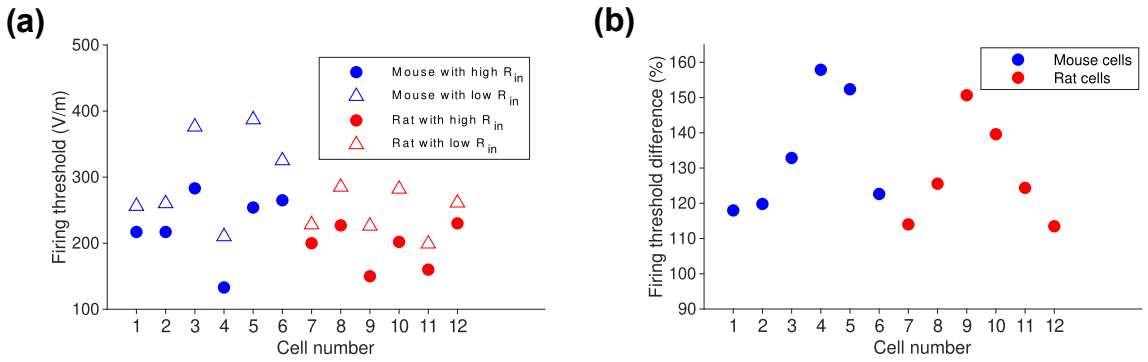

Figure 3.32. Decreased input resistance associated with increased firing threshold in both rat and mouse cells

Versions of cells with lowered (rat-like) input resistance always exhibit higher firing thresholds than those with higher (mouse-like) input resistances. *(a)*: Firing thresholds of all cells (1-6 mouse, in blue; 7-12 rat, in red) tuned to reach both lower and higher input resistance. *(b)*: Difference between firing threshold for low R_{in} and high R_{in} versions of each cell, as a percentage.

We see that for every one of the 12 cells we tested, there was a higher firing threshold for the version of that cell which was tuned to a lower input resistance. For the mouse morphologies, the lower input resistance (rat-like) cells had a between a 18% and 58% higher firing threshold than the low input resistance, and for the rat morphologies, the rat-like variant cells had between a 13% and 50% higher threshold for low input resistance over high input resistance.

Since the real rat cells had a 10% higher LTP induction threshold than their mouse counterparts, it is possible that this observed lower input resistance for mouse cells is responsible for the difference in TMS stimulation intensity required to elicit LTP, as our simple modelling here showed substantial increases in firing threshold from our scaling of relevant parameters.

Chapter 4

Discussion

In this work we have developed a toolbox for linking macro-scale simulation of brain stimulation with electric fields in SimNIBS, to meso-scale simulation of neurons and their action potential, to the micro-scale of synaptic plasticity and calcium dynamics. Additionally, we have explored some of the behaviors of cells when exposed to magnetic simulation, including the localized nature of synaptic plasticity and pharmacological perturbations to it, propagation of action potentials through axons, and the causes of the difference in firing threshold between two species of rodent. It is obvious that TMS has an effect; however, it affects so many scales of the brain's structure at once that approaches at many different levels need to be synthesized to gain a complete picture. While the tools we have created do not entirely solve this problem, the tools allow us to investigate many of the phenomena induced by TMS at appropriate scales.

4.1 NeMo-TMS: Unifying scales of neuroscientific simulation of transcranial magnetic simulation

When a brain is subjected to transcranial magnetic stimulation, large areas of the brain are activated. This is an inevitable consequence of the fact that the field must be strong enough to penetrate the skull, and penetrate far enough into the brain tissue to stimulate the target area.

Improving coil design means that this is an improving area of technology - more recent treatment protocols involve targeting deeper areas of the brain than the superficial targets in the cortex (Samoudi et al. 2018) using more advanced coil designs like the H-coil (Gutierrez et al. 2022), achieved through more sophisticated coil geometries than the classical figure-of-eight TMS coil. As the stimulation targets deeper areas in the brain, the resulting interaction between magnetic field, brain tissue, and electric

field will become more complicated, and, as such, the marriage of SimNIBS to NEURON and calcium modelling that NeMo-TMS offers becomes more attractive.

It is worth noting, however, that there are certain important effects that NeMo-TMS can not capture. While the various local connectivity regimes in localized cell clusters is somewhat well known for many brain regions such as the hippocampus (Maller et al. 2019; Witter 2010) and cortical columns (Schubert, Kötter, and Staiger 2007), there are always going to be limitations associated with modelling single cells with simulated input pathways. Considering that large volumes of brain tissue are activated by the TMS pulse (Huerta and Volpe 2009), in areas with recurrent connectivity, interneuron networks, glia, and other such features, all of which will presumably in some way be activated by a TMS pulse, a single-cell approach will inevitably be limited.

However, even with this in mind, modelling single neurons embedded within a volume of brain matter is still extremely useful. When TMS is used in a clinical context, in order to have a beneficial effect on the patient, the correct dosing must be applied; in this case dosing can refer to session length, TMS field intensity, and amount of sessions. There are several methods of calibrating the dosing; these include AMT(active motor threshold), EF (electric-field-based intensity selection) FL (functional lesion threshold), FXD (fixed intensity), PT (phosphene threshold), RMT (resting motor threshold), and TT, tolerability threshold.

Of these, the motor threshold based approaches are the most common(Turi, Lenz, et al. 2021). In the motor threshold based approach, the motor cortex of the patient is stimulated with ever-increasing TMS pulses until a movement in the hand with 50% of trials. (Herbsman et al. 2009; Pridmore et al. 1998). Some fraction of this threshold (for example, 120%) is then applied to the actual target of the TMS stimulus, which for major depressive disorder, is within the dorsolateral prefrontal cortex (DLPFC) (Pascual-Leone, Rubio, et al. 1996; Balconi and Ferrari 2013), although alternate prefrontal targets have been suggested as possibly effective locations. (M. Zhang et al. 2021).

NeMo-TMS has been recently used (Turi, Hananeia, et al. 2022) as a tool in aiding this dosing process for TMS research. In their paper, Turi et al. used NeMo-TMS to place human layer 5 cells (specifically the Aberra(Aman S. Aberra, Angel V. Peterchev, and Grill. 2018) model included in the NeMo-TMS release (Sina Shirinpour et al. 2021)) in both the motor cortex and the DLPFC, and found that the methods used to calibrate the dose based on motor threshold produced variable electric fields in the motor cortex and DLPFC. They proposed combining NeMo-TMS with scans of the patient's head to produce personalized calibration based on simulated electric fields using NeMo-TMS.

NeMo-TMS, however, does have a major shortcoming: The calcium simulation is only one-way. This means that the calcium modelling is entirely done after the full run of the NEURON simulation, and is fully reliant on the produced voltage trace. This means that there is no feedback element: the NEURON

simulation is unable of using the results of the calcium simulation internally. This could be important, as there exist channels which influence local membrane voltage that are dependent on Ca^{2+} ions to open, such as calcium-activated potassium channels (K_{Ca} channels)(Vergara et al. 1998; Kshatri, Gonzalez-Hernandez, and Giraldez 2018), and sodium ion channels can be blocked or otherwise influenced by the presence of Ca^{2+} ions. (Armstrong and Cota 1999; Shah, Chagot, and Chazin 2006).

While NEURON models do include modelling of calcium accumulation (such as via the CaDynamicsE2 mod (Hay et al. 2011)), these are very simplified relative to reaction-diffusion treatments. As such, crucial dynamics of the neuron's spiking pattern may be missing when there is no feed-back simulation of calcium dynamics. However, implementing such a solution would be extremely difficult, as it would require real-time communication between two distinct simulation frameworks, and the attendant increase in computational resources required to run the simulation.

4.2 Synaptic plasticity in response to repetitive magnetic simulation

rMS has been shown to induce LTP in a subset of proximal synapses (Lenz, Platschek, et al. 2015). We have extended NeMo-TMS with a plasticity model that allows investigation of location-specific effects within the cell with high precision. While this is not the first attempt to model plasticity induced by repetitive magnetic stimulation (Robinson 2011) by several different stimulus protocols (P. Fung and Robinson 2014; Wilson, Goodwin, et al. 2014; Wilson, Park K Fung, et al. 2016; Wilson, Fulcher, et al. 2018), all of these approaches did not represent individual neurons with detailed morphology - they used mean-field models of averaged groups of neurons. By combining multi-compartmental modelling with a voltage-based plasticity rule, we have explored a more granular level of detail, enabling examination of location-dependent effects in the somata and dendrites of the cell.

We have introduced a detailed and robust phenomenological model of synaptic plasticity into the NeMo-TMS toolbox and used it to replicate data and make predictions about location and frequency dependence of plasticity induced by rMS. While the model we chose is very detailed (Ebner et al. 2019), it is reasonable to question why a simpler model of synaptic plasticity was not chosen. After all, the model we chose has a great many free parameters, which can result in extremely laborious manual tuning process, as the outcomes of the simulation show great sensitivity to parameters such as initial weights, LTP/LTD amplitudes, and the saturation/decay rates of various internal variables.

Initially, we attempted to use the mSTDP model (Benuskova and Abraham 2007) to reproduce the results of Lenz et al (Lenz, Platschek, et al. 2015) in the reduced model of the CA1 pyramidal cell before it was decided to move on to a more detailed model (Hananeia, Ebner, et al. 2024). We were

unable to reproduce any of the rMS-based result sets for the combination of the mSDTP model, the reduced morphology, and NeMo-TMS. We were, however, able to induce LTP in the model by synaptic stimulation as in Ikegaya (Ikegaya, Ishizaka, and Matsuki. 2002). We believe this reason is several-fold: Firstly, the mSTDP model relies on pairings of somatic spikes and presynaptic events to make any changes to the weight of the synapse in question. While spike-based models of plasticity have seen wide use, we believe that subthreshold events within the cell can be responsible for an important part of plasticity induction (Johnston et al. 2003; Fino, Deniau, and Venance 2009; Seong, Behnia, and Carter 2014). In addition to EPSPs, active dendrites of cells can also produce dendritic spikes (Golding, Staff, and Spruston 2002), which unless specifically accounted for are invisible to spiking based models. Since rMS depolarizes not just the soma (or indeed not just the axon), but the entire cell, we made the assumption that local voltage-based events were perhaps necessary to understanding the plasticity effects of rMS.

Notably, our model reproduces the result of Lenz (2015) (Lenz, Platschek, et al. 2015), where proximal synapses strongly potentiate, whereas no LTP is observed in distal synapses. This is likely possible because of the voltage-based nature of the model - as a backpropagating action potential spreads through the neuron, the potential attenuates, and more distal synapses experience less local depolarization from the same spike. Spiking-based models would also be able to reproduce some of this effect, since spike timing dependent plasticity accounts for the attenuation of bAPs with its rapid exponential decline on the LTP ampltitude with time. However, a spiking based model would be unable to reproduce the effect that local inhibitory synapses can play, and local inhibition is known to have an effect on regulating LTP/LTD (Debanne, Gähwiler, and Thompson 1996).

We predict a rapid decrease in induced LTP amplitude with lower stimulation frequency than 10Hz. This frequency dependence likely occurs because the model's internal variables decay on a long enough timescale that subsequent TMS pulses and their attendant backpropagating action potentials boost the LTP variables (specifically C, T, and N) to higher values than individual paired pulses could. Given that these mechanisms have close biological correlates with equivalent time scales (Ebner et al. 2019), it is reasonable to conclude that a similar fall-off at lower stimulation frequencies will be observed in-vitro as well.

Our comparison of forced somatic spikes at 10Hz versus rMS suggests that this is likely the case (Figure 3.22), as the electrical pairing protocol proved totally unable to produce LTP amplitudes anywhere near that of rMS. Additionally, since we observed a notable difference in LTP induction between monophasic and biphasic stimulus (with biphasic causing less sustained depolarization in the dendrite) (Figure 3.21), it seems likely that co-operative effects between the local depolarization at the site of the synapse and the backpropagating action potential are responsible for the large induced LTP for 10Hz rMS. Although

the influence of the rMS pulse in causing a somatic action potential lies nearly strictly with the axon, the difference in LTP induction between these two stimulus regimes shows that rMS has important effects on the soma and dendrites as well.

Motivated by the strong distance dependence we observed for LTP induced by low-frequency rMS, we investigated under what circumstances LTP could be induced in the distal tuft synapses of the CA1 pyramidal cell. These synapses do not connect to CA3 via the Schaffer collaterals, instead projecting from layer III of the entorhinal cortex (Megıas et al. 2001; Takahashi and Magee 2009), and these synapses have limited effect on the soma of the cell on account of their distance (Jarsky et al. 2005).

The study of Kim et al (Y. Kim et al. 2015) provided some circumstances under which LTP could be induced at these distal synapses. To investigate this, we replicated their theta-burst protocol and found that in the absence of inhibition, we were able to induce LTP in these distal synapses with local electrical stimulation, although not to the same amplitudes as observed in that study with our chosen set of parameters.

Since theta-burst stimulus is often used as a TMS delivery protocol (S. W. Chung, Hoy, and Fitzgerald 2015; L. Oberman et al. 2011), we applied it to the cell along with coincident activation of all synapses. We found that rMS-TBS produced consistent LTP in all areas in the cell without significant attenuation over distance (Figure 3.23). In these simulations, magnetic stimulation produced a somatic action potential with almost every stimulus, with depolarization at the distal tuft similar with or without inhibition, contrasted with local electric stimulation where dendritic spikes were eliminated in the presence of inhibition, leading to substantial reduction in induced LTP. (Figure 3.24).

Therefore, because of these strong backpropagating action potentials rMS-TBS was able to induce LTP in these distal synapses, unlike local electrical TBS when LTP was blocked by inhibition. In the case where we simulated TTX treatment of the dendrites by blocking dendritic sodium conductances, LTP was prevented in all cases, since the backpropagating action potentials were unable to be sustained all the way to the tuft without active sodium conductance, and local dendritic spikes were likewise prevented.

We found that rMS at high frequency (such as in our theta-burst stimulation) is able to overcome the block that inhibition otherwise places on LTP induction at the distal tuft synapses at the tuft. Examining the voltage traces from these events, we see (Fig 3.24) presumed dendritic spikes. This co-operative interplay of large somatic spiking events with dendritic subthreshold events shows that spiking is not the totality of causative factors for LTP induction.

It is worth noting, however, that in clinical use, theta burst magnetic stimulation to facilitate treatment is usually not administered in protocols similar to those of Kim et al. Typically, in clinical use, an

intermittent theta burst protocol is used when a higher frequency protocol than a 10Hz TMS protocol is desired. (Bulteau, Veronique Sébille, et al. 2017; Bulteau, Laurin, et al. 2022; Morriss et al. 2024). An intermittent theta burst protocol might be structured as follows: 3 stimuli at 50 Hz (burst) separated at a theta frequency (200ms between bursts), in groups of 10 bursts, with a delay of 10 seconds between groups. The protocol used is shown below in Figure 4.1.

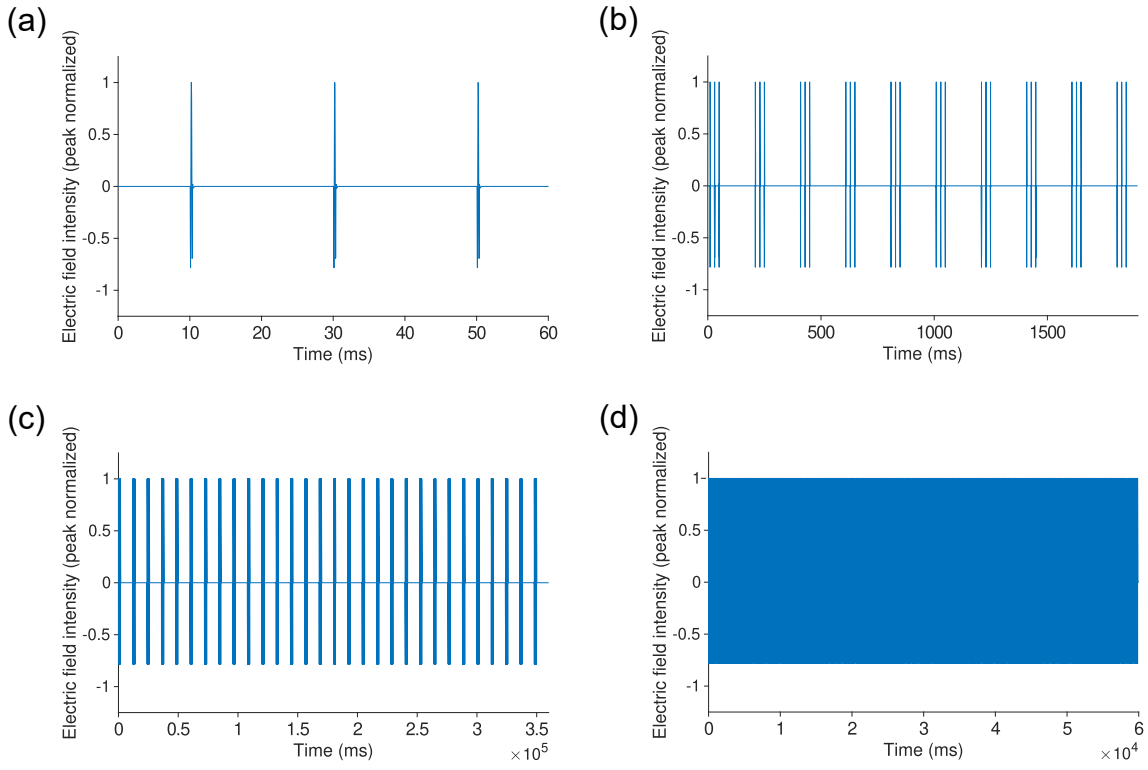

Figure 4.1. Stimulus protocol for intermittent and continuous theta burst stimulation
TMS stimulus protocol for intermittent and continuous theta burst stimulus viewed at different time scales. (a): Single burst, 10 are contained in a train. (b): Single group of 10 bursts. (c): Full 900 pulse intermittent TBS train; contains 30 trains separated by 10 seconds. (d): Full 900 pulse continuous TBS train; contains 30 trains with no inter-train interval.

This intermittency may be key. Compared to continuous theta burst stimulus, where there is no delay between burst groups, intermittent TBS has been found to have different effects clinically and in experiment. (Aceves-Serrano et al. 2022; Thimm and Funke 2015; C.-W. Lee et al. 2023). Intermittent TBS is known to induce LTP-like effects, whereas continuous TBS induces LTD-like effects (Suppa et al. 2016).

We performed a brief simulation with our model and found that our model exhibited no difference in observed plasticity between intermittent and continuous theta burst stimulation; both induced strong LTP of identical magnitude (Figure 4.2).

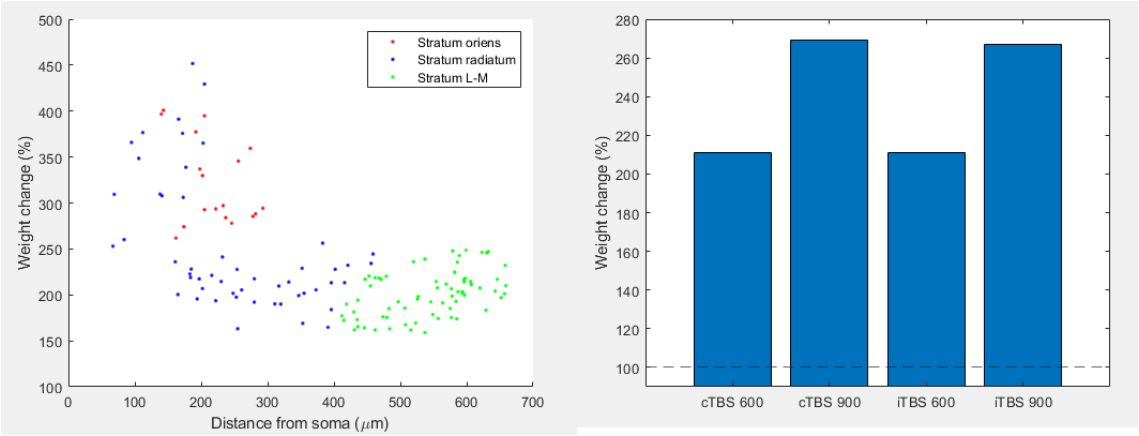

Figure 4.2. Model shows no difference between intermittent and continuous theta burst stimulation

No observed difference in induced LTP from intermittent or continuous theta burst stimulus *(a)*: Distance profile of induced LTP from 900-pulse intermittent theta burst stimulus *(b)*: Mean LTP amplitude for intermittent and continuous theta burst stimulation, 600 and 900 pulses.

We also compared the difference between 600 and 900 pulse intermittent and continuous TBS protocols. A 900 pulse iTBS protocol has been found to be potentiating, with a similar 600 pulse protocol having no effect or being depressive (Private communication, Christos Galanis, 2023). We do not observe any such difference between the 600 and 900 pulse protocols; indeed, the 600 pulse protocol produces almost exactly two thirds of the mean LTP of the 900 pulse protocol for both intermittent and continuous TBS.

This highlights a key limitation of the Ebner(Ebner et al. 2019) plasticity model: it does not feature metaplasticity. Given that metaplasticity results in higher cell activity causing greater difficulty in inducing LTP (and indeed a switch to LTD with sufficiently high activity within the history window)(Bienenstock, L. N. Cooper, and Munro 1982)(Benuskova and Abraham 2007), it is reasonable to assume that the "rest periods" between theta burst clusters allow the cell's activity levels to stabilize and the LTP/LTD threshold to favor LTP before the next stimulus onset, whereas without such a rest period, the cell may come to favor LTD or suppress further LTP.

Augmenting the Ebner model to include metaplasticity may make reproduction of such results possible. A proposed way to do this is with a similar sliding threshold that is used in the mSTDP(Benuskova and Abraham 2007) model, with the $< c(t) >$ multiplier applied to the LTP/LTD amplitudes in the Ebner model (as in Eq. 2.4 and 2.5), a modification which has been previously made to other models (Hananeia and Benuskova 2016). However, whether to apply these only to the presynaptic pathways, only to the postsynaptic pathways, or both, is an open question, since the actual synaptic mechanisms of metaplasticity remain somewhat elusive (Zorumski and Izumi 2012; Wankerl et al. 2010). Including metaplasticity would also significantly increase the amount of time required to tune the model, since

weight increases/decreases are not linear with metaplasticity, abbreviated simulations would be of little help for tuning.

When we examine the effect of pharmacological perturbation on induced rMS 3.19, we find that our model was able to reproduce the effect of a calcium-free solution and blockade of NMDA receptors. Our simulated application of TTX to the dendrites showed that even if the soma is allowed to spike, backpropagation of the action potential into the dendritic tree being severely limited by the lack of active Na^+ channels prevented the induction of LTP. However, it is worth noting that simulated blockade of the L-type calcium channel (Ca_L), which is known to be important for certain LTP pathways distinct to the NMDA-dependent pathway (Huber, Mauk, and Kelly 1995; Weisskopf, Bauer, and J. E. LeDoux 1999; Plumbly et al. 2019), did not produce the result exhibited in Lenz (2015)(Lenz, Platschek, et al. 2015), where there was no significant difference in EPSP amplitude between a control cell and one that had been treated with nifedipine, a specific L-type calcium antagonist. This likely shows a limitation of the plasticity model - with the L-type pathway eliminated, the NMDA pathway was still able to induce large amounts of LTP, implying that there is some interaction between the presynaptic LTP pathway and the NMDA pathway.

This result brings the earlier limitation of NeMo-TMS into focus: many mechanisms of synaptic plasticity rely on calcium, and calcium diffusion is certain to have some role in mediating how LTP works. (Evans and Blackwell 2015), especially at locations within the cell (such as the human cortical neuron's "calcium hot spot", a location near the distal tuft where there is a high concentration of voltage-gated CA^{2+} receptors (Hay et al. 2011)). The model that we implement is not a biophysical model (Ebner et al. 2019); although it does have internal variables that correspond to various signaling pathways, these are entirely internal to the model. A combination of a calcium-aware synaptic plasticity model and an improvement to NeMo-TMS that is able to incorporate calcium diffusion results into the NEURON simulation could perhaps reproduce the expected shutdown of LTP from application of nifedipine.

Another effect that we do not account for is inhibitory plasticity. In our model, we presume inhibitory synapses are non-plastic: this is known not to be the case (Vogels, Sprekeler, et al. 2011; Vogels, Froemke, et al. 2013; Capogna, Castillo, and Maffei 2021; Gandolfi et al. 2020). Inhibitory plasticity may be important in the context of rMS, since rMS has been shown to cause reduction in strength of GABAergic inhibitory synapses (Lenz, Galanis, et al. 2016; Lenz and Vlachos 2016). This reduction of inhibitory synaptic strength will lead to an increase in the overall excitability of the cell; this is known as disinhibition (Möhler and U. Rudolph 2017; Artinian and Lacaille 2018), and serves as an LTP-independent pathway for experience to increase the cell's firing rate. Disinhibition could be important as a mechanism of action for TMS (Vlachos, Funke, and Ziemann. 2017; R. Cash et al. 2010), and incorporation of a robust model of inhibitory plasticity into NeMo-TMS could prove useful, especially

when excitation/inhibition balance is a possible factor in some of the mental illnesses that TMS is used to treat.

Modifications to the inhibitory circuits in the targeted neurons may also play some part in explaining why cTBS does not have an equivalent LTP-like effect to an equivalent iTBS protocol. Such effects may combine with metaplasticity in non-intuitive ways.

Additionally, this is strictly a single-cell model, and any network effects are thus impossible to observe. Although the CA1 region does not feature significant direct recurrent connections (connections from CA1 axons to their parent cells or other CA1 neurons), there are recurrent connections to inhibitory interneurons in the region. Additionally, the hippocampus is known to have gap junctions (Spruston 2001; Beheshti, Hosseini, et al. 2014; Beheshti, Eivani, and Moshtaghian 2015), which are not modelled in this simulation, and may have difficult to predict network effects on synaptic plasticity, especially when gap junctions themselves may be uniquely affected by magnetic stimulation.

Additionally, we entirely neglect the effect of neuromodulation. Further work could implement some of the additional features we neglected, and perhaps shed further light on the dynamics of LTP induction by rMS.

4.3 Species difference in induction of long-term potentiation and induction of action potentials

Rodent CA1 pyramidal neurons are usually seen as morphologically similar (Routh et al. 2009), and as we see from our visual comparison of reconstructed adult neurons from the two species (Figures 3.27, 3.28, 3.29), they are of similar size, with apical dendrite lengths of 400 - 500 $\mu\ m$. Despite this, the rat neurons in slice culture were observed to require 10 percent greater stimulus intensity to produce long-term potentiation in response to TMS.

Because we had observed that no LTP is observed below the TMS firing threshold (Figure 3.20), we made an assumption that some factor that influences the firing threshold would be responsible for the higher amount of stimulus necessary to elicit LTP from rat cells.

Since we have established that axon morphology (along with, of course, stimulation intensity and stimulation angle, but in this case angle was kept constant) is nearly wholly determinant for the firing threshold, we presumed there would be some systematic difference between mouse and rat CA1 axonal branching structures. We could not observe any - there was no visible difference between the two cells' axon structures (Figures 3.27, 3.28, 3.29), and we could not see any significant difference between TMS firing threshold between the species, aside from a greater variance on the mouse cells.

Input resistance is mediated by both intrinsic properties and the overall size of the cell - smaller cells tend to have a higher input resistance, and thus be more excitable (Cuntz, Bird, et al. 2021). However, although the rat is a larger animal, and thus should have larger cells, we do not see rat cells being sufficiently larger in our dataset to explain this. Also, we measured input resistance with default parameters in the Jarsky model for the cells in our collection, and found results between 65 - 120 $M\Omega$ - middling between the expected values for the mouse (150 $M\Omega$) and rat (70 $M\Omega$).

Because of this, we concluded that intrinsic properties must be responsible, and we were able to derive a possible explanation in the raised input resistance of the rat cell, presumably caused by the greater presence of A-type potassium (Kv4) channels in rat cells (Private commmunication, Christos Galanis). When tuning these values, A-type potassium levels in the axon were chiefly responsible for the change in the TMS spike induction threshold. Because tuning the input resistance to mouse-like and rat-like values yielded a substantial difference in firing threshold, we feel reasonable to conclude this is a substantial contributing factor.

There could, however, be other contributing factors. We only examine a single cell; cells in slice cultures still have attendant interneurons, glia, and other local networks. As these would inevitably be stimulated by the TMS pulse, differences in the morphologies or intrinsic properties of these other cells could be a factor, especially when TMS is known to induce disinhibition (R. F. Cash et al. 2016), which can facilitate boosting of LTP.

Modelling of this problem not as a factor of only spike threshold, but with a full plasticity simulation such as that used in Section 3.3. However, this would have attendant problems. Firstly, the models of our rat and mouse cells are extremely morphologically complex and detailed. Although it would be trivial to add the plasticity model we used in Section 3.3 to the model, actually running it would be more complicated, since dozens to hundreds the amount of compute time would be required. Additionally, plasticity models are extremely sensitive to parameters, which would magnify the compute time issue, since many runs of the simulation would be needed to successfully set the parameters to a large and detailed morphology.

Another factor that could be missed is simply sample size. While we did not observe sufficiently different axonal morphology diversity between the two species, it is very possible that if we had a larger data set to examine with the same quality of axon reconstruction, meaningful differences might emerge. However, the availability of cell reconstructions with detailed axons is scant; most axons available in the literature have either their axons removed, their axons cut, or only have single unbranching axons reconstructed. This is, of course, a result of the extreme labor requirement in reconstructing dendritic and axonal morphologies by hand, as is still the standard practice in morphological studies (Donohue and Ascoli 2011), as the overwhelming bulk of morphologies available on the NeuroMorpho

database (Ascoli, Donohue, and Halavi 2007) are manually reconstructed, although recent development in automatic reconstruction tools is promising (Radojević and Meijering 2019; Januszewski et al. 2018; Y. Liu et al. 2022).

Publications

The research contained within this doctoral thesis was used for the purpose of three different publications, one of which is in preparation.

Open-source toolbox for multi-scale modelling of single neurons under transcranial magnetic stimulation.

Brain Stimulation: Basic, Translational, and Clinical Research in Neuromodulation, 2021

Sina Shirinpour and Nicholas Hananeia and James Rosado and Harry Tran, Christos Galanis and Andreas Vlachos and Peter Jedlicka and Gillian Queisser and Alexander Opitz.

Multi-scale modelling of location- and frequency-dependent synaptic plasticity induced by transcranial magnetic stimulation in the dendrites of pyramidal neurons

In preparation, available as preprint on BioRxiv:
https://www.biorxiv.org/content/10.1101/2024.07.03.601851v1

Nicholas Hananeia and Christian Ebner and Christos Galanis and Alexander Opitz and Andreas Vlachos and Peter Jedlicka

---

Axon morphology and intrinsic cellular properties determine repetitive transcranial magnetic stimulation threshold for plasticity

Frontiers in Cellular Neuroscience, 2024

Christos Galanis and Lena Neuhaus and Nicholas Hananeia and Zsolt Turi and Peter Jedlicka and Andreas Vlachos

---

Acknowledgements

I am very grateful for the wisdom, insight, support, and guidance of my doctoral supervisor, Prof. Dr. Peter Jedlicka in the years of my PhD studies; he has been a continuous source of both professional and personal support throughout my time studying in Germany.

I am also extremely thankful to Prof. Dr. Christian Heiliger, for his agreement to supervise my thesis for submission in the faculty of Physics.

I thank my collaborators and colleagues; particularly Dr. Sina Shirinpour, for our ongoing collaboration in the development and deployment of the NeMo-TMS tool, and Christian Ebner, for his ready help with understanding the behavior of his synaptic plasticity model.

I would additionally like to thank the Federal Ministry of Education and Research, Germany , for providing funding for the research that underlies this thesis. (BMBF, 01GQ2205B to PJ, 01GQ2205A to AV). Additionally, I thank the FAZIT-Stiftung for their financial aid in the year of 2022-2023.

As a note of personal thanks, I would like to thank everyone who has supported me personally during my journey to completing my doctoral thesis. I thank my colleagues in my research group - Martin, Nina, Moritz, and Alex, for countless hours of company and personal support, as well as endless insights without which this work would have been impossible. Finally, I thank my parents back home in New Zealand, whose daily video calls have kept me sane in my journey on the other side of the world, especially during the tribulations brought by the pandemic.

Declaration

I declare that I have written this dissertation single-handedly without any unauthorized help of another party, and only with the assistance acknowledged herein. I have appropriately acknowledged and cited all text passages that are derived verbatim from or are based on the content of published work of others, and all information relating to verbal communications. I consent to the use of anti-plagiarism software to check my thesis. I have abided by the principles of good scientific conduct laid down in the charter of the Justus Liebig University Giessen in carrying out the investigations discussed in the dissertation.

Giessen, September 18, 2024,

Nicholas Hananeia.

Bibliography

Abbott, Larry F (1999). "Lapicque's introduction of the integrate-and-fire model neuron (1907)". In: *Brain research bulletin* 50.5-6, pp. 303–304.

Aberra, Aman S, Boshuo Wang, Warren M Grill, and Angel V Peterchev (2020). "Simulation of transcranial magnetic stimulation in head model with morphologically-realistic cortical neurons". In: *Brain stimulation* 13.1, pp. 175–189.

Aberra, Aman S., Angel V. Peterchev, and Warren M. Grill. (2018). "Biophysically realistic neuron models for simulation of cortical stimulation." In: *Journal of neural engineering* 15.6, p. 066023.

Abraham, Wickliffe C (2008). "Metaplasticity: tuning synapses and networks for plasticity". In: *Nature Reviews Neuroscience* 9.5, pp. 387–387.

Aceves-Serrano, Lucero, Jason L Neva, Jonathan Munro, Martin Parent, Lara A Boyd, and Doris J Doudet (2022). "Continuous but not intermittent theta burst stimulation decreases striatal dopamine release and cortical excitability". In: *Experimental Neurology* 354, p. 114106.

Alekseichuk, I, S Shirinpour, and A Opitz (2020). *Finite element method (FEM) models for translational research in non-invasive brain stimulation.*

Alekseichuk, Ivan, Kathleen Mantell, Sina Shirinpour, and Alexander Opitz (2019). "Comparative modeling of transcranial magnetic and electric stimulation in mouse, monkey, and human". In: *Neuroimage* 194, pp. 136–148.

Amaral, David G (1993). "Emerging principles of intrinsic hippocampal organization". In: *Current opinion in neurobiology* 3.2, pp. 225–229.

Andersen, Per (1975). "Organization of hippocampal neurons and their interconnections". In: *The Hippocampus: Volume 1: Structure and Development*. Springer, pp. 155–175.

Andrade-Talavera, Yuniesky, Andre Fisahn, and Antonio Rodriguez-Moreno (2023). "Timing to be precise? An overview of spike timing-dependent plasticity, brain rhythmicity, and glial cells interplay within neuronal circuits". In: *Molecular Psychiatry*, pp. 1–12.

Arai, Noritoshi, Shingo Okabe, Toshiaki Furubayashi, Yasuo Terao, Kaoru Yuasa, and Yoshikazu Ugawa (2005). "Comparison between short train, monophasic and biphasic repetitive transcranial magnetic stimulation (rTMS) of the human motor cortex". In: *Clinical neurophysiology* 116.3, pp. 605–613.

Armstrong, CM and Gabriel Cota (1999). "Calcium block of Na+ channels and its effect on closing rate". In: *Proceedings of the National Academy of Sciences* 96.7, pp. 4154–4157.

Artinian, Julien and Jean-Claude Lacaille (2018). "Disinhibition in learning and memory circuits: new vistas for somatostatin interneurons and long-term synaptic plasticity". In: *Brain research bulletin* 141, pp. 20–26.

Ascoli, Giorgio A, Duncan E Donohue, and Maryam Halavi (2007). "NeuroMorpho. Org: a central resource for neuronal morphologies". In: *Journal of Neuroscience* 27.35, pp. 9247–9251.

Balconi, Michela and Chiara Ferrari (2013). "Repeated transcranial magnetic stimulation on dorsolateral prefrontal cortex improves performance in emotional memory retrieval as a function of level of anxiety and stimulus valence". In: *Psychiatry and Clinical Neurosciences* 67.4, pp. 210–218.

Barranca, Victor J, Asha Bhuiyan, Max Sundgren, and Fangzhou Xing (2022). "Functional implications of dale's law in balanced neuronal network dynamics and decision making". In: *Frontiers in Neuroscience* 16, p. 801847.

Beheshti, Siamak, Mehdi Eivani, and Jamal Moshtaghian (2015). "Gap junctions of the hippocampal CA1 area are crucial for memory consolidation". In: *Physiology and Pharmacology* 19.3, pp. 177–184.

Beheshti, Siamak, Seyyed Akbar Mir Seyyed Hosseini, Maryam Noorbakhshnia, and Mehdi Eivani (2014). "Role of hippocampal CA1 area gap junction channels on morphine state-dependent learning". In: *European Journal of Pharmacology* 745, pp. 196–200.

Beining, Marcel, Lucas Alberto Mongiat, Stephan Wolfgang Schwarzacher, Hermann Cuntz, and Peter Jedlicka (2017). "T2N as a new tool for robust electrophysiological modeling demonstrated for mature and adult-born dentate granule cells". In: *Elife* 6, e26517.

Bekkers, John M (2000). "Distribution and activation of voltage-gated potassium channels in cell-attached and outside-out patches from large layer 5 cortical pyramidal neurons of the rat". In: *The Journal of physiology* 525.3, pp. 611–620.

Benarroch, Eduardo E (2013). "HCN channels: function and clinical implications". In: *Neurology* 80.3, pp. 304–310.

Bennett, Michael VL and R Suzanne Zukin (2004). "Electrical coupling and neuronal synchronization in the mammalian brain". In: *Neuron* 41.4, pp. 495–511.

Benuskova, Lubica and Wickliffe C Abraham (2007). "STDP rule endowed with the BCM sliding threshold accounts for hippocampal heterosynaptic plasticity". In: *Journal of computational neuroscience* 22, pp. 129–133.

Bestmann, Sven and John W Krakauer (2015). "The uses and interpretations of the motor-evoked potential for understanding behaviour". In: *Experimental brain research* 233, pp. 679–689.

Bi, Guo-qiang and Mu-ming Poo (1998). "Synaptic modifications in cultured hippocampal neurons: dependence on spike timing, synaptic strength, and postsynaptic cell type". In: *Journal of neuroscience* 18.24, pp. 10464–10472.

Bianchi, Daniela, Addolorata Marasco, Alessandro Limongiello, Cristina Marchetti, Helene Marie, Brunello Tirozzi, and Michele Migliore (2012). "On the mechanisms underlying the depolarization block in the spiking dynamics of CA1 pyramidal neurons". In: *Journal of computational neuroscience* 33, pp. 207–225.

Bianchi, Daniela, Rosanna Migliore, Paola Vitale, Machhindra Garad, Paula A Pousinha, Helene Marie, Volkmar Lessmann, and Michele Migliore (2022). "Membrane electrical properties of mouse hippocampal CA1 pyramidal neurons during strong inputs". In: *Biophysical Journal* 121.4, pp. 644–657.

Bienenstock, Elie L, Leon N Cooper, and Paul W Munro (1982). "Theory for the development of neuron selectivity: orientation specificity and binocular interaction in visual cortex". In: *Journal of Neuroscience* 2.1, pp. 32–48.

Blais, B. S. and L. Cooper (2008). "BCM theory". In: *Scholarpedia* 3.3. revision #91041, p. 1570. DOI: 10.4249/scholarpedia.1570.

Bolwig, Tom G and Max Fink (2009). "Electrotherapy for melancholia: the pioneering contributions of Benjamin Franklin and Giovanni Aldini". In: *The journal of ECT* 25.1, pp. 15–18.

Borges, Ricardo and Antonio G Garcia (2021). "One hundred years from Otto Loewi experiment, a dream that revolutionized our view of neurotransmission". In: *Pflugers Archiv-European Journal of Physiology* 473.6, pp. 977–981.

Breit, Markus, Martin Stepniewski, Stephan Grein, Pascal Gottmann, Lukas Reinhardt, and Gillian Queisser (2016). "Anatomically detailed and large-scale simulations studying synapse loss and synchrony using NeuroBox". In: *Frontiers in Neuroanatomy* 10, p. 8.

Brown, Richard E, Thaddeus WB Bligh, and Jessica F Garden (2021). "The Hebb synapse before Hebb: theories of synaptic function in learning and memory before, with a discussion of the long-lost synaptic theory of William McDougall". In: *Frontiers in Behavioral Neuroscience* 15, p. 732195.

Bullitt, Elizabeth (1990). "Expression of c-fos-like protein as a marker for neuronal activity following noxious stimulation in the rat". In: *Journal of Comparative Neurology* 296.4, pp. 517–530.

Bulteau, Samuel, Andrew Laurin, et al. (2022). "Intermittent theta burst stimulation (iTBS) versus 10 Hz high-frequency repetitive transcranial magnetic stimulation (rTMS) to alleviate treatment-resistant unipolar depression: A randomized controlled trial (THETA-DEP)". In: *Brain Stimulation* 15.3, pp. 870–880.

Bulteau, Samuel, Veronique Sébille, et al. (2017). "Efficacy of intermittent Theta Burst Stimulation (iTBS) and 10-Hz high-frequency repetitive transcranial magnetic stimulation (rTMS) in treatment-resistant unipolar depression: study protocol for a randomised controlled trial". In: *Trials* 18, pp. 1–10.

Burkitt, Anthony N (2006). "A review of the integrate-and-fire neuron model: I. Homogeneous synaptic input". In: *Biological cybernetics* 95, pp. 1–19.

Capogna, Marco, Pablo E Castillo, and Arianna Maffei (2021). "The ins and outs of inhibitory synaptic plasticity: Neuron types, molecular mechanisms and functional roles". In: *European Journal of Neuroscience* 54.8, pp. 6882–6901.

Carnevale, T. (2007). "Neuron simulation environment". In: *Scholarpedia* 2.6. revision #154131, p. 1378. DOI: 10.4249/scholarpedia.1378.

Casanova, Manuel F, Estate M Sokhadze, Emily L Casanova, and Xiaoli Li (2020). "Transcranial magnetic stimulation in autism spectrum disorders: Neuropathological underpinnings and clinical correlations". In: *Seminars in pediatric neurology*. Vol. 35. Elsevier, p. 100832.

Cash, RFH, Ulf Ziemann, Kevin Murray, and Gary W Thickbroom (2010). "Late cortical disinhibition in human motor cortex: a triple-pulse transcranial magnetic stimulation study". In: *Journal of Neurophysiology* 103.1, pp. 511–518.

Cash, Robin FH, Takenobu Murakami, Robert Chen, Gary W Thickbroom, and Ulf Ziemann (2016). "Augmenting plasticity induction in human motor cortex by disinhibition stimulation". In: *Cerebral Cortex* 26.1, pp. 58–69.

Cassidy, Jessica M, Bernadette T Gillick, and James R Carey (2014). "Priming the brain to capitalize on metaplasticity in stroke rehabilitation". In: *Physical therapy* 94.1, pp. 139–150.

Casula, Elias P, Giorgio Leodori, Jaime Ibáñez, Alberto Benussi, Vishal Rawji, Sara Tremblay, Anna Latorre, John C Rothwell, and Lorenzo Rocchi (2022). "The Effect of Coil Orientation on the Stimulation of the Pre–Supplementary Motor Area: A Combined TMS and EEG Study". In: *Brain Sciences* 12.10, p. 1358.

Chervyakov, Alexander V., Andrey Yu Chernyavsky, Dmitry O. Sinitsyn, and Michael A. Piradov. (2015). "Possible mechanisms underlying the therapeutic effects of transcranial magnetic stimulation." In: *Frontiers in human neuroscience* 9, p. 303.

Chou, Ying-hui, Patrick T Hickey, Mark Sundman, Allen W Song, and Nan-kuei Chen (2015). "Effects of repetitive transcranial magnetic stimulation on motor symptoms in Parkinson disease: a systematic review and meta-analysis". In: *JAMA neurology* 72.4, pp. 432–440.

Chung, Sung Wook, Kate E Hoy, and Paul B Fitzgerald (2015). "Theta-burst stimulation: A new form of TMS treatment for depression?" In: *Depression and anxiety* 32.3, pp. 182–192.

Cimino, Guido (1999). "Reticular theory versus neuron theory in the work of Camillo Golgi." In: *Physis; rivista internazionale di storia della scienza* 36.2, pp. 431–472.

Cole, Jonathan C, Carolyn Green Bernacki, Amanda Helmer, Narsimha Pinninti, and John P O'reardon (2015). "Efficacy of transcranial magnetic stimulation (TMS) in the treatment of schizophrenia: a review of the literature to date". In: *Innovations in clinical neuroscience* 12.7-8, p. 12.

Connors, Barry W and Michael A Long (2004). "Electrical synapses in the mammalian brain". In: *Annu. Rev. Neurosci.* 27, pp. 393–418.

Cuntz, Hermann, Alex D Bird, Martin Mittag, Marcel Beining, Marius Schneider, Laura Mediavilla, Felix Z Hoffmann, Thomas Deller, and Peter Jedlicka (2021). "A general principle of dendritic constancy: A neuron's size-and shape-invariant excitability". In: *Neuron* 109.22, pp. 3647–3662.

Cuntz, Hermann, Alexander Borst, and Idan Segev (2007). "Optimization principles of dendritic structure". In: *Theoretical Biology and Medical Modelling* 4, pp. 1–8.

Cuntz, Hermann, Friedrich Forstner, Alexander Borst, and Michael Häusser (2010). "One rule to grow them all: a general theory of neuronal branching and its practical application". In: *PLoS computational biology* 6.8, e1000877.

– (2011). *The TREES toolbox—probing the basis of axonal and dendritic branching.*

Cutsuridis, Vassilis, Bruce P Graham, Stuart Cobb, and Imre Vida (2019). *Hippocampal microcircuits: a computational modeler's resource book.* Springer.

Debanne, Dominique, Beat H Gähwiler, and Scorr M Thompson (1996). "Cooperative interactions in the induction of long-term potentiation and depression of synaptic excitation between hippocampal CA3-CA1 cell pairs in vitro." In: *Proceedings of the National Academy of Sciences* 93.20, pp. 11225–11230.

Deng, Zhi-De, Sarah H Lisanby, and Angel V Peterchev (2013). "Electric field depth–focality tradeoff in transcranial magnetic stimulation: simulation comparison of 50 coil designs". In: *Brain stimulation* 6.1, pp. 1–13.

Di Lazzaro, Vincenzo et al. (2021). "Diagnostic contribution and therapeutic perspectives of transcranial magnetic stimulation in dementia". In: *Clinical neurophysiology* 132.10, pp. 2568–2607.

Donohue, Duncan E and Giorgio A Ascoli (2011). "Automated reconstruction of neuronal morphology: an overview". In: *Brain research reviews* 67.1-2, pp. 94–102.

Ebner, Christian, Claudia Clopath, Peter Jedlicka, and Hermann Cuntz. (2019). "Unifying long-term plasticity rules for excitatory synapses by modeling dendrites of cortical pyramidal neurons." In: *Cell reports* 29.13, pp. 4295–4307.

Evans, RC and KT Blackwell (2015). "Calcium: amplitude, duration, or location?" In: *The Biological Bulletin* 228.1, pp. 75–83.

Feldman, Daniel E (2012). "The spike-timing dependence of plasticity". In: *Neuron* 75.4, pp. 556–571.

Fino, Elodie, Jean-Michel Deniau, and Laurent Venance (2009). "Brief subthreshold events can act as Hebbian signals for long-term plasticity". In: *PLoS One* 4.8, e6557.

Fritschy, Jean-Marc (2008). "Epilepsy, E/I balance and GABAA receptor plasticity". In: *Frontiers in molecular neuroscience* 1, p. 201.

Fung, PK and PA Robinson (2014). "Neural field theory of synaptic metaplasticity with applications to theta burst stimulation". In: *Journal of theoretical biology* 340, pp. 164–176.

Galanis, Christos, Lena Neuhaus, Nicholas Hananeia, Zsolt Turi, Peter Jedlicka, and Andreas Vlachos (2024). "Axon morphology and intrinsic cellular properties determine repetitive transcranial magnetic stimulation threshold for plasticity". In: *Frontiers in Cellular Neuroscience* 18, p. 1374555.

Gandolfi, Daniela, Albertino Bigiani, Carlo Adolfo Porro, and Jonathan Mapelli (2020). "Inhibitory plasticity: from molecules to computation and beyond". In: *International Journal of Molecular Sciences* 21.5, p. 1805.

Gaynes, Bradley N et al. (2014). "Repetitive transcranial magnetic stimulation for treatment-resistant depression: a systematic review and meta-analysis". In: *The Journal of clinical psychiatry* 75.5, p. 29758.

Gazdag, Gábor and Gabor S Ungvari (2019). "Electroconvulsive therapy: 80 years old and still going strong". In: *World journal of psychiatry* 9.1, p. 1.

Golding, Nace L, Nathan P Staff, and Nelson Spruston (2002). "Dendritic spikes as a mechanism for cooperative long-term potentiation". In: *Nature* 418.6895, pp. 326–331.

Gomez-Tames, Jose, Atsushi Hamasaka, Ilkka Laakso, Akimasa Hirata, and Yoshikazu Ugawa (2018). "Atlas of optimal coil orientation and position for TMS: A computational study". In: *Brain stimulation* 11.4, pp. 839–848.

Groden, Moritz, Hannah M Moessinger, Barbara Schaffran, Javier DeFelipe, Ruth Benavides-Piccione, Hermann Cuntz, and Peter Jedlicka (2024). "A biologically inspired repair mechanism for neuronal reconstructions with a focus on human dendrites". In: *PLOS Computational Biology* 20.2, e1011267.

Guillery, Rainer W (2005). "Observations of synaptic structures: origins of the neuron doctrine and its current status". In: *Philosophical Transactions of the Royal Society B: Biological Sciences* 360.1458, pp. 1281–1307.

Gutierrez, Mario Ibrahin, Irais Poblete-Naredo, Jorge Airy Mercado-Gutierrez, Cinthya Lourdes Toledo-Peral, Jimena Quinzaños-Fresnedo, Oscar Yanez-Suarez, and Josefina Gutierrez-Martinez (2022). "Devices and Technology in Transcranial Magnetic Stimulation: A Systematic Review". In: *Brain Sciences* 12.9, p. 1218.

Hallett, Mark (2007). "Transcranial magnetic stimulation: a primer". In: *Neuron* 55.2, pp. 187–199.

Hananeia, Nicholas and Lubica Benuskova (2016). "Computational simulation of dentate gyrus granule cell—The role of metaplasticity". In: *Neurocomputing* 175, pp. 300–309.

Hananeia, Nicholas, Christian Ebner, Christos Galanis, Hermann Cuntz, Alexander Opitz, Andreas Vlachos, and Peter Jedlicka (2024). "Multi-scale modelling of location-and frequency-dependent synaptic plasticity induced by transcranial magnetic stimulation in the dendrites of pyramidal neurons". In: *bioRxiv*, pp. 2024–07.

Harmelech, Tal, Yiftach Roth, and Aron Tendler (2021). "Deep TMS H7 coil: features, applications & future". In: *Expert Review of Medical Devices* 18.12, pp. 1133–1144.

Hay, Etay, Sean Hill, Felix Schürmann, Henry Markram, and Idan Segev (2011). "Models of neocortical layer 5b pyramidal cells capturing a wide range of dendritic and perisomatic active properties". In: *PLoS computational biology* 7.7, e1002107.

Hebb, DO (1949). "The Organization of Behavior: A Neuropsychological Theory". In: *(No Title)*.

Hellmann, Julian, Rene Jüttner, Clarisse Roth, Malek Bajbouj, Imke Kirste, Isabella Heuser, Karen Gertz, Matthias Endres, and Golo Kronenberg (2012). "Repetitive magnetic stimulation of human-derived neuron-like cells activates cAMP-CREB pathway". In: *European archives of psychiatry and clinical neuroscience* 262, pp. 87–91.

Herbsman, Tal et al. (2009). "Motor threshold in transcranial magnetic stimulation: The impact of white matter fiber orientation and skull-to-cortex distance". In: *Human brain mapping* 30.7, pp. 2044–2055.

Hodgkin, Alan L and Andrew F Huxley (1952). "A quantitative description of membrane current and its application to conduction and excitation in nerve". In: *The Journal of physiology* 117.4, p. 500.

Horih, Sami I (1989). "Basic neurochemistry: molecular, cellular, and medical aspects". In: *Neurology* 39.3, pp. 460–460.

Hormuzdi, Sheriar G, Mikhail A Filippov, Georgia Mitropoulou, Hannah Monyer, and Roberto Bruzzone (2004). "Electrical synapses: a dynamic signaling system that shapes the activity of neuronal networks". In: *Biochimica et Biophysica Acta (BBA)-Biomembranes* 1662.1-2, pp. 113–137.

Hsu, Wan-Yu, Chia-Hsiung Cheng, Kwong-Kum Liao, I-Hui Lee, and Yung-Yang Lin (2012). "Effects of repetitive transcranial magnetic stimulation on motor functions in patients with stroke: a meta-analysis". In: *Stroke* 43.7, pp. 1849–1857.

Huang, Ying-Zu, Rou-Shayn Chen, John C Rothwell, and Hsin-Yi Wen (2007). "The after-effect of human theta burst stimulation is NMDA receptor dependent". In: *Clinical Neurophysiology* 118.5, pp. 1028–1032.

Huber, KIMBERLY M, MICHAEL D Mauk, and PAUL T Kelly (1995). "Distinct LTP induction mechanisms: contribution of NMDA receptors and voltage-dependent calcium channels". In: *Journal of neurophysiology* 73.1, pp. 270–279.

Huerta, Patricio T and Bruce T Volpe (2009). "Transcranial magnetic stimulation, synaptic plasticity and network oscillations". In: *Journal of neuroengineering and rehabilitation* 6, pp. 1–10.

Ikegaya, Yuji, Yoko Ishizaka, and Norio Matsuki. (2002). "BDNF attenuates hippocampal LTD via activation of phospholipase C: implications for a vertical shift in the frequency–response curve of synaptic plasticity." In: *European Journal of Neuroscience* 16.1, pp. 145–148.

Isaac, John (2001). "Protein phosphatase 1 and LTD: synapses are the architects of depression". In: *Neuron* 32.6, pp. 963–966.

Izhikevich, Eugene M (2003). "Simple model of spiking neurons". In: *IEEE Transactions on neural networks* 14.6, pp. 1569–1572.

Januszewski, Michał et al. (2018). "High-precision automated reconstruction of neurons with flood-filling networks". In: *Nature methods* 15.8, pp. 605–610.

Jarsky, Tim, Alex Roxin, William L Kath, and Nelson Spruston (2005). "Conditional dendritic spike propagation following distal synaptic activation of hippocampal CA1 pyramidal neurons". In: *Nature neuroscience* 8.12, pp. 1667–1676.

Ji, Ru-Rong, Thomas E Schlaepfer, Carlos D Aizenman, Charles M Epstein, Dike Qiu, Justin C Huang, and Fabio Rupp (1998). "Repetitive transcranial magnetic stimulation activates specific regions in rat brain". In: *Proceedings of the National Academy of Sciences* 95.26, pp. 15635–15640.

Johnston, Daniel, Brian R Christie, Andreas Frick, Richard Gray, Dax A Hoffman, Lalania K Schexnayder, Shigeo Watanabe, and Li-Lian Yuan (2003). "Active dendrites, potassium channels and synaptic plasticity". In: *Philosophical Transactions of the Royal Society of London. Series B: Biological Sciences* 358.1432, pp. 667–674.

Josselyn, Sheena A, Stefan Köhler, and Paul W Frankland (2017). "Heroes of the engram". In: *Journal of Neuroscience* 37.18, pp. 4647–4657.

Kalil, Katherine, Gyorgyi Szebenyi, and Erik W Dent (2000). "Common mechanisms underlying growth cone guidance and axon branching". In: *Journal of neurobiology* 44.2, pp. 145–158.

Kase, Daisuke and Keiji Imoto (2012). "The role of HCN channels on membrane excitability in the nervous system". In: *Journal of signal transduction* 2012.

Kida, Hiroyuki, Yasumasa Tsuda, Nana Ito, Yui Yamamoto, Yuji Owada, Yoshinori Kamiya, and Dai Mitsushima (2016). "Motor training promotes both synaptic and intrinsic plasticity of layer II/III pyramidal neurons in the primary motor cortex". In: *Cerebral cortex* 26.8, pp. 3494–3507.

Kim, Jinhyun, Dong-Sheng Wei, and Dax A Hoffman (2005). "Kv4 potassium channel subunits control action potential repolarization and frequency-dependent broadening in rat hippocampal CA1 pyramidal neurones". In: *The Journal of physiology* 569.1, pp. 41–57.

Kim, Yujin, Ching-Lung Hsu, Mark S. Cembrowski, Brett D. Mensh, and Nelson Spruston. (2015). "Dendritic sodium spikes are required for long-term potentiation at distal synapses on hippocampal pyramidal neurons." In: *Elife* 4, e06414.

King, Emily S and Alexander D Tang (2022). "Intrinsic plasticity mechanisms of repetitive transcranial magnetic stimulation". In: *The Neuroscientist*, p. 10738584221118262.

Kinjo, Megumi, Masataka Wada, Shinichiro Nakajima, Sakiko Tsugawa, Tomomi Nakahara, Daniel M Blumberger, Masaru Mimura, and Yoshihiro Noda (2021). "Transcranial magnetic stimulation neurophysiology of patients with major depressive disorder: a systematic review and meta-analysis". In: *Psychological medicine* 51.1, pp. 1–10.

Kirkwood, Alfredo, Marika G Rioult, and Mark F Bear (1996). "Experience-dependent modification of synaptic plasticity in visual cortex". In: *Nature* 381.6582, pp. 526–528.

Kole, Maarten HP, Susanne U Ilschner, Björn M Kampa, Stephen R Williams, Peter C Ruben, and Greg J Stuart (2008). "Action potential generation requires a high sodium channel density in the axon initial segment". In: *Nature neuroscience* 11.2, pp. 178–186.

Kshatri, Aravind S, Alberto Gonzalez-Hernandez, and Teresa Giraldez (2018). "Physiological roles and therapeutic potential of Ca2+ activated potassium channels in the nervous system". In: *Frontiers in molecular neuroscience* 11, p. 258.

Lamprecht, Raphael and Joseph LeDoux (2004). "Structural plasticity and memory". In: *Nature Reviews Neuroscience* 5.1, pp. 45–54.

Larson, John, Darryl Wong, and Gary Lynch (1986). "Patterned stimulation at the theta frequency is optimal for the induction of hippocampal long-term potentiation". In: *Brain research* 368.2, pp. 347–350.

Lau, C Geoffrey and R Suzanne Zukin (2007). "NMDA receptor trafficking in synaptic plasticity and neuropsychiatric disorders". In: *Nature Reviews Neuroscience* 8.6, pp. 413–426.

Lee, Chi-Wei et al. (2023). "Different synaptic mechanisms of intermittent and continuous theta-burst stimulations in a severe foot-shock induced and treatment-resistant depression in a rat model". In: *Experimental Neurology* 362, p. 114338.

Lee, Chong Hyun and Peter C Ruben (2008). "Interaction between voltage-gated sodium channels and the neurotoxin, tetrodotoxin". In: *Channels* 2.6, pp. 407–412.

Lee, Hey-Kyoung, Michaela Barbarosie, Kimihiko Kameyama, Mark F Bear, and Richard L Huganir (2000). "Regulation of distinct AMPA receptor phosphorylation sites during bidirectional synaptic plasticity". In: *Nature* 405.6789, pp. 955–959.

Lee, Hey-Kyoung, Kogo Takamiya, et al. (2003). "Phosphorylation of the AMPA receptor GluR1 subunit is required for synaptic plasticity and retention of spatial memory". In: *Cell* 112.5, pp. 631–643.

Lefaucheur, Jean-Pascal et al. (2020). "Evidence-based guidelines on the therapeutic use of repetitive transcranial magnetic stimulation (rTMS): an update (2014–2018)". In: *Clinical neurophysiology* 131.2, pp. 474–528.

Lenz, Maximilian, Christos Galanis, et al. (2016). "Repetitive magnetic stimulation induces plasticity of inhibitory synapses". In: *Nature communications* 7.1, p. 10020.

Lenz, Maximilian, Steffen Platschek, et al. (2015). "Repetitive magnetic stimulation induces plasticity of excitatory postsynapses on proximal dendrites of cultured mouse CA1 pyramidal neurons". In: *Brain Structure and Function* 220, pp. 3323–3337.

Lenz, Maximilian and Andreas Vlachos (2016). "Releasing the cortical brake by non-invasive electromagnetic stimulation? rTMS induces LTD of GABAergic neurotransmission". In: *Frontiers in neural circuits* 10, p. 96.

Lin, Richard C and Richard H Scheller (2000). "Mechanisms of synaptic vesicle exocytosis". In: *Annual review of cell and developmental biology* 16.1, pp. 19–49.

Lisman, John (1989). "A mechanism for the Hebb and the anti-Hebb processes underlying learning and memory." In: *Proceedings of the National Academy of Sciences* 86.23, pp. 9574–9578.

Liu, Yufeng, Gaoyu Wang, Giorgio A Ascoli, Jiangning Zhou, and Lijuan Liu (2022). "Neuron tracing from light microscopy images: automation, deep learning and bench testing". In: *Bioinformatics* 38.24, pp. 5329–5339.

Lorentzen, Rasmus, Tuan D Nguyen, Alexander McGirr, Fredrik Hieronymus, and Søren D Østergaard (2022). "The efficacy of transcranial magnetic stimulation (TMS) for negative symptoms in schizophrenia: a systematic review and meta-analysis". In: *Schizophrenia* 8.1, p. 35.

Losonczy, Attila and Jeffrey C Magee (2006). "Integrative properties of radial oblique dendrites in hippocampal CA1 pyramidal neurons". In: *Neuron* 50.2, pp. 291–307.

Lüscher, Christian and Robert C Malenka (2012). "NMDA receptor-dependent long-term potentiation and long-term depression (LTP/LTD)". In: *Cold Spring Harbor perspectives in biology* 4.6, a005710.

Ma, Jun, Zhanchi Zhang, Yuhong Su, Lin Kang, Dandan Geng, Yanyong Wang, Feng Luan, Mingwei Wang, and Huixian Cui (2013). "Magnetic stimulation modulates structural synaptic plasticity and regulates BDNF–TrkB signal pathway in cultured hippocampal neurons". In: *Neurochemistry international* 62.1, pp. 84–91.

Magee, Jeffrey C (1998). "Dendritic hyperpolarization-activated currents modify the integrative properties of hippocampal CA1 pyramidal neurons". In: *Journal of Neuroscience* 18.19, pp. 7613–7624.

Malinow, Roberto (2003). "AMPA receptor trafficking and long-term potentiation". In: *Philosophical Transactions of the Royal Society of London. Series B: Biological Sciences* 358.1432, pp. 707–714.

Maller, Jerome J, Thomas Welton, Matthew Middione, Fraser M Callaghan, Jeffrey V Rosenfeld, and Stuart M Grieve (2019). "Revealing the hippocampal connectome through super-resolution 1150-direction diffusion MRI". In: *Scientific reports* 9.1, p. 2418.

Manis, Paul B (2022). "Delayed rectifier and A-Type potassium channels". In: *Encyclopedia of Computational Neuroscience*. Springer, pp. 1163–1177.

Markram, Henry, Joachim Lübke, Michael Frotscher, and Bert Sakmann (1997). "Regulation of synaptic efficacy by coincidence of postsynaptic APs and EPSPs". In: *Science* 275.5297, pp. 213–215.

McDougall, William (1901). "On the seat of the psycho-physical processes". In: *Brain* 24.4, pp. 579–630.

Megıas, M., Z. S. Emri, T. F. Freund, and A. I. Gulyas. (2001). "Total number and distribution of inhibitory and excitatory synapses on hippocampal CA1 pyramidal cells." In: *Neuroscience* 102.3, pp. 527–540.

Meng, Y, Ravi L Hadimani, Lawrence J Crowther, Z Xu, J Qu, and DC Jiles (2015). "Deep brain transcranial magnetic stimulation using variable "Halo coil" system". In: *Journal of Applied Physics* 117.17.

Menon, Parvathi, Nimeshan Geevasinga, Con Yiannikas, James Howells, Matthew C Kiernan, and Steve Vucic (2015). "Sensitivity and specificity of threshold tracking transcranial magnetic stimulation for diagnosis of amyotrophic lateral sclerosis: a prospective study". In: *The Lancet Neurology* 14.5, pp. 478–484.

Migliore, Rosanna et al. (2018). "The physiological variability of channel density in hippocampal CA1 pyramidal cells and interneurons explored using a unified data-driven modeling workflow". In: *PLoS computational biology* 14.9, e1006423.

Mittag, Martin, Laura Mediavilla, Stefan Remy, Hermann Cuntz, and Peter Jedlicka (2023). "Modelling the contributions to hyperexcitability in a mouse model of Alzheimer's disease". In: *The Journal of Physiology*.

Möhler, Hanns and Uwe Rudolph (2017). "Disinhibition, an emerging pharmacology of learning and memory". In: *F1000Research* 6.

Moradi Chameh, Homeira, Scott Rich, Lihua Wang, Fu-Der Chen, Liang Zhang, Peter L Carlen, Shreejoy J Tripathy, and Taufik A Valiante (2021). "Diversity amongst human cortical pyramidal neurons revealed via their sag currents and frequency preferences". In: *Nature communications* 12.1, p. 2497.

Morris, Andrew P (1999). "The regulation of epithelial cell cAMP-and calcium-dependent chloride channels." In: *Advances in Pharmacology (San Diego, Calif.)* 46, pp. 209–251.

Morris, RG (1989). "Synaptic plasticity and learning: selective impairment of learning rats and blockade of long-term potentiation in vivo by the N-methyl-D-aspartate receptor antagonist AP5". In: *Journal of Neuroscience* 9.9, pp. 3040–3057.

Morriss, Richard et al. (2024). "Connectivity-guided intermittent theta burst versus repetitive transcranial magnetic stimulation for treatment-resistant depression: a randomized controlled trial". In: *Nature Medicine*.

Müller-Dahlhaus, Florian and Andreas Vlachos (2013). "Unraveling the cellular and molecular mechanisms of repetitive magnetic stimulation". In: *Frontiers in molecular neuroscience* 6, p. 50.

Oberman, Lindsay, Dylan Edwards, Mark Eldaief, and Alvaro Pascual-Leone (2011). "Safety of theta burst transcranial magnetic stimulation: a systematic review of the literature". In: *Journal of Clinical Neurophysiology* 28.1, p. 67.

Oberman, Lindsay M, Alexander Rotenberg, and Alvaro Pascual-Leone (2015). "Use of transcranial magnetic stimulation in autism spectrum disorders". In: *Journal of autism and developmental disorders* 45, pp. 524–536.

Okun, M. and I. Lampl (2009). "Balance of excitation and inhibition". In: *Scholarpedia* 4.8. revision #150430, p. 7467. DOI: 10.4249/scholarpedia.7467.

Pannese, Ennio (1999). "The Golgi stain: invention, diffusion and impact on neurosciences". In: *Journal of the History of the Neurosciences* 8.2, pp. 132–140.

Parent, André (2004). "Giovanni Aldini: from animal electricity to human brain stimulation". In: *Canadian journal of neurological sciences* 31.4, pp. 576–584.

Pascual-Leone, Alvaro, Belen Rubio, Federico Pallardo, and Maria Dolores Catala (1996). "Rapid-rate transcranial magnetic stimulation of left dorsolateral prefrontal cortex in drug-resistant depression". In: *The Lancet* 348.9022, pp. 233–237.

Pascual-Leone, Alvaro, Josep Valls-Sole, Eric M Wassermann, and Mark Hallett (1994). "Responses to rapid-rate transcranial magnetic stimulation of the human motor cortex". In: *Brain* 117.4, pp. 847–858.

Pereda, Alberto E (2014). "Electrical synapses and their functional interactions with chemical synapses". In: *Nature Reviews Neuroscience* 15.4, pp. 250–263.

Petroff, Ognen AC (2002). "Book review: GABA and glutamate in the human brain". In: *The Neuroscientist* 8.6, pp. 562–573.

Pfister, Jean-Pascal and Wulfram Gerstner (2006). "Triplets of spikes in a model of spike timing-dependent plasticity". In: *Journal of Neuroscience* 26.38, pp. 9673–9682.

Plumbly, William, Nick Brandon, Tarek Z Deeb, Jeremy Hall, and Adrian J Harwood (2019). "L-type voltage-gated calcium channel regulation of in vitro human cortical neuronal networks". In: *Scientific Reports* 9.1, p. 13810.

Pridmore, Saxby, J Americo Fernandes Filho, Ziad Nahas, Chris Liberatos, and Mark S George (1998). "Motor threshold in transcranial magnetic stimulation: a comparison of a neurophysiological method and a visualization of movement method". In: *The journal of ECT* 14.1, pp. 25–27.

Quevedo, Joao, Mônica Vianna, Doriana Daroit, Antônio G Born, Carlos R Kuyven, Rafael Roesler, and Jorge A Quillfeldt (1998). "L-type voltage-dependent calcium channel blocker nifedipine enhances memory retention when infused into the hippocampus". In: *Neurobiology of learning and memory* 69.3, pp. 320–325.

Radojević, Miroslav and Erik Meijering (2019). "Automated neuron reconstruction from 3D fluorescence microscopy images using sequential Monte Carlo estimation". In: *Neuroinformatics* 17.3, pp. 423–442.

Robinson, PA (2011). "Neural field theory of synaptic plasticity". In: *Journal of Theoretical Biology* 285.1, pp. 156–163.

Rotem, Assaf and Elisha Moses (2008). "Magnetic stimulation of one-dimensional neuronal cultures". In: *Biophysical Journal* 94.12, pp. 5065–5078.

Routh, Brandy N, Daniel Johnston, Kristen Harris, and Raymond A Chitwood (2009). "Anatomical and electrophysiological comparison of CA1 pyramidal neurons of the rat and mouse". In: *Journal of neurophysiology* 102.4, pp. 2288–2302.

Rowland, Laura M, Richard AE Edden, Kimberly Kontson, He Zhu, Peter B Barker, and L Elliot Hong (2013). "GABA predicts inhibition of frequency-specific oscillations in schizophrenia". In: *The Journal of neuropsychiatry and clinical neurosciences* 25.1, pp. 83–87.

Rudolph, Stephanie, Ming-Chi Tsai, Henrique von Gersdorff, and Jacques I Wadiche (2015). "The ubiquitous nature of multivesicular release". In: *Trends in neurosciences* 38.7, pp. 428–438.

Samoilova, Marina, Kirsten Wentlandt, Yana Adamchik, Alexander A. Velumian, and Peter L. Carlen. (2008). "Connexin 43 mimetic peptides inhibit spontaneous epileptiform activity in organotypic hippocampal slice cultures." In: *Experimental neurology* 210.2, pp. 762–775.

Samoudi, Amine M, Emmeric Tanghe, Luc Martens, and Wout Joseph (2018). "Deep transcranial magnetic stimulation: improved coil design and assessment of the induced fields using MIDA model". In: *BioMed Research International* 2018.

Sáray, Sára et al. (2021). "HippoUnit: A software tool for the automated testing and systematic comparison of detailed models of hippocampal neurons based on electrophysiological data." In: *PLoS computational biology* 17.1, e1008114.

Saturnino, Guilherme B, Kristoffer H Madsen, and Axel Thielscher (2019). "Electric field simulations for transcranial brain stimulation using FEM: an efficient implementation and error analysis". In: *Journal of neural engineering* 16.6, p. 066032.

Scharfman, Helen E and Catherine E Myers (2013). "Hilar mossy cells of the dentate gyrus: a historical perspective". In: *Frontiers in neural circuits* 6, p. 106.

Schubert, Dirk, Rolf Kötter, and Jochen F Staiger (2007). "Mapping functional connectivity in barrel-related columns reveals layer-and cell type-specific microcircuits". In: *Brain Structure and Function* 212, pp. 107–119.

Seong, Hannah J, Rudy Behnia, and Adam G Carter (2014). "Impact of subthreshold membrane potential on synaptic responses at dendritic spines of layer 5 pyramidal neurons in the prefrontal cortex". In: *Journal of neurophysiology* 111.10, pp. 1960–1972.

Shah, Vikas N, Benjamin Chagot, and Walter J Chazin (2006). "Calcium-dependent regulation of ion channels". In: *Calcium binding proteins* 1.4, p. 203.

Shirinpour, Sina, Nicholas Hananeia, James Rosado, Christos Galanis Harry Tran, Andreas Vlachos, Peter Jedlicka, Gillian Queisser, and Alexander Opitz. (2021). "Open-source toolbox for multi-scale modeling of single neurons under transcranial magnetic stimulation." In: *Brain Stimulation: Basic, Translational, and Clinical Research in Neuromodulation* 14.6, p. 1697.

Shouval, Harel Z, Mark F Bear, and Leon N Cooper (2002). "A unified model of NMDA receptor-dependent bidirectional synaptic plasticity". In: *Proceedings of the National Academy of Sciences* 99.16, pp. 10831–10836.

Shouval, Harel Z and Georgios Kalantzis (2005). "Stochastic properties of synaptic transmission affect the shape of spike time–dependent plasticity curves". In: *Journal of neurophysiology* 93.2, pp. 1069–1073.

Sjöström, J. and W. Gerstner (2010). "Spike-timing dependent plasticity". In: *Scholarpedia* 5.2. revision #184913, p. 1362. DOI: 10.4249/scholarpedia.1362.

Sjöström, Per Jesper, Gina G Turrigiano, and Sacha B Nelson (2001). "Rate, timing, and cooperativity jointly determine cortical synaptic plasticity". In: *Neuron* 32.6, pp. 1149–1164.

Smith, Marie-Claire and Cathy M Stinear (2016). "Transcranial magnetic stimulation (TMS) in stroke: ready for clinical practice?" In: *Journal of Clinical Neuroscience* 31, pp. 10–14.

Sohal, Vikaas S and John LR Rubenstein (2019). "Excitation-inhibition balance as a framework for investigating mechanisms in neuropsychiatric disorders". In: *Molecular psychiatry* 24.9, pp. 1248–1257.

Song, Insuk and Richard L Huganir (2002). "Regulation of AMPA receptors during synaptic plasticity". In: *Trends in neurosciences* 25.11, pp. 578–588.

Spruston, Nelson (2001). "Axonal gap junctions send ripples through the hippocampus". In: *Neuron* 31.5, pp. 669–671.

Spruston, Nelson, Michael Häusser, and Greg Stuart (2013). "Chapter 11 - Information Processing in Dendrites and Spines". In: *Fundamental Neuroscience (Fourth Edition)*. Ed. by Larry R. Squire, Darwin Berg, Floyd E. Bloom, Sascha du Lac, Anirvan Ghosh, and Nicholas C. Spitzer. Fourth Edition. San Diego: Academic Press, pp. 231–260. ISBN: 978-0-12-385870-2. DOI: https://doi.org/10.1016/B978-0-12-385870-2.00011-1. URL: https://www.sciencedirect.com/science/article/pii/B9780123858702000111.

Staff, Nathan P, Hae-Yoon Jung, Tara Thiagarajan, Michael Yao, and Nelson Spruston (2000). "Resting and active properties of pyramidal neurons in subiculum and CA1 of rat hippocampus". In: *Journal of neurophysiology* 84.5, pp. 2398–2408.

Suminaite, Daumante, David A Lyons, and Matthew R Livesey (2019). "Myelinated axon physiology and regulation of neural circuit function". In: *Glia* 67.11, pp. 2050–2062.

Suppa, A, Y-Z Huang, K Funke, MC Ridding, B Cheeran, V Di Lazzaro, U Ziemann, and JC Rothwell (2016). "Ten years of theta burst stimulation in humans: established knowledge, unknowns and prospects". In: *Brain stimulation* 9.3, pp. 323–335.

Takahashi, Hiroto and Jeffrey C Magee (2009). "Pathway interactions and synaptic plasticity in the dendritic tuft regions of CA1 pyramidal neurons". In: *Neuron* 62.1, pp. 102–111.

Tamariz, Elisa and Alfredo Varela-Echavarria (2015). "The discovery of the growth cone and its influence on the study of axon guidance". In: *Frontiers in neuroanatomy* 9, p. 51.

Tang, Alexander D, Ivan Hong, Laura J Boddington, Andrew R Garrett, Sarah Etherington, John NJ Reynolds, and Jennifer Rodger (2016). "Low-intensity repetitive magnetic stimulation lowers action potential threshold and increases spike firing in layer 5 pyramidal neurons in vitro". In: *Neuroscience* 335, pp. 64–71.

Tavosanis, Gaia (2012). "Dendritic structural plasticity". In: *Developmental neurobiology* 72.1, pp. 73–86.

Thimm, Andreas and Klaus Funke (2015). "Multiple blocks of intermittent and continuous theta-burst stimulation applied via transcranial magnetic stimulation differently affect sensory responses in rat barrel cortex". In: *The Journal of physiology* 593.4, pp. 967–985.

Thome, Christian et al. (2014). "Axon-carrying dendrites convey privileged synaptic input in hippocampal neurons". In: *Neuron* 83.6, pp. 1418–1430.

Todd, Gabrielle, Stanley C Flavel, and Michael C Ridding (2009). "Priming theta-burst repetitive transcranial magnetic stimulation with low-and high-frequency stimulation". In: *Experimental Brain Research* 195, pp. 307–315.

Tokay, Tursonjan, Norman Holl, Timo Kirschstein, Volker Zschorlich, and Rüdiger Köhling (2009). "High-frequency magnetic stimulation induces long-term potentiation in rat hippocampal slices". In: *Neuroscience Letters* 461.2, pp. 150–154.

Tomko, Matus, Lubica Benuskova, and Peter Jedlicka. (2021). "A new reduced-morphology model for CA1 pyramidal cells and its validation and comparison with other models using HippoUnit." In: *Scientific reports* 11.1, pp. 1–16.

Tremblay, Sara et al. (2019). "Clinical utility and prospective of TMS–EEG". In: *Clinical Neurophysiology* 130.5, pp. 802–844.

Turi, Zsolt, Nicholas Hananeia, Sina Shirinpour, Alexander Opitz, Peter Jedlicka, and Andreas Vlachos (2022). "Dosing Transcranial Magnetic Stimulation of the Primary Motor and Dorsolateral Prefrontal Cortices With Multi-Scale Modeling". In: *Frontiers in Neuroscience* 16, p. 929814.

Turi, Zsolt, Maximilian Lenz, Walter Paulus, Matthias Mittner, and Andreas Vlachos (2021). "Selecting stimulation intensity in repetitive transcranial magnetic stimulation studies: A systematic review between 1991 and 2020". In: *European Journal of Neuroscience* 53.10, pp. 3404–3415.

Ueno, Shoogo and Masaki Sekino (2021). "Figure-eight coils for magnetic stimulation: from focal stimulation to deep stimulation". In: *Frontiers in human neuroscience* 15, p. 805971.

Vergara, Cecilia, Ramon Latorre, Neil V Marrion, and John P Adelman (1998). "Calcium-activated potassium channels". In: *Current opinion in neurobiology* 8.3, pp. 321–329.

Vlachos, Andreas, Klaus Funke, and Ulf Ziemann. (2017). "Assessment and modulation of cortical inhibition using transcranial magnetic stimulation." In: *e-Neuroforum* 23.1, pp. 9–17.

Vlachos, Andreas, Florian Müller-Dahlhaus, Johannes Rosskopp, Maximilian Lenz, Ulf Ziemann, and Thomas Deller (2012). "Repetitive magnetic stimulation induces functional and structural plasticity of excitatory postsynapses in mouse organotypic hippocampal slice cultures". In: *Journal of Neuroscience* 32.48, pp. 17514–17523.

Vogels, Tim P, Robert C Froemke, et al. (2013). "Inhibitory synaptic plasticity: spike timing-dependence and putative network function". In: *Frontiers in neural circuits* 7, p. 119.

Vogels, Tim P, Henning Sprekeler, Friedemann Zenke, Claudia Clopath, and Wulfram Gerstner (2011). "Inhibitory plasticity balances excitation and inhibition in sensory pathways and memory networks". In: *Science* 334.6062, pp. 1569–1573.

Vucic, Steve et al. (2023). "Clinical diagnostic utility of transcranial magnetic stimulation in neurological disorders. Updated report of an IFCN committee". In: *Clinical Neurophysiology*.

Wang, John Q, Anish Arora, Lu Yang, Nikhil K Parelkar, Guochi Zhang, Xianyu Liu, Eun Sang Choe, and Limin Mao (2005). "Phosphorylation of AMPA receptors: mechanisms and synaptic plasticity". In: *Molecular neurobiology* 32, pp. 237–249.

Wang, Xin, Zhiqi Mao, Zhipei Ling, and Xinguang Yu (2020). "Repetitive transcranial magnetic stimulation for cognitive impairment in Alzheimer's disease: a meta-analysis of randomized controlled trials". In: *Journal of Neurology* 267, pp. 791–801.

Wankerl, Katharina, David Weise, Reinhard Gentner, Jost-Julian Rumpf, and Joseph Classen (2010). "L-type voltage-gated Ca2+ channels: a single molecular switch for long-term potentiation/long-term depression-like plasticity and activity-dependent metaplasticity in humans". In: *Journal of Neuroscience* 30.18, pp. 6197–6204.

Wassermann, Eric M. and Trelawny Zimmermann. (2012). "Transcranial magnetic brain stimulation: therapeutic promises and scientific gaps." In: *Pharmacology & therapeutics* 133.1, pp. 98–107.

Weiler, Marina et al. (2023). "Transcriptional changes in the rat brain induced by repetitive transcranial magnetic stimulation (rTMS)". In: *Frontiers in Human Neuroscience* 17, p. 1215291.

Weisskopf, Marc G, Elizabeth P Bauer, and Joseph E LeDoux (1999). "L-type voltage-gated calcium channels mediate NMDA-independent associative long-term potentiation at thalamic input synapses to the amygdala". In: *Journal of Neuroscience* 19.23, pp. 10512–10519.

Westenbroek, Ruth E, Michael K Ahlijanian, and William A Catterall (1990). "Clustering of L-type Ca2+ channels at the base of major dendrites in hippocampal pyramidal neurons". In: *Nature* 347.6290, pp. 281–284.

Wilson, Marcus T, Ben D Fulcher, Park K Fung, Peter A Robinson, Alex Fornito, and Nigel C Rogasch (2018). "Biophysical modeling of neural plasticity induced by transcranial magnetic stimulation". In: *Clinical Neurophysiology* 129.6, pp. 1230–1241.

Wilson, Marcus T, Park K Fung, Peter A Robinson, Jonathan Shemmell, and John NJ Reynolds (2016). "Calcium dependent plasticity applied to repetitive transcranial magnetic stimulation with a neural field model". In: *Journal of computational neuroscience* 41, pp. 107–125.

Wilson, Marcus T, DP Goodwin, Philip W Brownjohn, Jonathan Shemmell, and John NJ Reynolds (2014). "Numerical modelling of plasticity induced by transcranial magnetic stimulation". In: *Journal of computational neuroscience* 36, pp. 499–514.

Wittenberg, Gayle M and Samuel S-H Wang (2006). "Malleability of spike-timing-dependent plasticity at the CA3–CA1 synapse". In: *Journal of Neuroscience* 26.24, pp. 6610–6617.

Witter, Menno P. (2010). "Connectivity of the Hippocampus". In: *Hippocampal Microcircuits: A Computational Modeler's Resource Book*. Ed. by Vassilis Cutsuridis, Bruce Graham, Stuart Cobb, and Imre Vida. New York, NY: Springer New York, pp. 5–26. ISBN: 978-1-4419-0996-1. DOI: 10.1007/978-1-4419-0996-1_1. URL: https://doi.org/10.1007/978-1-4419-0996-1_1.

Yizhar, Ofer et al. (2011). "Neocortical excitation/inhibition balance in information processing and social dysfunction". In: *Nature* 477.7363, pp. 171–178.

Zhang, Min, Runhua Wang, Xin Luo, Si Zhang, Xiaomei Zhong, Yuping Ning, and Bin Zhang (2021). "Repetitive transcranial magnetic stimulation target location methods for depression". In: *Frontiers in Neuroscience* 15, p. 695423.

Ziemann, Ulf (2004). "TMS induced plasticity in human cortex". In: *Reviews in the Neurosciences* 15.4, pp. 253–266.

– (2017). "Thirty years of transcranial magnetic stimulation: where do we stand?" In: *Experimental brain research* 235.4, pp. 973–984.

Zorumski, Charles F and Yukitoshi Izumi (2012). "NMDA receptors and metaplasticity: mechanisms and possible roles in neuropsychiatric disorders". In: *Neuroscience & Biobehavioral Reviews* 36.3, pp. 989–1000.